AWARD NUMBER: W81XWH-18-1-0506

TITLE: Engineering Biomaterial-Based Therapies for Improved Lymphatic Function and the Resolution of Chronic Inflammation in Posttraumatic Osteoarthritis

PRINCIPAL INVESTIGATOR: Brandon Dixon

CONTRACTING ORGANIZATION: Georgia Tech Research Corporation

REPORT DATE: SEPTEMBER 2020

TYPE OF REPORT: Annual

PREPARED FOR: U.S. Army Medical Research and Materiel Command
Fort Detrick, Maryland 21702-5012

REPORT DOCUMENTATION PAGE

Form Approved
OMB No. 0704-0188

1. REPORT DATE	2. REPORT TYPE	3. DATES COVERED
SEPTEMBER 2020	Annual	15 Aug 2019 – 14 Aug 2020

4. TITLE AND SUBTITLE
Engineering Biomaterial-Based Therapies for Improved Lymphatic Function and the Resolution of Chronic Inflammation in Posttraumatic Osteoarthritis

5a. CONTRACT NUMBER
W81XWH-18-1-0506

5b. GRANT NUMBER
W81XWH-18-1-0506

5c. PROGRAM ELEMENT NUMBER

6. AUTHOR(S)
Brandon Dixon

E-Mail: dixon@gatech.edu

5d. PROJECT NUMBER

5e. TASK NUMBER

5f. WORK UNIT NUMBER

7. PERFORMING ORGANIZATION NAME(S) AND ADDRESS(ES)

Georgia Tech Research Corporation
505 10th St NW
Atlanta GA 30318-5775

8. PERFORMING ORGANIZATION REPORT NUMBER

9. SPONSORING / MONITORING AGENCY NAME(S) AND ADDRESS(ES)

U.S. Army Medical Research and Materiel Command
Fort Detrick, Maryland 21702-5012

10. SPONSOR/MONITOR'S ACRONYM(S)

11. SPONSOR/MONITOR'S REPORT NUMBER(S)

12. DISTRIBUTION / AVAILABILITY STATEMENT

Approved for Public Release; Distribution Unlimited

13. SUPPLEMENTARY NOTES

14. ABSTRACT
In year 2 of the project, we demonstrated that lymphatic function was reduced during mid- and late- stages of osteoarthritis in the rat medial meniscus transection model. This reduction may be due to cytokines and inflammation found in osteoarthritis synovial fluid. In addition, we provided evidence that biomaterials (such as hyaluronan, liposomes and PEG microgels) can be intra-articularly injected into rat knees to increase retention of drugs within the joint for as long as 3 weeks. The application of these carriers in conjunction with therapeutics (such as resolvins, hyaluronan, exercise and mesenchymal stem cells) will be investigated in year 3 to treat osteoarthritis.

15. SUBJECT TERMS

NONE LISTED

16. SECURITY CLASSIFICATION OF:			17. LIMITATION OF ABSTRACT	18. NUMBER OF PAGES	19a. NAME OF RESPONSIBLE PERSON
a. REPORT	b. ABSTRACT	c. THIS PAGE			USAMRMC
Unclassified	Unclassified	Unclassified	Unclassified	76	19b. TELEPHONE NUMBER *(include area code)*

TABLE OF CONTENTS

1. INTRODUCTION:

Osteoarthritis (OA) is associated with chronic unresolved inflammation that is a key driver of disease development and progression. The central dogma in the OA field is that chronic inflammation is an inherent problem of production, i.e. the tissues of the joint continuously produce inflammatory cytokines, proteases, and other pathologic factors. The clearance of these factors has always been thought to be rapid and thus, is assumed not to be rate limiting in disease progression. Additionally, downstream communication from clearance (such as at the lymph node) has been largely neglected. These assumptions have received little attention and in part, because the tools to truly test these hypotheses have been limited. However, in all other peripheral tissue diseases, the functional process and communication between the tissue, the lymphatic vessel conduit, and the lymph nodes is critical in the resolution of inflammation. Thus, the ***overall objective*** of this PRMRP grant is to develop biomaterial-based therapies that can be integrated with imaging modalities to both: 1) elucidate the role of lymphatic function in normal and diseased joints; and 2) promote joint clearance and the resolution of chronic inflammation by delivering inflammation resolving lipid mediators using controlled-release nanoparticles. Our ***central hypothesis*** is that lymphatic function is a critical component in OA disease progression and regenerative therapies that improve lymphatic function and the resolution of chronic inflammation will attenuate OA disease development and progression. Thus, the following Specific Aims were designed:

Aims 1: *To develop a set of biomaterial-based tools to quantitatively interrogate lymphatic clearance function.*

Aims 2: *To evaluate lymphatic function during the pathogenesis of OA in the rat medial meniscus transection (MMT)-induced OA model.*

Aims 3: *To engineer novel intra-articular therapeutics to improve lymphatic function and resolution of inflammation during post traumatic OA.*

2. KEYWORDS:

osteoarthritis, intra-articular delivery, knee clearance, lymphatics, inflammation, resolvin

3. ACCOMPLISHMENTS:

What were the major goals of the project?

Specific Aim 1: Develop NIR tools to assess lymphatic function and clearance of various sized particles from intra-articular injection.	**Emory Site 1**	**GA Tech Site 2**	**Expected Timeline**	**Complete**
Major Task 1 – *Determine the clearance kinetics of 2kDa and 40kDa PEG's from intra-articular injections into the knee joint and their uptake into lymphatics.*				
Subtask 1 – Determine the clearance kinetics and localization of 2kDa PEG-NIR particles	Willett	Dixon	8 - 10/18	100%
Subtask 2 – Determine the clearance kinetics and localization of 40kDa PEG-NIR particles	Willett	Dixon	9 - 12/18	100%
Milestone(s) Achieved	Willett	Dixon	12/18	100%
Local IACUC Approval	Willett	Dixon	Approved	100%
Milestone Achieved: ACURO Approval	Willett	Dixon	Approved	100%
Major Task 2 – *Determine the retention and clearance kinetics of PEG-liposome carriers from intra-articular injections into the knee joint and their uptake into lymphatics.*				
Subtask 1 - Determine the clearance kinetics and localization of 500nm NIR-labelled liposome carriers	Willett	Garcia & Dixon	1 - 3/19	80%
Subtask 2 – Determine the clearance kinetics and localization of 500nm liposome carriers containing 40kDa PEG-NIR	Willett	Garcia & Dixon	1 - 3/19	80%
Subtask 3 – Determine the clearance kinetics and localization of 900nm NIR-labelled liposome carriers	Willett	Garcia & Dixon	3 - 5/19	80%
Subtask 4 – Determine the clearance kinetics and localization of 900nm liposome carriers containing 40kDa PEG-NIR	Willett	Garcia & Dixon	3 - 5/19	50%
Milestone(s) Achieved:	Willett	Garcia & Dixon	5/19	75%
Specific Aim 2: Apply NIR technology to assess lymphatic function and clearance of materials within osteoarthritic joints.				
Major Task 3 - *Determine the effect of OA on lymphatic function and clearance of small particles.*				
Subtask 1 – Determine the clearance kinetics and localization of 2kDa PEG particles in MMT-induced OA animals at early, mid and late stage	Willett	Dixon	4/19-1/20	100%
Subtask 2 – Determine the clearance kinetics and localization of 40kDa PEG particles in MMT-induced OA animals at early, mid and late stage	Willett	Dixon	4/19-1/20	100%
Milestone(s) Achieved:	Willett	Dixon	1/20	100%
Major Task 4 – *Determine the effect of OA on lymphatic architect and clearance of PEG-liposome carriers.*				
Subtask 1 - Determine the clearance kinetics and localization of NIR-labelled liposome carriers in MMT-induced OA animals at early, mid and late stage	Willett	Dixon	6/19-8/20	50%
Subtask 2 - Determine the clearance kinetics and localization of liposome carriers containing 40kDa PEG-NIR in MMT-induced OA animals at early, mid and late stage	Willett	Dixon	6/19-8/20	50%
Milestone(s) Achieved:	Willett	Dixon	8/20	
Specific Aim 3: Administer resolvin therapies in liposome nanoparticles to treat OA and correct for lymphatic dysfunction.				
Major Task 5 – *Determine the Effects of Resolvins to treat OA.*				
Subtask 1 – Fabrication and assessment of liposome carriers containing Resolvins D1 and E1	Willett	Garcia & Dixon	5 - 7/20	20%
Subtask 2 – Determine the efficacy of Resolvins to treat early stage of OA	Willett	Garcia & Dixon	6 - 10/20	20%
Milestone(s) Achieved:	Willett	Garcia & Dixon	10/20	
Major Task 6 – *Determine the effect of PEG-liposome carriers containing resolvins on the progression of OA and their ability to improve lymphatic function during late stage OA.*				
Subtask 1 - Effect of Resolvin to treat mid to late stage of OA by using different therapeutic regimen	Willett	Garcia & Dixon	9/20-7/21	0%
Milestone(s) Achieved:	Willett	Garcia & Dixon	7/21	
Final analyses & manuscript preparation.	Willett	Garcia & Dixon	5 - 7/21	

What was accomplished under these goals?

In Fiscal Year 1 (FY1) of the project, we had completed (100%) Major Task 1 and published the results in our manuscript provided in FY1 report. For FY2, we focused our efforts on Major Tasks 2, 3, 4 and initiated work on Major Task 5. We provide results and discussion of these Major Tasks below.

Major Task 2 – *Determine the retention and clearance kinetics of PEG-liposome carriers from intra-articular injections into the knee joint and their uptake into lymphatics.*
Subtask 1 - Determine the clearance kinetics and localization of 500nm NIR-labelled liposome carriers
Subtask 2 – Determine the clearance kinetics and localization of 500nm liposome carriers containing 40kDa PEG-NIR
Subtask 3 – Determine the clearance kinetics and localization of 900nm NIR-labelled liposome carriers
Subtask 4 – Determine the clearance kinetics and localization of 900nm liposome carriers containing 40kDa PEG-NIR

The goal of Major Task 2 is to develop near-infrared (NIR) based approaches to detect the clearance of drug delivery vehicles from the joint space. In FY2 we published a review article, "Biomaterial strategies for improved intra-articular drug delivery," describing the retention and clearance of biomaterials to treat osteoarthritis (DOI: 10.1002/jbm.a.37074, provided in Appendices). We describe different biomaterial-based systems and particles that can prolong the retention of drugs within the joint (Figure 1). We have also

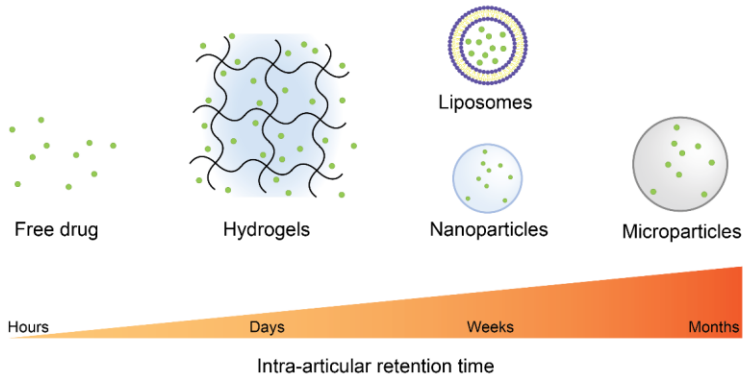

Figure 1: Drug delivery systems typically used for intra-articular (IA) drug administration and their IA retention time. Free small and macromolecule drugs are cleared from the joint space in few hours. The use of drug delivery vehicles increases drug IA retention time, typically in a size-dependent manner. Nano-scale vehicles such as nanoparticles and liposomes are generally retained up to a couple of weeks, whereas microparticles can be retained in the joint space up to a month. (Adapted from Mancipe Castro *et al*. 2020, J Biomed Mater Res)

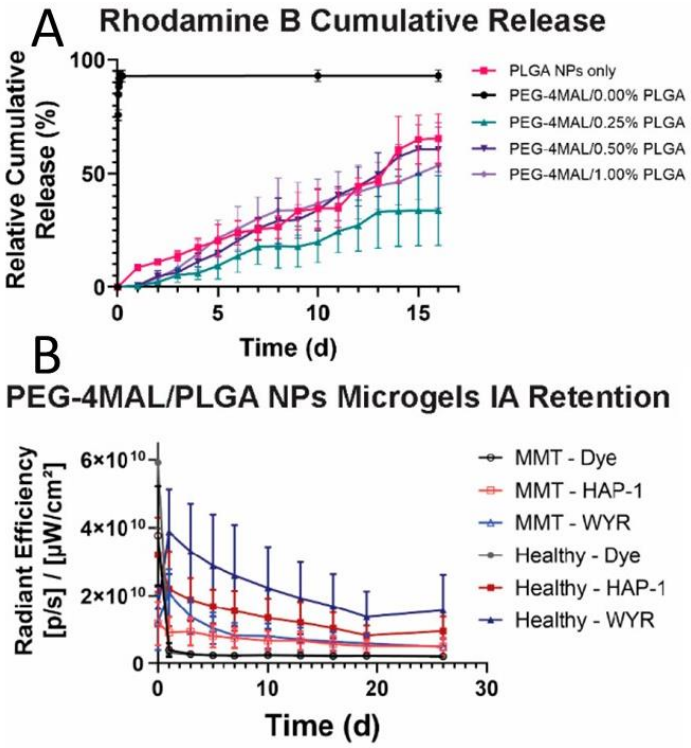

Figure 2: A) Rhodamine B release profile from empty microgels, nanocomposite microgels, and PLGA nanoparticles. Rhodamine B rapidly diffuses out of empty PEG-4MAL microgels, whereas microgels containing PLGA NPs and PLGA NPs alone exhibited a zero-order release. B) Radiant efficiency of different formulations of microgels as a function of time (mean ± SD, n = 9) within naïve and osteoarthritis (MMT) rat knee joints. Free dye was cleared within a day and microgels (HAP-1 and WYR) were retained in knee joints beyond 3 weeks *in vivo*. (Adapted from Mancipe Castro *et al*., 2020, ACS Biomater Science Eng)

published a research article where we engineered 4-arm-poly(ethylene glycol)-maleimide (PEG-4MAL) microgel as a drug carrier system to treat osteoarthritis, "Articular cartilage- and synoviocyte-binding poly(ethylene glycol) nano-composite microgels as intra-articular drug delivery vehicles for the treatment of osteoarthritis" (provided in Appendices). With these microgels, we found that fluorophores can be released with zero-order kinetics over 16 days *in vitro* and can be retained within rat knee joints for over 3 weeks (Figure 2). In this FY2, we have additionally developed and characterized

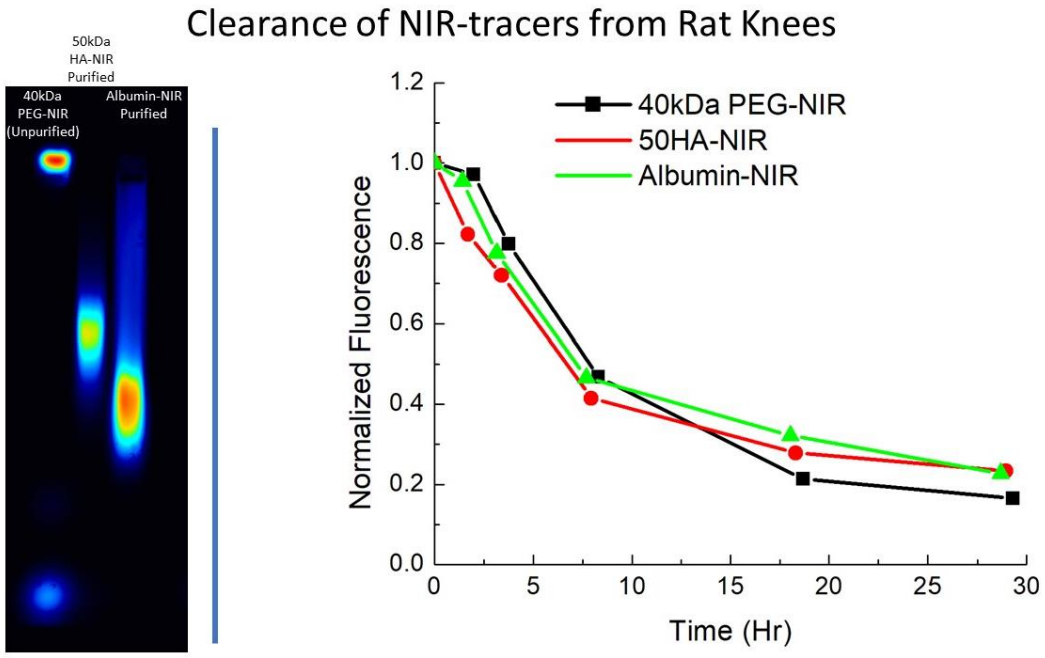

Figure 3: Fabrication and clearance of NIR conjugates from rat knees. Left image, NIR dyes were conjugated to 40kDa polyethylene glycol (PEG), 50kDa hyaluronan (HA, purified) and albumin (~66kDa, purified) and separated on SDS-PAGE. Right panel, Purified NIR-conjugates (e.g. PEG, HA and Albumin) were intra-articularly injected into rat knees. Clearance kinetics were similar for each construct (n = 7).

hyaluronan and liposome-based drug carriers tagged with NIR dyes. Hyaluronan is a natural extracellular matrix found in the synovial fluid of joints, is currently being used as a viscosupplement to treat knee osteoarthritis and may also be used as a drug carrier. We have fabricated hyaluronan tagged with NIR dyes and found that this biomaterial clears similarly to 40kDa PEG-NIR and albumin-NIR (~66kDa) (Figure 3). We have also fabricated liposomes for intra-articular drug delivery cargo. We found that liposomes (900 nm) with the composition of 80% 1, 2, dipalmitoyl-*sn*-glycero-3-phospocholine (DPPC), 15% cholesterol and 5% 1,2-distearoyl-*sn*-glycero - 3 - phosphoethanolamine - N - [amino (polyethylene glycol)-2000] (DSPE-PEG) are stable for days *in vitro* at 37°C. To track the clearance of liposomes *in vivo*, we attached NIR dye Cy5.5 to DSPE-PEG and co-injected the 900 nm carrier into rat knees with or without 40kDa PEG-NIR (Figure 4). In this initial experiment, we found that liposomes were retained in the knee joint for nearly 1.5 days before being cleared. Residual liposomes were retained for at least a week before NIR signal returned to near baseline. In contrast, NIR signal for 40kDa PEG-NIR (observed under the 800 channel) returned to near baseline within 24 hours.

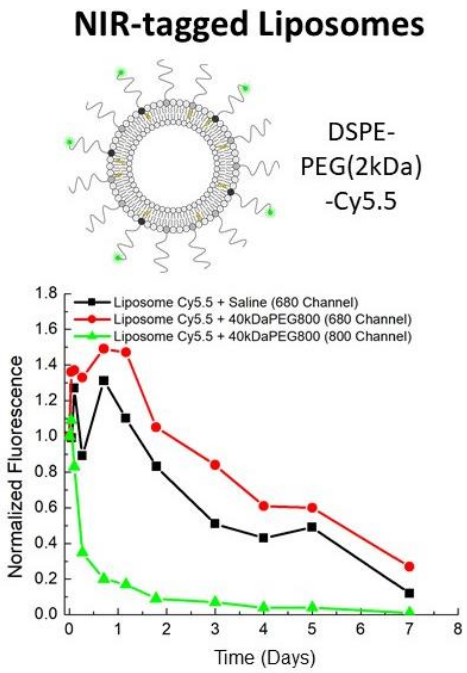

Figure 4: Illustration of liposome construct containing Cy5.5 dye. Lewis rat was given intra-articular injection of liposomes in saline (black) into left knee joint or was given liposomes and 40kDa PEG-NIR into the right knee joint. NIR images were captured at various times and calculated normalized fluorescence intensity were plotted. Similar results were found for 2 rats.

Research activities involving liposome synthesis were subsequently shut down from mid-March until early July due to COVID-19. Upon return and resumption of liposome synthesis, we have encountered numerous stability issues associated with the 900 nm liposome that caused them to spontaneously assemble into varying particles of diverse and smaller sizes. After troubleshooting these issues with a variety of formulation strategies, as well as replacing all the lipids used in the synthesis with fresh lipids, we decided to pivot to a new formulation approach in August. Since we are a bit agnostic to the actual biomaterial used to deliver the cargo, provided that the particle fits a particular size profile to achieve the desired kinetics, we are now optimizing PLGA-based nanoparticles in both free suspension, as well embed in larger microgels (similar to Figure 2). We are now characterizing the kinetics of these particles with our NIR system *in vivo*.

Major Task 3 - *Determine the effect of OA on lymphatic function and clearance of small particles.*
Subtask 1 – Determine the clearance kinetics and localization of 2kDa PEG particles in MMT-induced OA animals at early, mid and late stage
Subtask 2 – Determine the clearance kinetics and localization of 40kDa PEG particles in MMT-induced OA animals at early, mid and late stage

For Major Task 3, our primary goal is to evaluate the effect of osteoarthritis on lymphatic function. To accomplish this, we first characterize the three different stages (e.g. early, mid, and late) of osteoarthritis that occurs in the medial meniscus transection (MMT) rat model (Figure 5). For this rat model, naïve (non-operated) and sham (surgical control) joints were used as negative controls to compare the effect of MMT induction on joint deterioration.

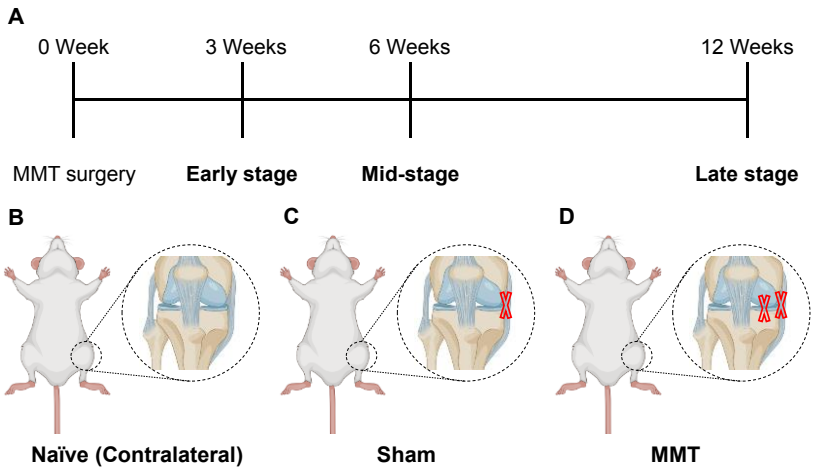

Figure 5: (A) Timeline for the medial meniscus transection (MMT) rat model used in our studies. Illustrations of naïve rat knee joint (B), a knee joint that had received sham operation --- transection of medial collateral ligament (C), and a knee joint that had received MMT surgery --- transection of medial collateral ligament and medial meniscus (D).

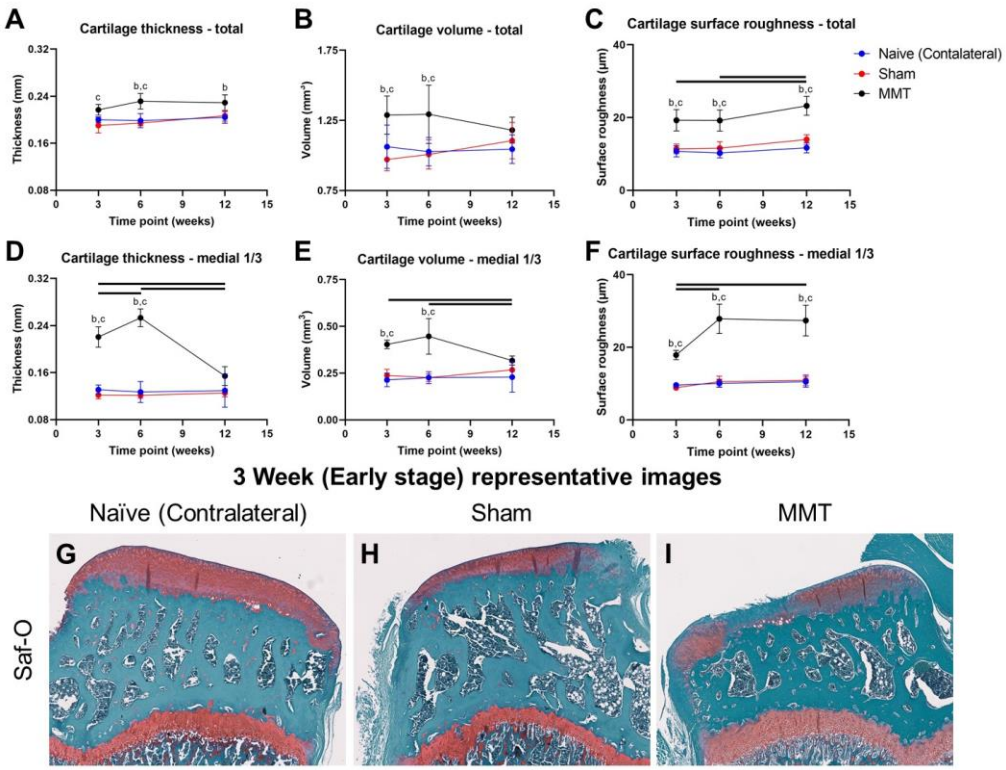

Figure 6: MMT-induced osteoarthritis in rat model. Cartilage thickness (A), volume (B) and surface roughness (C) were significantly elevated during osteoarthritis development in rats. No significance was found between naïve and sham-operated knees. Representative safranin-O staining of rat tibia from naïve (G), Sham (H) and MMT (I) animals at 3-weeks post-surgery. n = 6-9 per group.

With contrast enhanced μCT imaging, we have quantified the changes to articular cartilage and bone. At early stage (3-weeks post-surgery), there was an increase in total articular cartilage volume, cartilage thickness and surface roughness of the tibia (Figure 6). The damage to the articular cartilage was found dominantly in the medial 1/3 portion of the tibia, which was consistent with the loss of joint stability from transection of the medial meniscus. As osteoarthritis developed in this model, there was increased lesion area of the articular cartilage with gradual deterioration down to the subchondral bone layer (Figure 7), which was consistently observed at mid-stage (6-weeks post-surgery). By 12-weeks post-surgery (late stage) there was an expansion of osteophyte and its mineralization (Figure 8).

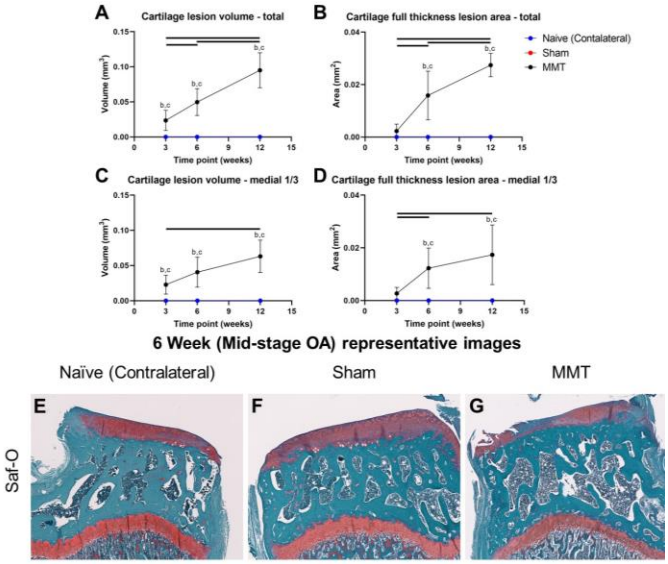

Figure 7: MMT-induced osteoarthritis in rat model. Cartilage lesion volume (A, C) and area (B, D) were significantly elevated during osteoarthritis development in rats. No significance was found between naïve and sham-operated knees. Representative safranin-O staining of rat tibia from naïve (E), Sham (F) and MMT (G) animals at 6-weeks post-surgery. n = 6-9 per group.

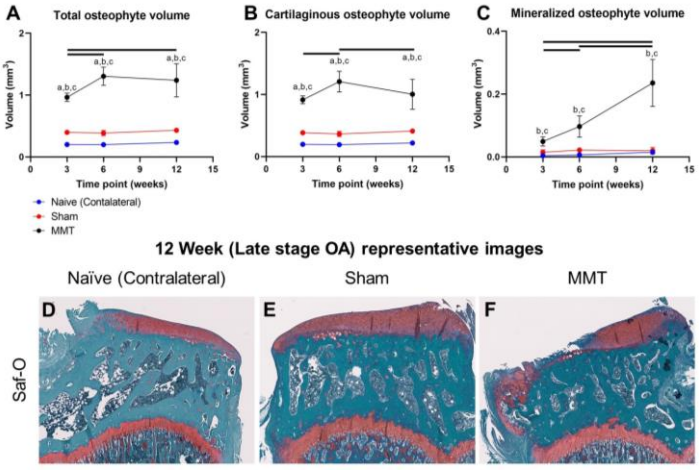

Figure 8: MMT-induced osteoarthritis in rat model. Total (A), cartilaginous (B) and mineralized (C) osteophyte volumes were significantly elevated during osteoarthritis development in rats. Representative safranin-O staining of rat tibia from naïve (D), Sham (E) and MMT (F) animals at 12-weeks post-surgery. n = 6-9 per group.

With this post-traumatic osteoarthritis model, we conducted studies to determine the effect of osteoarthritis development on clearance and lymphatic function using two specialized techniques: 1) knee clearance of lymphatic-specific particles and 2) *ex vivo* assessment of lymphatic vessel pump function. We did not find a significant effect of MMT-induced osteoarthritis on clearance of the smaller tracer (e.g. free dye) which was cleared through the venous circulation (Figure 9). Interestingly, both OA and sham surgery animals showed a gradual reduction in lymphatic clearance (e.g. 40kDa PEG) that eventually returned to normal by week 21. However, for sham surgery the peak of this effect occurred in week 6 and resolved by week 9, while OA animals have reduced function in weeks 9 and 18 that resolved in week 21. This suggested that OA may affect lymphatic function at mid- to late-stages.

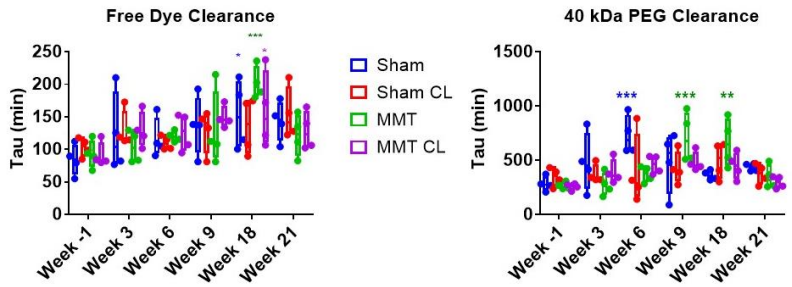

Figure 9: Effect of MMT-induced osteoarthritis to knee clearance. Rats received either Sham or MMT surgeries to their left hindlimb; the contralateral right hindlimb did not receive any surgical manipulation. Knee clearance studies with free NIR dye and 40kDa PEG-NIR (lymphatic-specific particle) were conducted one week before surgery (Week -1) and at 3-, 6-, 9-, 18- and 21- weeks post-surgery. Time constants (Tau) were calculated and box plots are shown for free dye and for 40kDa PEG-NIR.

In FY1, we demonstrated that the ejection fraction of isolated lymphatic vessels may be increased in MMT-induced osteoarthritis animals around 9 weeks post-surgery. To investigate more directly the effect of the synovial fluid environment on lymphatic function, we tested the effect of human synovial fluid, collected from healthy or osteoarthritis knee patients, in the *ex vivo* lymphatic pump function assay. Human synovial fluids were commercially available or donated by Emory's orthopaedic physician (courtesy of Dr. Kenneth Mautner). Isolated rat femoral lymphatic vessels, the primary collecting vessel that we have identified as responsible for draining the knee joint in the rat, responded to changes in pressure (from 1, to 3, to 5 mm of H_2O) with increased contraction frequency and with decreased contraction amplitude (Figure 10). When synovial fluid collected from a healthy donor were perfused through the lumen of the vessel for 1 hour or for 2 hours, there was a marked increase in contraction frequency at 1 and 3 mm of H_2O. When the vessel was treated for more than 12 hours (overnight) with healthy synovial fluid, the vessel diameter was increased with irregular contraction frequency occurring at each pressure step.

When synovial fluid collected from osteoarthritis patients were perfused through the lumen of the vessel, there was a marked increase in the vessel tone and a decrease in the amplitude frequency of contraction with the intrinsic pumping of the vessel being completely lost after 2 hours of incubation

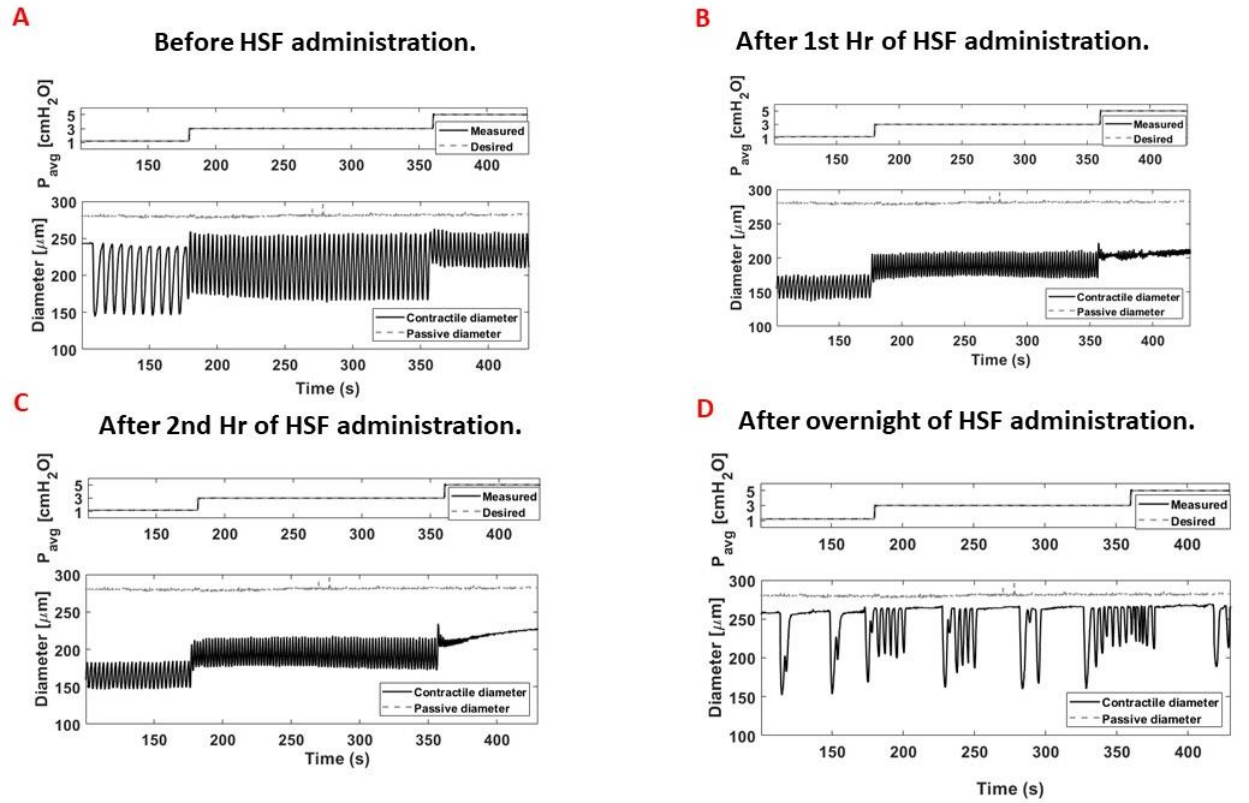

Figure 10: Effect of healthy synovial fluid on *ex vivo* lymphatic pump function. Rat femoral lymphatic vessels were isolated and placed into physiological saline chamber attached to pressure controls. Images of vessels were captured. Changes to vessel diameter were measured. The vessels were assessed before (A), 1 hr (B), 2 hr (C) and 24 hr (D) after treatment with synovial fluid (diluted 1:10 in physiological saline) collected from a healthy patient.

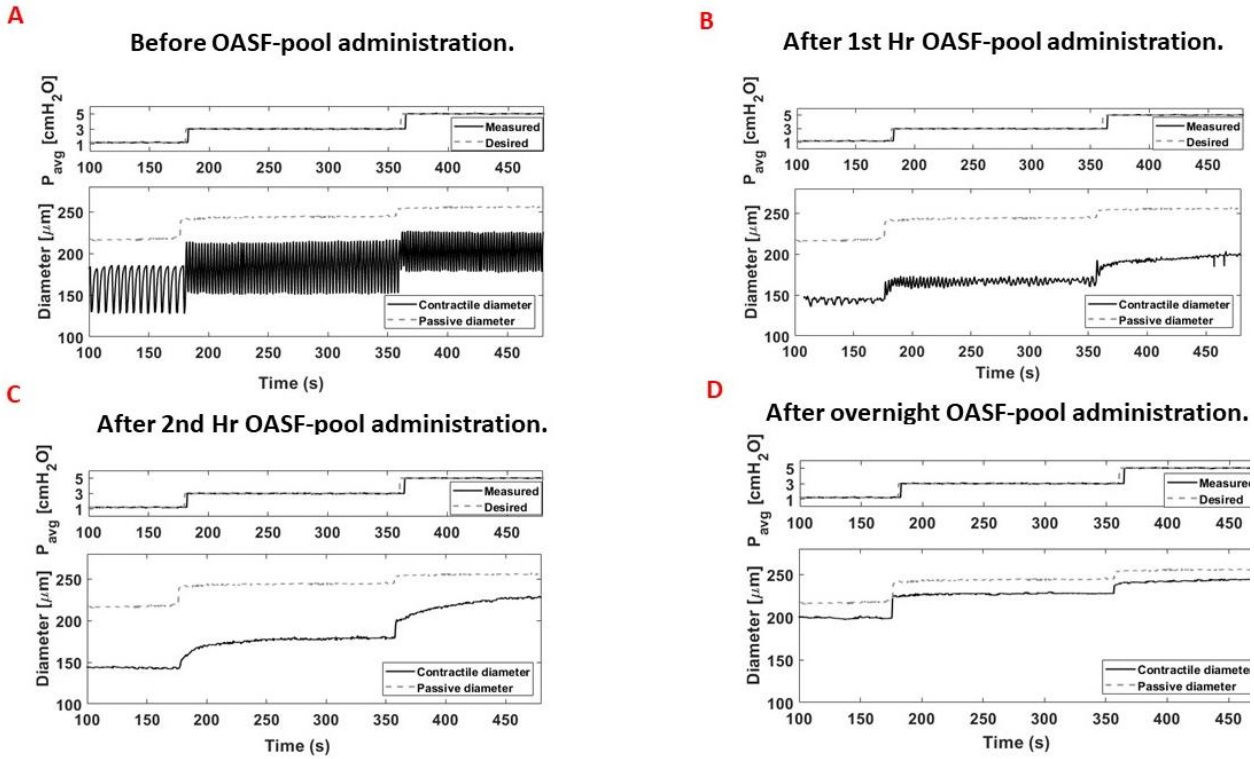

Figure 11: Effect of osteoarthritis synovial fluid on *ex vivo* lymphatic pump function. Rat femoral lymphatic vessels were isolated and placed into physiological saline chamber attached to pressure controls. Images of vessels were captured. Changes to vessel diameter were measured. The vessels were assessed before (A), 1 hr (B), 2 hr (C) and 24 hr (D) after treatment with synovial fluid (diluted 1:10 in physiological saline) collected from knee osteoarthritis patients.

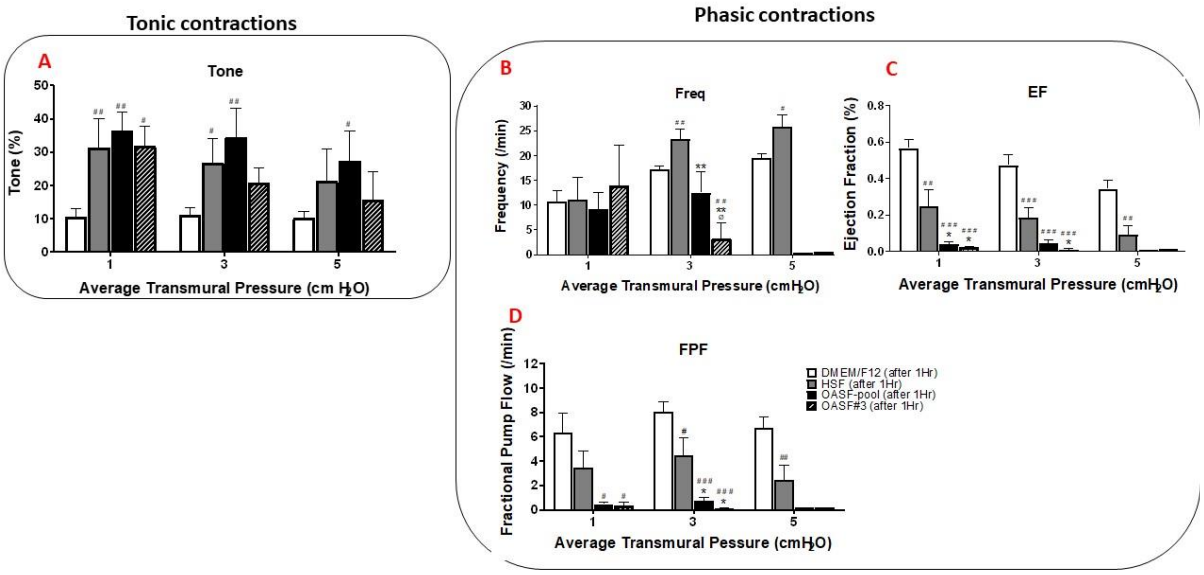

Figure 12: Effect of human synovial fluid on ex vivo lymphatic pump function after 1-hour treatment. Lymphatic vessel Tone (A), Frequency (B), Ejection Fraction (C), and Fractional Pump Flow (D) was average for untreated vessels (DMEM/F12), treated with healthy synovial fluid (HSF), osteoarthritis synovial fluid pooled from 6 patients (OASF pool) and osteoarthritis fluid from an individual patient (OASF#3). n = 3-7 per group.

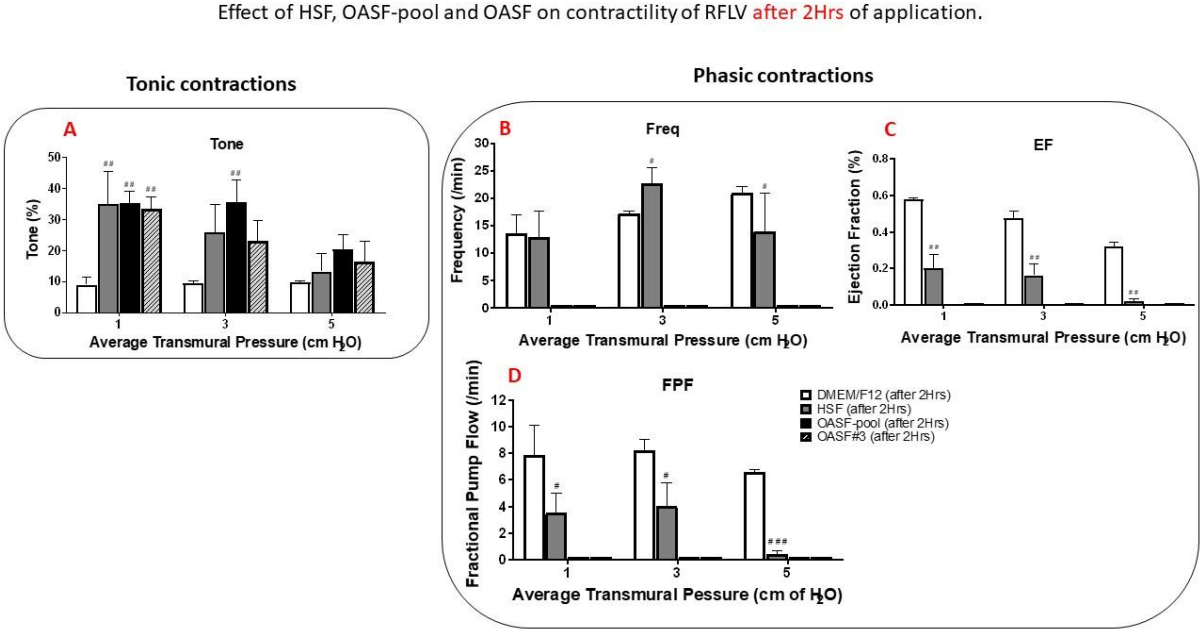

Figure 13: Effect of human synovial fluid on ex vivo lymphatic pump function after 2-hours treatment. Lymphatic vessel Tone (A), Frequency (B), Ejection Fraction (C), and Fractional Pump Flow (D) was average for untreated vessels (DMEM/F12), treated with healthy synovial fluid (HSF), osteoarthritis synovial fluid pooled from 6 patients (OASF pool) and osteoarthritis fluid from an individual patient (OASF#3). n = 3-7 per group.

(Figure 11). From these data, we calculated the effect of synovial fluid on lymphatic tone, frequency, ejection fraction and fractional pump flow during 1- and 2- hours treatment (Figures 12 and 13). Overall, synovial fluid from osteoarthritis patients (either a pooled sample of 6 patients or from an individual osteoarthritis donor) caused a significant increase in vessel tone and a significant reduction of intrinsic lymphatic pump function at 1 hour and an ablation of lymphatic pump function at 2 hours. These effects were not observed with synovial fluid from a healthy donor.

To determine the constituent(s) that were in the synovial fluid and that may contribute to changes of lymphatic function, inflammatory markers (Figure 14) and hyaluronan content (Figure 15) were measured. Using a commercially available multiplex array, we found that each osteoarthritis patient sample had varying increases of cytokines and inflammatory markers relative to the normal healthy donor synovial fluid sample. Interestingly, osteoarthritis sample #3 showed a moderate increase of most markers and was alone effective in reducing lymphatic contraction. Collectively, no one specific cytokine or inflammatory marker was consistently increased across the 6 osteoarthritis samples. Multivariate analysis will be conducted to determine if there is a group of markers that may explain the inhibition of lymphatic pump function.

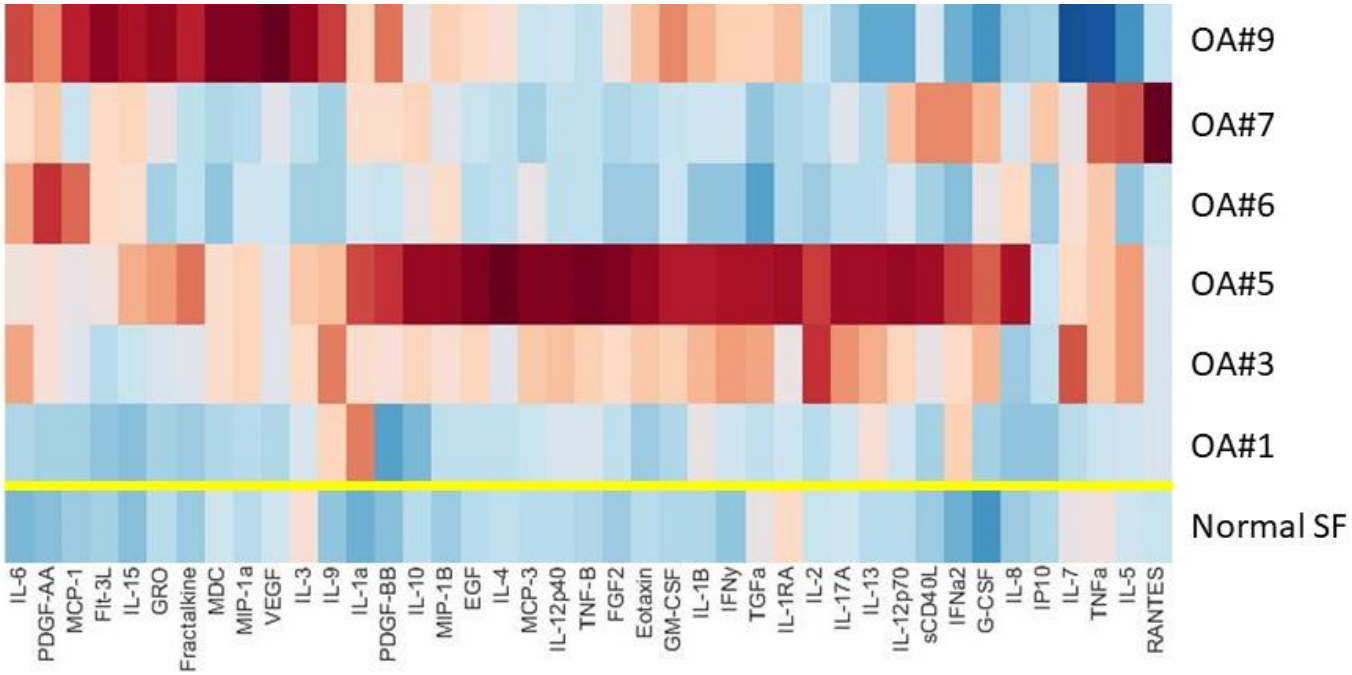

Figure 14: Multiplex Luminex analysis of inflammatory markers found in synovial fluid. Equi-volume of synovial fluid collected from healthy donor (Normal SF) and 6 knee osteoarthritis individuals (OA# 1, 3, 5, 6, 7 and 9) were loaded into Luminex multiplex platform to detect 40 inflammatory and cytokine markers. The image is a representative color map of the relative expression profile (dark blue is low and red is high expression). These synovial fluid samples were also used in the *ex vivo* lymphatic vessel studies.

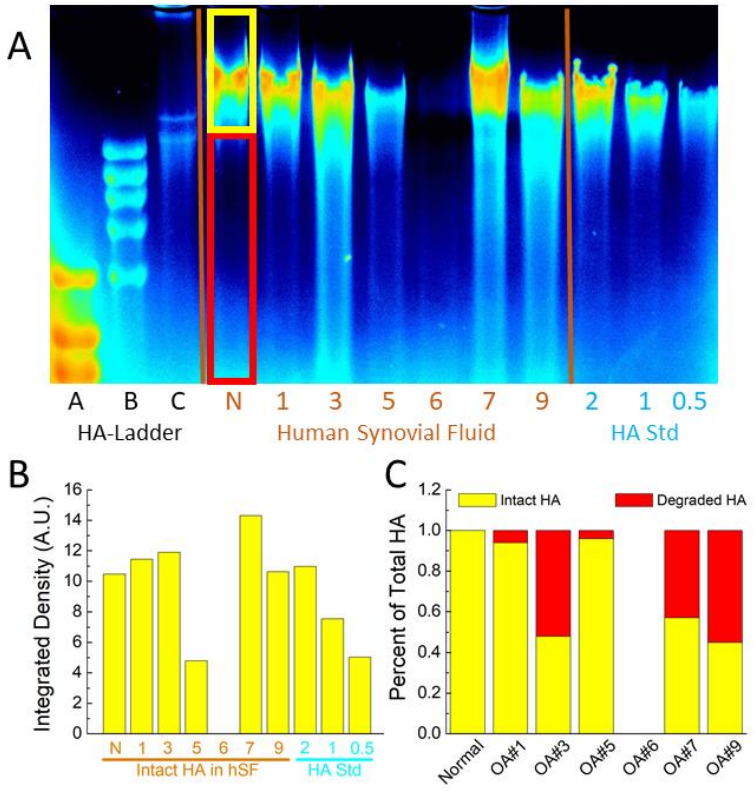

Figure 15: Hyaluronan (HA) content found in synovial fluid collected from healthy normal knee and from osteoarthritis knees.
A) Equi-volume of synovial fluid were electrophorized through 1% agarose gel and stained with Stains-all to detect hyaluronan. Lanes A, B and C were loaded with Low-, High- and Mega- HA ladders, respectively. Lane N was loading healthy, normal synovial fluid; Lanes 1, 3, 5, 6, 7, and 9 were loaded with synovial fluids from knee osteoarthritis donors #1, 3, 5, 6, 7 and 9, respectively. Purified 2.5MDa HA standards were loaded at differing amounts (2, 1 and 0.5 µg). Color intensity map where black/blue is low and red is high.
B) Measured integrated density of fixed area for each sample in the range of 1.5-6MDa range.
C) Relative integrated density of intact HA (range 1.5-6MDa) and degraded HA (range 300kDa – 1.5MDa).

As for hyaluronan (HA) content, synovial fluid samples were electrophoresed through 1% agarose gels and stained with Stains-All to detect hyaluronan. With this technique, the relative amount and integrity of hyaluronan can be assessed. For healthy synovial fluid, there was a distinct band that was ~3MDa in size for hyaluronan (yellow box in Figure 15). For synovial fluid collected from osteoarthritis patients, we found varying HA amounts in the samples (Figure 15B). Also, we found that HA were degraded in some of the samples and categorized the OA patients into 3 groups: 1) a group (e.g. #1 and #5) that was very similar to normal, 2) a group (e.g. #3, #7 and #9) that had intact and degraded HA, suggesting a catabolic environment of the joint, and 3) a sample (#6) that had little to no HA, suggesting a highly catabolic joint environment. We are conducting additional studies to determine if these results can be correlated to Kellgren-Lawrence scores (a clinical assessment based on morphological changes to the knee joint observed from x-ray.)

Major Task 4 – *Determine the effect of OA on lymphatic architect and clearance of PEG-liposome carriers.*
Subtask 1 - Determine the clearance kinetics and localization of NIR-labelled liposome carriers in MMT-induced OA animals at early, mid and late stage
Subtask 2 - Determine the clearance kinetics and localization of liposome carriers containing 40kDa PEG-NIR in MMT-induced OA animals at early, mid and late stage

The results from Major Task 3 suggested that osteoarthritis can impede lymphatic function. For Major Task 4, we focused our efforts 1) to altered lymphatic structure and morphology and 2) to retention and localization of drug carriers in the knee joint during osteoarthritis progression.

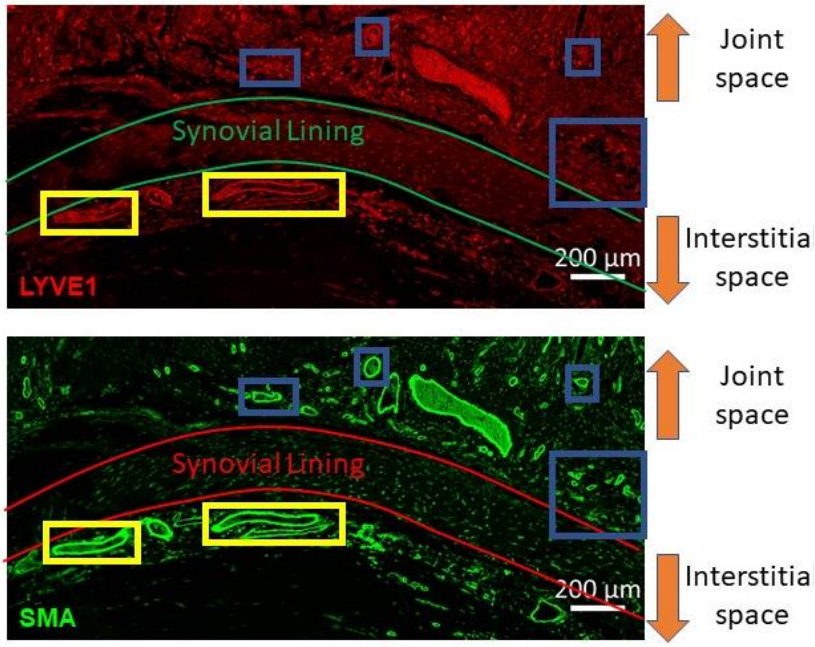

Figure 16: Representative fluorescent images of rat knee joint stained with lymphatic-specific hyaluronan receptor LYVE-1 (LYVE1) or vascular-specific smooth muscle actin (SMA). Naïve rat knee joints were fixed in 10% formalin, decalcified with Osteosoft, embedded in paraffin, sectioned into 5µm sagittal section and stained with antibodies recognizing LYVE-1 (red) or SMA (green). Blue boxed area highlights vessels labeled with SMA but not with LYVE-1, suggesting that these are blood vessels and not lymphatics. Yellow boxed area highlights vessels labeled with both SMA and LYVE-1, suggesting that these are lymphatic vessels.

To determine the impact of osteoarthritis on lymphatic structures, immunohistology studies were conducted to identify lymphatic vessels within the knee joints. Lymphatic vessel endothelial receptor 1 (LYVE-1) is specifically expressed by lymphatic endothelial cells (LECs), which line lymphatic vessels, and is not expressed by vascular endothelial cells, which line blood vessels, such as capillaries, arteries, and veins. Smooth muscle actin (SMA) is used to identify both lymphatic and blood vessels in a tissue sample. In the knee joint (Figure 16), we found lymphatic vessels primarily within the interstitial space, were relatively larger than blood vessels and were irregular spherical shape. Similar results were also found for antibodies recognizing VEGFR3 and podoplanin, which were lymphatic-specific markers in this tissue bed (data not shown). We have prepared slides from MMT-induced osteoarthritis at 3-weeks post-surgery and were delayed in staining due to months of remote work from COVID-19. These studies have resumed and will be included in FY3 report.

Since synovial fluid impeded lymphatic function (in Major Task 3), we assessed the effect of synovial fluid on lymphatic endothelial cell metabolism, migration, and propagation (Figure 17). No marked effect was found on cell morphology, metabolic activity, proliferation, or migration when LECs were treated with healthy normal synovial fluid or with synovial fluid collected from osteoarthritis patients. These findings suggested that synovial fluid-induced changes to lymphatic pump function was not attributed to gross damage of LECs. We are conducting additional experiments to determine if LECs can be apoptotic when treated with 10% synovial fluid.

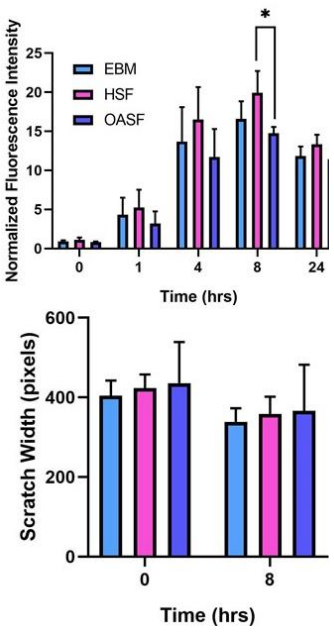

Figure 17: Effect of synovial fluid on lymphatic endothelial cells (LECs). LECs were cultured in endothelial basal media (EBM), 10% synovial fluid collected from healthy donor (HSF) or 10% synovial fluid collected for osteoarthritis patients (pooled samples). Top panel, LECs metabolic activity was measured using Alamar Blue assay for up to 24 hours. Bottom panel, scratch assay was used to determine if synovial fluid affected migration and proliferation of LECs.

For localization of drug delivery carriers, we have found that microgels can be targeted to the synovial lining after intra-articular injection into rat knees (Figure 18). Microgels, with or without HAP-1 peptides, were found within the synovial lining of rat knees. This provides evidence that microgel drug carrier can be retained within the joint capsule and possibly release drugs into the adjoining lymphatics and inflammatory cells during osteoarthritis progression. We have also found alginate microcapsules embedded within the infrapatellar fat pad of rat knee joints out to 9 days post-injection (McKinney *et al*. 2019, "Therapeutic efficacy of intra-articular delivery of encapsulated human mesenchymal stem cells on early stage osteoarthritis.") We are continuing this method of work for our liposome drug carrier studies.

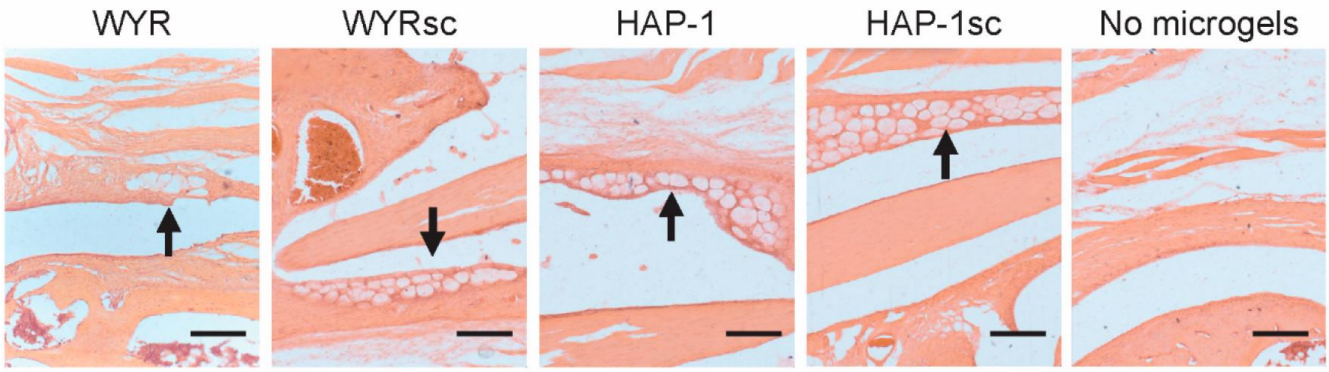

Figure 18: *In vivo* localization of peptide-functionalized PEG-4MAL nanocomposite microgels. Representative images of the synovial membrane 2 weeks after intra-articular administration of PEG-4MAL microgels. Black arrows denote the accumulation of peptide-functionalized microgels within the synovial membrane, which appear as circular white pockets (scale bar 200 μm). Adapted from Mancipe Castro *et al*., 2020, ACS Biomater Science Eng.

Major Task 5 – *Determine the Effects of Resolvins to treat OA.*
Subtask 1 – Fabrication and assessment of liposome carriers containing Resolvins D1 and E1
Subtask 2 – Determine the efficacy of Resolvins to treat early stage of OA

The goal of major task 5 is to promote the resolution of chronic inflammation as a treatment for OA. Though much of the direct resolving work in this aim has been delayed due to the pandemic, we have begun to investigate the effects of two treatments—exercise and human mesenchymal stem cells (hMSCs) — on OA development in terms of lymphatic function, resolution of chronic inflammation and ultimately protection of cartilage. As mentioned in Major Task 4, alginate microspheres can reside in the synovial layer of rat knees.

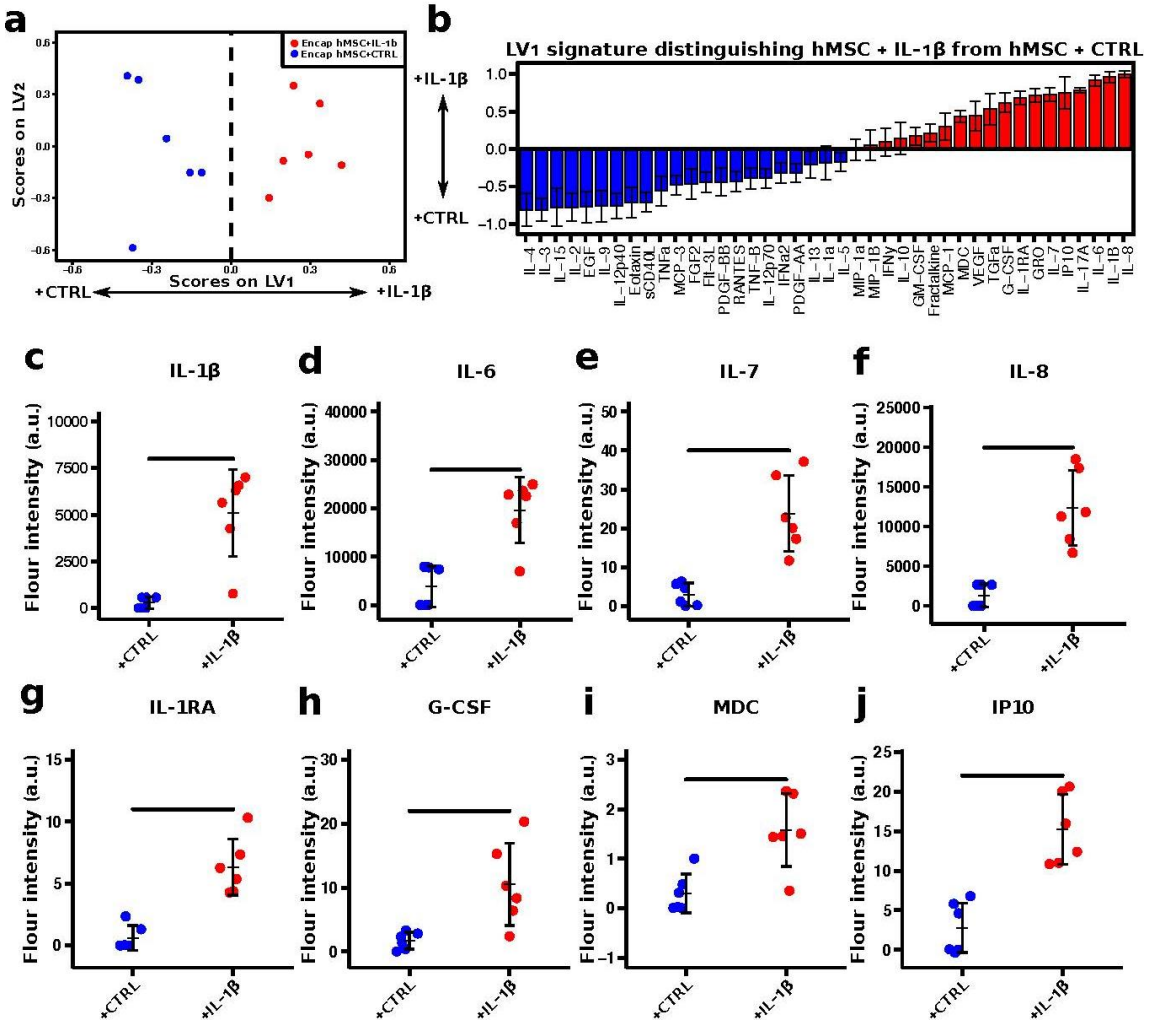

Figure 19: Secretomes from encapsulated hMSC in the presence of IL-1 stimulation, an interleukin elevated in synovial fluid of osteoarthritis patients. (a) PLSDA analysis on encapsulated hMSC identified a single latent variable, LV1, that distinguished between Encap hMSC + CTRL on the left and Encap hMSC + IL-1β to the right. (b) The weighted profiles of cytokines showed relative expression of cytokines in CTRL conditions (blue) and IL-1β conditions (red). Error bars on each cytokine were computed by PLSDA model regeneration using iterative (1000 iterations) leave one out cross validation (LOOCV). (c-j) All cytokines that showed increased expression with IL-1β stimulation were assessed independently, using t-test with Bonferroni correction, for significance between CTRL and IL-1β conditions, with all significant findings presented. Encap hMSCs + IL-1β yielded increased expression in pro-inflammatory (IL-1β, IL-6, IL-7, IL-8), anti-inflammatory (IL-1RA), and chemotactic (G-CSF, MDC, IP10) cytokines. Data presented as mean +/- SD. n = 6 for all groups. Horizontal black bars indicate significant differences between individual MMT groups.

We previously reported (McKinney *et al*. 2019, "Therapeutic efficacy of intra-articular delivery of encapsulated human mesenchymal stem cells on early stage osteoarthritis") that hMSCs may have a chondroprotective effect in the MMT rat model. MSCs have also been shown to be immunomodulatory and can promote the resolution of inflammation, much in a manner similar to resolving based lipid mediators (Barry & Murphy, 2013; Horie *et al*., 2012). To identify some of the putative secretomes from hMSCs in response to a simulated OA microenvironment, we analyzed cytokines secreted by encapsulated hMSCs *in vitro* (Figure 19). Our studies showed that encapsulated hMSCs secreted more IL-6, IL-7, IL-8, IL-1RA, G-CSF, MDC and IP10 when placed in an osteoarthritic environment. These factors have been shown to be involved in resolving chronic inflammation by directing an acute inflammatory response and could be key elements to induce chondroprotection *in vivo*. Additional studies in FY3 will determine if any or their combination can be used with

liposome drug carriers to treat osteoarthritis and the effects that they have on lymphatic function and its resolution of chronic inflammation in OA.

NSAID use after, but not before, hMSC injection reduces treatment efficacy

In this study, we investigated whether NSAID use impacts the efficacy of hMSC treatment in the rat knee osteoarthritis model. We hypothesized that NSAIDs will reduce the efficacy of hMSC therapy in treating post-traumatic osteoarthritis. The following groups were used 1) Sham, 2) MMT with no drug (PTOA group), 3) MMT with hMSC therapy and no drug (no NSAID group), 4) MMT with naproxen for 2 weeks prior to hMSC treatment (pre-NSAID group), 5) MMT with naproxen for 3 weeks after hMSC treatment (post-NSAID group) and 6) MMT with naproxen 2 weeks prior to and 3 weeks after hMSC treatment (full-NSAID group). Animals received hMSC treatment at 4 weeks post-surgery after mild OA has developed. The study ended at mid-stage osteoarthritis (7 weeks post-surgery).

NSAID use, regardless of timing, had little effect on the efficacy of hMSC therapy (Figure 20). Cartilage thickness ($p>0.67$), cartilage attenuation ($p>0.10$), cartilage surface roughness ($p>0.80$), and mineralized osteophyte volume ($p>0.57$) were all similar among hMSC treated groups, regardless of NSAID use. Pain significantly differed across groups ($p=0.05$). We tested for post hoc differences among groups using a t-test without correction for multiple comparisons. Here, we observed a significant drop in the withdrawal threshold with MMT surgery ($p=0.04$), which was recovered with injection of hMSCs (vs sham $p=0.81$; vs MMT $p=0.03$). While there was no effect of pre-NSAID use on the withdrawal threshold, the withdrawal threshold was lower in the post-NSAID and full NSAID groups.

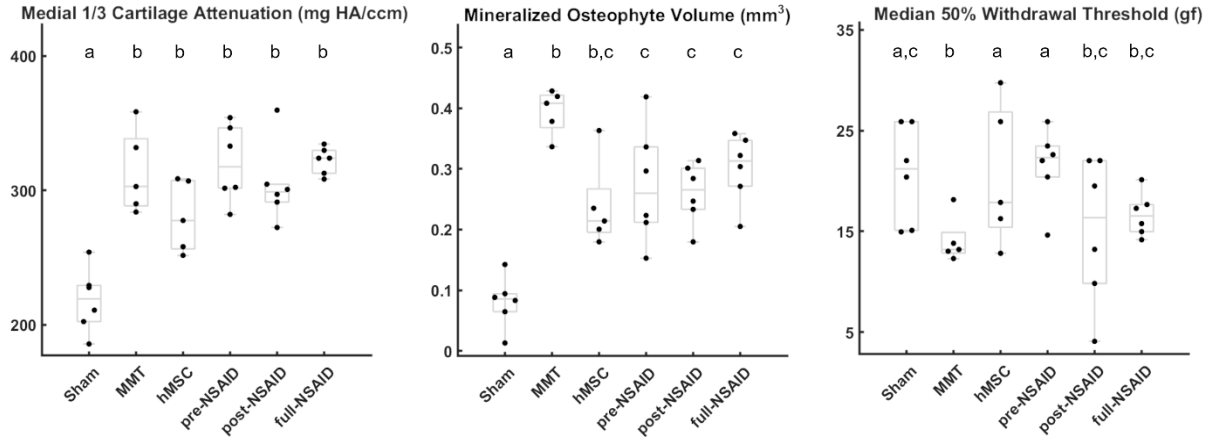

Figure 20: Morphological and pain outcomes. MMT surgery induced osteoarthritis, as evidenced by increases in cartilage attenuation, and mineralized osteophyte volume. Injected hMSCs alleviated signs of osteoarthritis, with a reduction in mineralized osteophyte volume. NSAIDs largely did not alter the therapeutic efficacy of hMSCs. Exploratory pain data suggests that MMT may reduce withdrawal threshold compared to sham animals, and hMSCs may return this threshold back to sham levels, with little interaction from NSAID use. Statistically similar groups are denoted by shared letters.

These data suggest that NSAID use prior to and following hMSC injection minimally alters the therapy's ability to slow joint degradation and reduce pain.

Exercise Treatment Promotes Intra-Articular Lymphatic Clearance and Attenuates PTOA

Exercise and rehabilitation are the gold standard treatment option for OA and the only treatments that have been shown clinically to modulate OA disease progression (Al-Khlaifat et al., 2016; Cagnin et al., 2019; Peeler & Ripat, 2018). Exercise also has been shown to promote lymphatic clearance and pumping function (in part through skeletal muscle contraction). In this study we sought to ask whether exercise could promote clearance of lymphatic targeting tracers (indicative of enhancing lymphatic function) and attenuate OA disease progression. Male Lewis rats received either Sham MMT surgery, with or without exercise (n=6/group). Exercised animals began treadmill walking (10 m/min) 21 d post-surgery, after early stage osteoarthritis has developed, and exercised 5 d/wk for up to 30 mins. Gait was measured at 3- and 6-weeks post-surgery. Cartilage and osteophyte morphology and cartilage

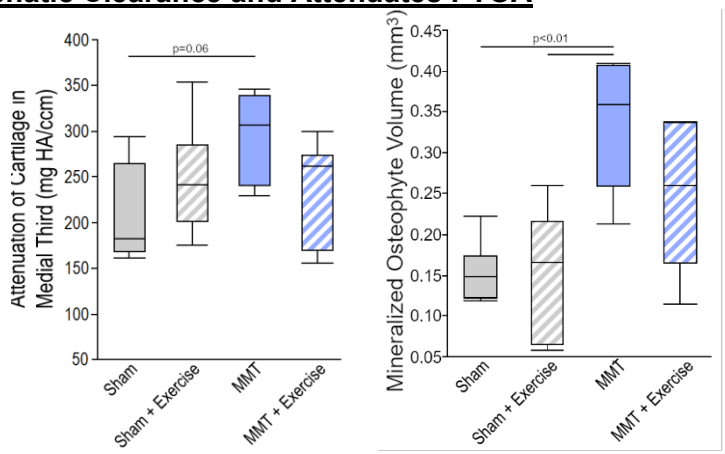

Figure 21: MMT-induced osteoarthritis increased cartilage attenuation and osteophyte volume, which were attenuated with exercise.

attenuation in the medial tibia were quantified using EPIC-μCT. There were no morphological differences due to exercise in the Sham animals (Figure 21). Exercise successfully attenuated signs of post-traumatic osteoarthritis in MMT animals. While MMT animals showed signs of increased cartilage attenuation (p=0.06) and mineralized osteophyte volume (p<0.01), these differences were not observed in the exercised MMT animals. Exercise also increased step frequency, decreased step length, and increased duty factor in all animals, regardless of surgery, suggesting a functional modification in these animals (Figure 22), that may be associated with observed morphological differences in the exercised MMT animals.

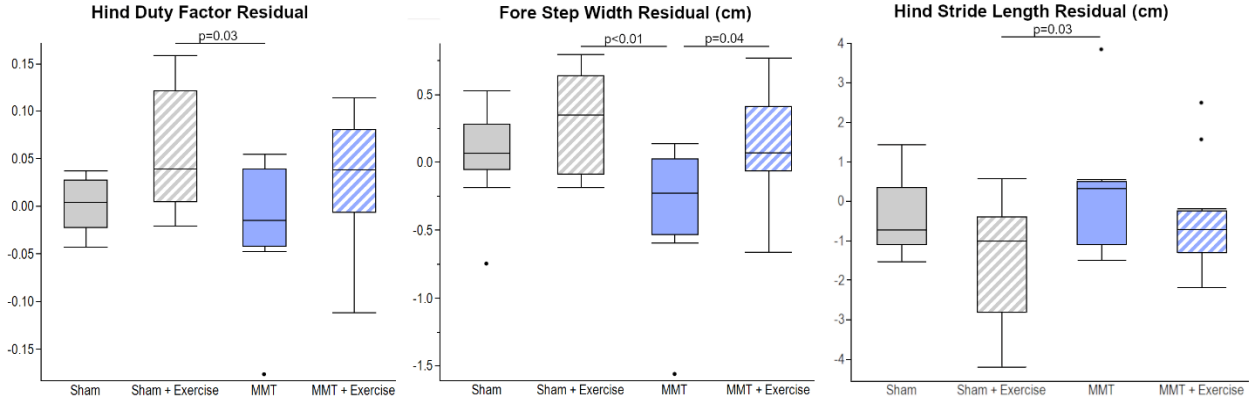

Figure 22: Exercise increased hind limb duty factor, fore step width, and hind stride length, regardless of surgery.

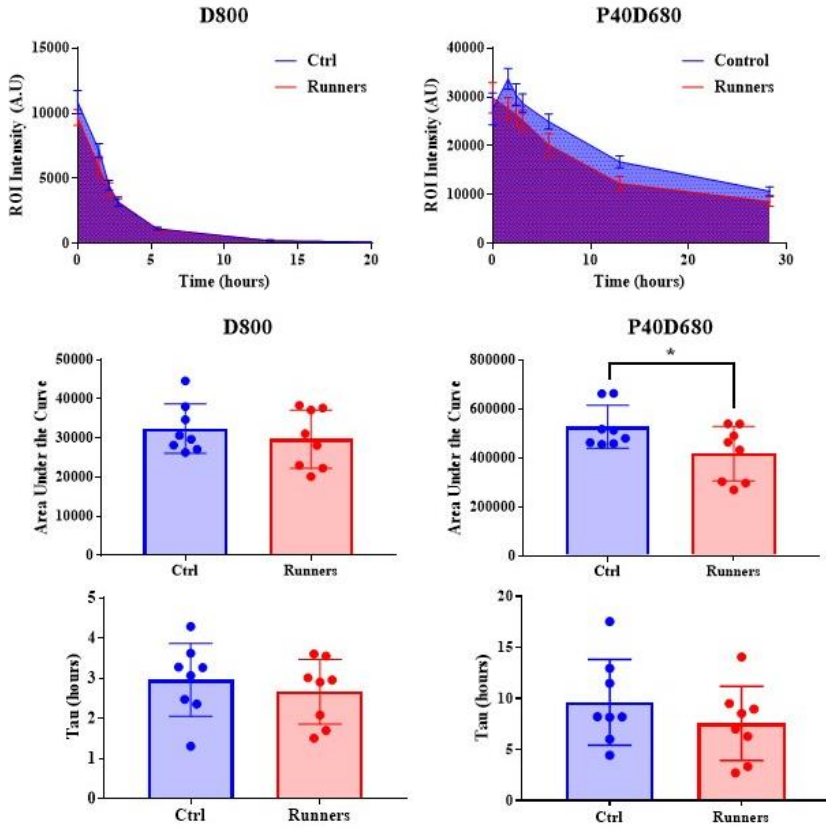

Figure 23: Exercise increases lymphatic clearance from knee joints. Rats were left to move freely after intra-articular injection (control) or were placed on an exercise regimen of 10m/min for 30 min after intra-articular injection (Runners). Free NIR dye (D800) and 40kDa PEG-NIR (P40D680) were co-injected in rat knees.

We also have preliminary evidence that exercise may increase knee clearance of lymphatic-specific particles (Figure 23). 40kDa PEG-NIR (a particle trafficked to lymphatics) clearance was faster (lower calculated Tau and decreased area under the curve) when rats were exercised for 30 min at a pace of 10m/min. We did not find a significant difference for the free dye; however, this may be due to low sampling acquisition. We will expand these studies by increasing the exercise frequency to match the study above. These data suggest that exercise can increase the lymphatic clearance of the knee joint, potentially playing a role in resolving chronic inflammation, clearing MMPs and fragmented aggrecan, and ultimately restoring the knee joint homeostasis.

What opportunities for training and professional development has the project provided?
These accomplishments were performed by our team of investigators at both sites, Emory University and Georgia Institute of Technology (GA Tech). The team of 12 scientists met monthly to present and discuss the ongoing data and the progress of the Department of Defense research project. This provided opportunity for graduate students, post-doctorates, and investigators to exchange ideas and assisted with any problems across institutions. Within each institution, graduate students and post-doctorates met weekly with their respective principal investigators to review studies and to plan for the week.
Hands-on technical training was provided to all graduate students at each site. Dr. Kaiser trained personnel at Emory and Dr. Nepiyushchikh trained students at GA Tech. Dr. Doan facilitated training at both Emory and GA Tech sites.
In addition to laboratory training, scientists received professional career development by attending and presenting at national science conferences and symposium.

How were the results disseminated to communities of interest?
In addition to presenting at regional and national conferences (see presentation list below), we have published our findings in peer-reviewed journals (see Appendices).

What do you plan to do during the next reporting period to accomplish the goals?
As we enter year 3 of our project, we will focus our efforts on therapeutics for osteoarthritis (Specific Aim 3). To this end, we have already conducted preliminary studies with hyaluronan, exercise and mesenchymal stem cells as various forms of therapies. In addition, we will incorporate resolvin into drug carriers and determine the ability of resolvin to potentiate the development of osteoarthritis. The completion of our goals in FY3 will validate existing therapeutics (such as hyaluronan and exercise) using our NIR technology and will provide new therapies (such as exosomes of mesenchymal stem cells and resolvin contained in liposome carriers) to treating the debilitating disease osteoarthritis.

4. IMPACT:

What was the impact on the development of the principal discipline(s) of the project?
We have developed multiple different novel biomaterial-based carriers for intra-articular drug delivery and shown that we can enhance retention in the joint. These technologies are now being tested with specific drugs including resolvins. The use of NIR imaging to assess knee clearance in animal model is a unique technique and provides an unmet technology to address the impact of size- and charge-based particle trafficking from diseased joints and overall joint homeostasis. This technique allows us to track drug delivery, drug retention and its release from the joint. This is critical to determine the efficacy of intra-articular injection of drugs and therapeutics to treat osteoarthritis. Because osteoarthritis is a chronic disease, the retention of drugs, and their potential to target downstream lymph nodes specific to the diseased joint within the affected joint is imperative. Additionally, we show the potential of exercise and MSC treatment to promote lymphatic function, resolve chronic inflammation and attenuate OA progression.

What was the impact on other disciplines?
In addition to osteoarthritis, the use of NIR imaging to increase our understanding of factors involved in clearance can be applied to other joint diseases, including rheumatoid arthritis and synovitis. These joint diseases may result from an impairment of lymphatic function and thus clearance measurements may shed light to their deficits. The biomaterial carriers developed could also be used for other chronic inflammatory diseases where lymphatic function may be a therapeutic target.

What was the impact on technology transfer?
Nothing to report.

What was the impact on society beyond science and technology?
Nothing to report.

5. CHANGES/PROBLEMS:

Changes in approach and reasons for change.
During FY2, we experienced laboratory shutdown due to the COVID-19 pandemic which changed our timeline for the proposed work (detailed in the below paragraph). This has delayed our progress on Major Tasks 2 and 4. However, we continued to make progress towards our goals from the original proposal, have expanded some of the approaches by developing additional biomaterials (e.g. hyaluronan and PEG microgels) to

complement our proposed drug carrier liposomes, and have expanded the treatments (such as exercise and MSCs) for the resolution of inflammation. These additions will improve our chance to deliver therapeutics for osteoarthritis (in specific aim 3), which will be fully addressed in FY3.

Actual or anticipated problems or delays and actions or plans to resolve them.
Some of our progress (specifically completion of Major Tasks 2 and 4) were delayed due to the COVID-19 pandemic. Laboratories and campuses were closed at both Emory and GA Tech in March 2020 and slowly began reopening in June of 2020. During this period, we worked remotely and shifted our efforts toward manuscript writing, discussion of DoD-related research articles, and data analysis. We used Zoom or Bluejeans for weekly virtual meetings. Since June 2020, the institutions have begun to allow researchers back in laboratories in a slow and phased manner with reduced capacities. We have re-initiated our efforts for the DoD project. We have modified our work schedule and operations to be compliant with institutional directives regarding safety during COVID-19. To date, we do not foresee any procedural modification that would impede the execution of the DoD project.

Changes that had a significant impact on expenditures.
No changes were made.

Significant changes in use or care of human subjects, vertebrate animals, biohazards, and/or select agents.

Significant changes in use or care of human subjects.
No human subjects were used in our project.

Significant changes in use or care of vertebrate animals.
No significant changes were introduced with regards to use of animals.

Significant changes in use of biohazards and/or select agents.
No significant changes were introduced with regards to biohazards and/or select agents.

6. PRODUCTS:

Publications, conference papers, and presentations.
Journal publications.
1) Mancipe Castro LM, Garcia AJ, Guldberg RE. Biomaterial strategies for improved intra-articular drug delivery. Journal of Biomedical Materials Research 2020: 1-11. Published and federal support was acknowledged.

2) Mancipe Castro LM, Sequeira A, Garcia AJ, Guldberg RE. Articular cartilage- and synoviocyte-binding poly(ethylene glycol) nanocomposite microgels as intra-articular drug delivery vehicles for the treatment of osteoarthritis. ACS Biomaterials Science & Engineering August 2020. Published and federal support was acknowledged.

3) McKinney JM, Pucha KA, Doan TN, Wang L, Weinstock LD, Tignor BT, Fowle KL, Levit RD, Wood LB, Willett NJ. Biomaterial encapsulation of human mesenchymal stromal cells modulates paracrine signaling response and enhances efficacy for treatment of established osteoarthritis. Biomaterial Science. Under peer-review.

Books or other non-periodical, one-time publications.
None.

Other publications, conference papers, and presentations.
Presentations that acknowledged Department of Defense funding
1) Kaiser J, McKinney JM, Raval S, Pucha K, Sok D, Fuller J, Willett N. “Implementation of Physical Therapy Improves the Therapeutic Efficacy of a Cellular Therapy in a Preclinical Model of Post-Traumatic Osteoarthritis.” 8th Annual International Symposium on Regenerative Rehabilitation. October 2019. (Conference Presentation).

2) Doan TN, Bernard, FC, Shaver JC, McKinney JM, Dixon, JB, Willett NJ. “In Vivo Clearance of Hyaluronan from the Rat Knee.” Orthopaedic Research Society Conference. February 2020. (Poster).

3) Kaiser J, Bernard F, Raval S, Dixon B, Willett N. “Mild Exercise Expedites Restoration of Synovial Fluid Homeostasis Through Increased Lymphatic Clearance.” Orthopaedic Research Society Conference. February 2020. (Poster).

4) Kaiser J, McKinney JM, Raval S, Pucha K, Sok D, Fuller J, Willett N. “Physical Therapy Improves Efficacy of Cellular Therapy on Joint Function, Cartilage Morphology, and Pain Symptoms in a Rodent Model of Post-Traumatic Osteoarthritis.” Orthopaedic Research Society Conference. February 2020. (Poster).

5) McKinney JM, Doan TN, Pucha KA, Wang L, Weinstock LD, Wood LB, Levit RD, Willett NJ. Therapeutic efficacy of encapsulated human mesenchymal stem cells in osteoarthritis. Orthopaedic Research Society (ORS) Annual Meeting. Phoenix, AZ, February 2020. (Poster).

6) Sok D, Kaiser J, Raval S, Willett NJ. “NSAIDs May Reduce Efficacy of Mesenchymal Stem Cell Therapy in a Rodent Model of Post-Traumatic Osteoarthritis.” Orthopaedic Research Society Conference. February 2020. (Poster).

7) Doan TN, Bernard, FC, Shaver JC, McKinney JM, Dixon, JB, Willett NJ. “In Vivo Clearance of Hyaluronan from the Rat Knee.” Musculoskeletal Research Symposium. Emory University, Atlanta, GA. April 2020. (Abstract submitted, Meeting was canceled due to COVID-19).

8) Bernard FC, Kaiser JM, Doan TN, Nepiyushchikh ZV, Raval SK, McKinney JM, Dixon JB, Willett NJ. “Integrated Bioengineering Techniques Investigating the Relationships Between Lymphatic Function and Osteoarthritis Progression.” 2020 Military Health System Research Symposium HSRS. July 2020. (Online Abstract).

9) Kaiser J, Raval S, Bernard F, McKinney J, Pucha K, Sok D, Dixon B, Willet J. “Exercise may Mediate Post-Traumatic Osteoarthritis Through Restoration of Joint Homeostasis.” American Society of Biomechanics. August 2020. (Poster).

Website(s) or other Internet site(s)
None.

Technologies or techniques
None to report.

Inventions, patent applications, and/or licenses
None to report.

Other Products
None.

7. PARTICIPANTS & OTHER COLLABORATING ORGANIZATIONS:

What individuals have worked on the project?

Participants at Emory University
1) Nick Willett (no change)
2) Thanh Doan (no change)
3) Jarred Kaiser (no change)
4) Jay McKinney (no change)

Participants at Georgia Institute of Technology
1) Brandon Dixon (no change)
2) Andres Garcia (no change)

3) Zhanna Nepiyushchikh (no change)
4) Fabrice Bernard (no change)
5) Lauren Liebman (no change)
6) Eleftheria (Ria) Michalaki
Project Role: Postdoctoral Fellow
Research ID: 0000-0003-3429-560
Month Worked: 9 months
Contribution to Project: Dr. Michalaki trained and assisted undergraduate students at GA Tech. She is involved with *ex vivo* lymphatic vessel studies and leads the *in vitro* lymphatic studies.
Funding Support: N/A
7) Lina Mancipe Castro

Has there been a change in the active other support of the PD/PI(s) or senior/key personnel since the last reporting period?
Nothing to report.

What other organizations were involved as partners?
No other organization was involved.

8. SPECIAL REPORTING REQUIREMENTS:

COLLABORATIVE AWARDS: Dr. Nick Willett leads the group at the Emory site and Dr. Brandon Dixon leads the group at the GA Tech site. Dr. Andres Garcia is a collaborating investigator at the GA Tech site. Their groups' efforts are specified in the SOW. Dr. Willett and Dr. Doan both have office spaces at Emory and GA Tech and they visit both sites weekly.

9. APPENDICES:

1) Mancipe Castro LM, Garcia AJ, Guldberg RE. Biomaterial strategies for improved intra-articular drug delivery. Journal of Biomedical Materials Research 2020: 1-11. Published and federal support was acknowledged.

2) Mancipe Castro LM, Sequeira A, Garcia AJ, Guldberg RE. Articular cartilage- and synoviocyte-binding poly(ethylene glycol) nanocomposite microgels as intra-articular drug delivery vehicles for the treatment of osteoarthritis. ACS Biomaterials Science & Engineering August 2020. Published and federal support was acknowledged.

3) McKinney JM, Pucha KA, Doan TN, Wang L, Weinstock LD, Tignor BT, Fowle KL, Levit RD, Wood LB, Willett NJ. Biomaterial encapsulation of human mesenchymal stromal cells modulates paracrine signaling response and enhances efficacy for treatment of established osteoarthritis. Biomaterial Science. Under peer-review.

Received: 23 May 2020 | Revised: 19 July 2020 | Accepted: 26 July 2020

DOI: 10.1002/jbm.a.37074

Society For Biomaterials

WILEY

REVIEW ARTICLE

Biomaterial strategies for improved intra-articular drug delivery

Lina M. Mancipe Castro[1,2] | Andrés J. García[1,2] | Robert E. Guldberg[3]

[1]Parker H. Petit Institute for Bioengineering and Biosciences, Georgia Institute of Technology, Atlanta, Georgia

[2]George W. Woodruff School of Mechanical Engineering, Georgia Institute of Technology, Atlanta, Georgia

[3]Phil and Penny Knight Campus for Accelerating Scientific Impact, 6231 University of Oregon, Eugene, Oregon

Correspondence
Andrés J. García, Parker H. Petit Institute for Bioengineering and Biosciences, Georgia Institute of Technology, 315 Ferst Dr NW, Atlanta, GA 30332.
Email: andres.garcia@me.gatech.edu

Robert E. Guldberg, Phil and Penny Knight Campus for Accelerating Scientific Impact, 6231 University of Oregon, Eugene, OR 97403.
Email: guldberg@uoregon.edu

Funding information
National Institute of Arthritis and Musculoskeletal and Skin Diseases, Grant/Award Numbers: R01AR062920, S10OD016264; U.S. Department of Defense, Grant/Award Number: PR171379

Abstract

Osteoarthritis (OA) is a joint degenerative disease that has become one of the leading causes of disability in the world. It is estimated that OA affects 50 million adults in the United States. Currently, there are no FDA-approved treatments that slow OA progression and its treatment is limited to pain management strategies and life style changes. Despite the discovery of several disease-modifying OA drugs (DMOADs) and promising results in preclinical studies, their clinical translation has been significantly limited because of poor intra-articular (IA) bioavailability and challenges in delivering these compounds to tissues of interest within the joint. Here, we review current OA treatments and their effectiveness at reducing joint pain, as well as novel targets for OA treatment and the challenges related to their clinical translation. Moreover, we discuss intra-articular (IA) drug delivery as a promising route of administration, describe its inherent challenges, and review recent advances in biomaterial-based IA drug delivery for OA treatment. Finally, we highlight the potential of tissue targeting in the development of effective IA drug delivery systems.

KEYWORDS

drug delivery, intra-articular, osteoarthritis, tissue-targeting

1 | INTRODUCTION

Osteoarthritis (OA) is a joint degenerative disease characterized by cartilage loss, which leads to joint pain, swelling and stiffness. OA affected 303 million people in the world in 2017[1] and it was estimated that 30.8 million adults in the United States suffered from OA in 2011.[2] OA prevalence in the United States has increased over the last years[3] and it is estimated to affect around 50 million people in 2020.[4] In 2008, around 14 million people over 25 years old were affected by knee OA alone and around 50% of those cases required a total knee replacement.[5] Annual medical care expenses associated with OA are approximately $185.5 billion dollars annually in the United States.[6] In a country with rapidly aging population and high incidence of obesity, the prevalence of OA is expected to increase.[7] A study conducted in Sweden estimated that 25% of adults over 45 years were diagnosed with OA in at least one joint, excluding the spine in 2014.[3] Additionally, countries like England have estimated the prevalence of knee OA alone to be as high as 19% in adults over 40 years.[8]

Despite the increasing prevalence of OA, no FDA-approved disease modifying OA drugs (DMOADs) exist[9] and its treatment is limited to pain management strategies and life style changes. Depending on the severity of the disease, OA patients require interventions ranging from weight management, physical therapy,[10] dietary supplements[11] and systemic administration of anti-inflammatory and analgesic drugs,[12,13] and in more severe cases, intra-articular (IA) injections of hyaluronic acid (HA)[14] and total joint replacement.[5] However, these treatment strategies present limited long-term benefits and do not prevent or slow OA progression.[10,15,16]

A variety of promising DMOAD candidates have been investigated.[17,18] However, achieving appropriate IA bioavailability after systemic administration remains a major challenge.[9] Intra-articular injection offers an attractive route of drug administration for OA treatment.[9] Nevertheless, free drugs injected in the IA space are

rapidly cleared, resulting in poor retention and insufficient drug concentrations in the tissues of interest.[19] This challenges evidence the need for biomaterial-based drug delivery vehicles able to improve the drug bioavailability into the relevant tissues.[9]

In the following sections, we discuss current understanding of OA pathophysiology as well as the effectiveness of current treatment strategies. Furthermore, a section summarizing novel OA targets and promising DMOAD candidates is presented. We also describe the advantages and unmet challenges of IA drug delivery and present recent advances on IA drug delivery systems.

2 | OA PATHOPHYSIOLOGY

According to its cause, osteoarthritis can be classified in idiopathic and secondary OA. The former has its origin on nontraumatic conditions, where factors such as age and gender have been identified to play a role.[20] It is estimated that by 2030, adults older than 65 years will account for around 50% of the total OA cases in the United States.[21] Additionally, the prevalence of OA in men over 60 years is 10%, whereas it is 13% in women, who additionally experience more severe symptoms.[7]

Secondary OA can develop as a result of metabolic disorders, traumatic events or mechanical misalignment.[10] In these cases, the etiology of OA is not fully understood, but it has been recently recognized that it is a multifactorial disease. Joint injury, abnormal joint development, metabolic disorders, obesity, age, biochemical reactions and inflammation have all been reported as possible OA causes.[10,20] Some research groups have suggested that these factors could elicit changes in joint biology, mechanics and structure leading to impaired joint remodeling and the associated progressive degenerative changes characteristic of OA.[22]

OA affects the joint as a whole and induces articular cartilage degeneration, subchondral bone remodeling and osteophyte formation, ligament laxity, weakening of peri-articular muscles and joint swelling[10] (Figure 1). The exact mechanisms involved in OA progression and the interplay between articular tissues remain under investigation.[23] However, recent research has identified biological mechanisms and measured biomarker levels that have been used to partly recreate OA progression.[9]

As OA advances, the articular cartilage experiences a continuous degeneration process characterized by partial surface lamina loss, chondrocyte hypertrophy and the appearance of cartilage fibrillations, calcified erosions and lesions.[9] These morphological damages are accompanied by cartilage matrix compositional changes such as proteoglycan depletion and collagen Type II cleavage.[23] Furthermore, the activation of the nuclear factor NF-κB in hypertrophic chondrocytes, synovium macrophages and fibroblasts leads to the up-regulation of catabolic proteins including matrix metalloproteinases (MMPs), aggrecanases, cathepsins and A disintegrin and metalloproteinase with thrombospondin motifs (ADAMTS).[4,9,23] Moreover, the expression of transforming growth factor beta (TGF-β) and vascular endothelial growth factor (VEGF) in chondrocytes, promotes blood vessel penetration into the hypertrophic cartilage and calcification.[23] This unbalanced bone remodeling induces subchondral bone sclerosis, cysts and osteophyte formation, which result in severe pain.[4,23] Furthermore, the synovial membrane is affected by the infiltration of T lymphocytes, neutrophils and macrophages,[23] which secrete pro-inflammatory mediators, cytokines and chemokines such as IL-1, IL-6, IL-15, TNF-α, nitric oxide and prostaglandins, which further exacerbate joint inflammation and cartilage degeneration.[25] Additionally, synoviocyte secretion of synovial fluid components is impaired, leading to poor viscous lubrication and shock absorption capacity.[9] In healthy patients, the hyaluronic acid concentration in the synovial fluid ranges from 2.5 to 4 mg/ml and has a molecular weight between 6,300 and 7,600 kDa; however, as a result of OA progression, its concentration and molecular weight decrease up to 1–2 mg/ml and 1,600–3,480 kDa, respectively.[26]

Despite advances on elucidating the mechanisms involved in OA progression, there is still much investigation needed to fully

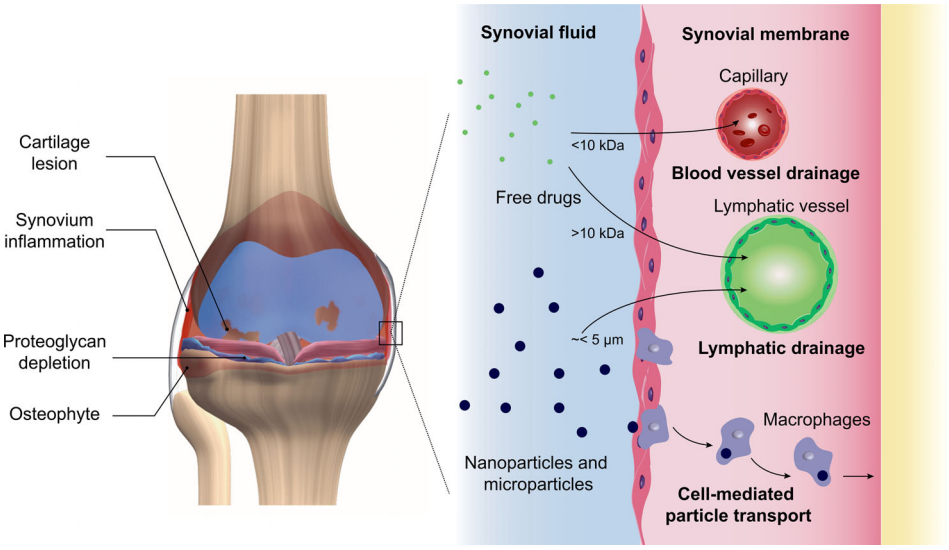

FIGURE 1 Schematic representation of an osteoarthritic knee presenting signs of cartilage degradation, bone remodeling and synovial membrane inflammation. Clearance mechanisms for free drugs and particulate drug delivery systems after IA injection. Molecules smaller than 10 kDa are eliminated from the joint space via blood vessels whereas larger molecules and particles in the nano-scale and up to few micros are eliminated via lymphatic drainage.[9] Synovial macrophages also play an important role at eliminating particulate drug delivery systems via phagocytosis[24]

comprehend OA pathophysiology. The lack of understanding of the underlying mechanisms of OA onset and development, in addition to difficulties in clinical trial design, as well as the need for more sensitive techniques to better detect changes related to OA progression,[27] are all limitations that have hindered the development of appropriate disease-modifying OA drugs (DMOADs).[4,9,23]

3 | CURRENT CLINICAL TREATMENTS FOR OSTEOARTHRITIS

3.1 | Nonpharmacological management

Nonpharmacological approaches constitute the first line of treatment at early stages of OA progression and intend to reduce pain and improve joint functionality. The absence of mechanic loading increases cartilage degeneration,[28] whereas excessive mechanic stimuli are also deleterious for joint health.[10] Therefore, physical therapy are key components of nonpharmacological OA treatment. Exercises types recommended for OA patients at this stage include proprioception, stretching and resistance.[10] In the case of overweighed patients, not only physical therapy is recommended, but an initial 10% weight loss is necessary in order to significantly reduce joint pain.[29] Even though weight loss has been associated with a significant reduction in the risk of developing symptomatic knee OA in female patients with a body mass index (BMI) greater than 25 kg m^{-2}, no effect of weight loss on OA was observed in women with BMI < 25 kg m^{-2}.[29] These results suggest that weight management strategies may only be effective in overweighed populations. However, given the progressive character of this disease, and the inability of many obese patients to maintain a significant weight loss over time,[29] patients often require pharmacological treatment.

An alternative to alleviate the pain is the use of dietary supplements, which account for US$25 billion annual sales.[11] Approximately 70% of OA patients take oral supplements for pain management, with glucosamine and chondroitin sulfate being the most consumed compounds, accounting for a third of the oral supplements market value (US$872 million annual sales).[11] Despite the high sales volume, oral supplements have failed to induce clinically significant improvements in pain management in OA patients. Liu et al. in a meta-analysis study reviewed 69 randomized placebo-controlled clinical trials that evaluated the effects of 20 individual oral supplements for the treatment of hand, hip or knee OA. The results demonstrated that no supplements exhibited a clinically important effect on pain or physical function in the long term (>6 months). Between 4 and 6 months, only undenatured Type II collagen and green-lipped mussel extract, a supplement rich in anti-inflammatory compounds such as omega-3, eicosapentaenoic acid and docosahexaenoic acid (DHA)],[30] showed a significant clinical effect on pain reduction.[11] Even though glucosamine and chondroitin sulfate are the most consumed dietary supplements among the OA population, according to Liu et al., these compounds only statistically improved pain scores at short term (<3 months), but their clinical effect is debatable.[11] Additionally, clinical trials and meta-analysis studies have shown that the use of glucosamine and chondroitin sulfate in combination does not induce a relevant reduction in pain compared to placebo in most OA patients.[31-33] Although glucosamine can be detected in the synovial fluid after oral administration,[34] insufficient IA concentrations could be related to the poor outcomes seen in clinical trials. In fact, 90% of orally administered glucosamine is absorbed, but its concentration in plasma is significantly reduced due to the first-pass effect, leading to a bioavailability of 26%–44%.[34] On the other hand, oral delivery of chondroitin sulfate is challenging due to its high molecular weight (10–50 kDa).[34] Around 90% of orally administered chondroitin sulfate is absorbed as low molecular weight derivatives[35] and exhibits a plasma bioavailability of 5%–15%.[34] These challenges in the oral delivery of glucosamine and chondroitin sulfate may explain why these compounds have not induced a clinically relevant reduction of OA symptoms in several clinical trials.

3.2 | Pharmacological management

Currently there are no approved DMOADs that reduce OA progression, thus treatment is limited to pain management and the regimen depends on the severity of the disease. Commonly used medications include cyclooxygenase inhibitors such as acetaminophen, systemic administration of opioids and nonsteroidal anti-inflammatory drugs (NSAIDs). However, their prolonged use is limited due to their secondary effects on the hepatic, gastrointestinal, renal and cardiac systems, especially in the elderly population that often presents a wide range of comorbidities.[9,10,36-38] Moreover, recent clinical studies have shown that acetaminophen is inferior to NSAIDs and not-superior than placebo for pain management in moderate and severe OA patients.[28] The use of topical NSAIDs is a safer alternative, but their use has only been shown to be effective during the first 2 weeks of use.[39] In the case of opioids, increasing awareness regarding their chronic use has limited their administration for long-term pain management. Also, studies have shown that opioids do not improve pain scores in OA patients compared to NSAIDs.[40,41]

In order to minimize adverse side effects associated with systemic administration of therapeutics and to improve drug's bioavailability in the joint space, intra-articular (IA) injections raise an alternative that offers a more localized treatment. IA injection of corticoids has been shown to reduce pain scores and increase joint functionality due to their anti-inflammatory and immunosuppressive effects. Corticoids reduce pain and inflammation by decreasing IL-1 production, prostaglandins, leukotrienes and metalloproteinases.[10,42,43] Several corticoids that have been FDA-approved for IA delivery as immediate release formulations include dexamethasone, beta-methasone, methylprednisolone, triamcinolone acetate and triamcinolone hexacetonide.[10] However, their long-term efficacy is questionable primarily due to the short retention time. For example, the IA half-life time of cortisone and dexamethasone solutions are 1.5 and 3.6 hr respectively.[44,45] In an attempt to improve the IA retention of these molecules, crystalline drug suspensions have been used. However,

around 10% of the patients experience crystal-induced "steroid flare", characterized by an acute synovitis,[46] which usually resolves within few days after injection.[47]

Finally, hyaluronic acid (HA) is the only formulation currently approved for OA treatment as a lubricating agent,[9,36,37,48] which intends to restore healthy synovial fluid properties.[10] Although clinical trials, systematic reviews and meta-analyses on the effects of HA injections on joint pain present confounding results, primarily due to a high variability in HA formulations, inappropriate blinding and small sample size, most evidence suggest that viscosupplementation may be a safe alternative to achieve clinically relevant pain reduction.[14] A meta-analysis study that evaluated 19 clinical trial publications, with a total of 4,485 patients revealed that overall, HA injection significantly improved pain scores, but its clinical effect was only 29% of the minimal important difference (MID).[15] However, some evidence suggest that high molecular weight or cross-liked HA formulations are able to induce a clinically relevant reduction in knee pain.[15,26] In fact, the use of cross-linked HA formulations led to pain improvements closer to the MID (95%) whereas noncross-linked formulations had a pain improvement of only 25%. However, if these studies are analyzed according to the clinical experimental design, double-blinded trials present a lower treatment effect (49% of MID) compared to studies with insufficient blinding (129% of MID).[15] Additionally, the use of HA injections did not have an important clinical effect on the Western Ontario and McMaster Universities Osteoarthritis (WOMAC) function or stiffness indexes.[15] Consistent with other meta-analysis studies, the clinical effect of viscosupplementation using HA is unclear, primarily due to the lack of good quality, appropriately blinded studies.[16]

4 | NOVEL TARGETS FOR OA TREATMENT AND DRUG CANDIDATES

Considering that OA affects the joint as a whole, in addition to pain, pathways related to inflammation, cartilage catabolism and subchondral bone remodeling have become targets of interest to develop DMOADs. Regarding inflammation, inhibition of the nuclear factor NF-κB or individual downstream proteins (IL-1β, TNF-α, β-NGF, MMPs) has been investigated.[17,18] For example, a phase I and II clinical study for a small molecule NF-κB inhibitor, SAR113945, demonstrated drug tolerability but failed to show effectiveness 56 days after intra-articular administration.[49] However, an analysis performed on a sub-population of the patients, who presented knee joint effusion at baseline demonstrated that IA injection of SAR113945 significantly reduced WOMAC scores of pain and physical function compared to placebo control.[49]

Compounds that inhibit cartilage catabolic activity have also been evaluated. For example, a phase II clinical trial demonstrated that recombinant human fibroblast growth factor 18 (Sprifermin)-treated patients presented a significant reduction in lateral femorotibial cartilage thickness and volume loss compared to placebo control ($p < .033$ and $p < .014$, respectively), when treated with 100 μg of Sprifermin. However, patients in all experimental groups, including placebo, exhibited improved symptoms as determined by the WOMAC index at 12 months, with less improvement for patients receiving 100 μg of Sprifermin compared to placebo ($p < .013$).[50] Another promising molecule, kartogenin (KGN), has been shown to promote chondrogenic differentiation and reduction of OA progression in preclinical animal models.[51-53] In fact, Kang et al. demonstrated that chondrocyte pellets treated with KGN present significantly higher expression of collagen Type II and aggrecan compared to nontreated pellets ($p < .001$).[51] Finally, DMOADs that affect subchondral bone such as the bone resorption inhibitor salmon calcitonin and the antiosteoporotic agent strontium ranelate have been suggested to have promising effects on OA progression.[9]

Another class of DMOAD candidates include senolytic agents and autophagy promoters. It has been observed in animal models of posttraumatic OA that senescent cells accumulate in the synovial membrane and the articular cartilage.[54] Also, a reduced expression of autophagy regulators, which participate in protective mechanisms in healthy cartilage, has been observed in pathological human cartilage samples.[55] Therefore, elimination of senescent cells (SnC), as well as reactivation of autophagy pathways have shown promising results at reducing OA progression in preclinical animal models. In fact, Jeon et al. used a transgenic mice model that allowed for selective elimination of senescent cells to demonstrate that removal of this cell population resulted in reduced cartilage degradation in a posttraumatic model of mice OA.[54] These results were also confirmed using pharmacological elimination of SnC via IA administration of the senolytic molecule UBX0101.[54] Moreover, Xia et al. demonstrated that IA delivery of cordycepin induce reactivation of autophagy markers in a mouse model of OA and significantly reduced joint degeneration compared to untreated joints.[55]

Although OA pathogenesis does not seem to have an inflammatory origin, some researchers believe that synovial inflammation plays a key role on disease progression and have suggested the use of antirheumatic drugs as possible OA treatments.[56,57] In fact, antirheumatic drugs have shown promising results on in vitro models and animal studies, but their efficiency in clinical trials is still questionable.[18] Persson et al. in a systematic review and meta-analysis study, evaluated placebo-controlled clinical trials that investigated the efficacy of FDA-approved antirheumatic drugs as possible OA treatments.[57] In the study, small molecule drugs and biologics were investigated, including hydroxychloroquine, methotrexate, anakinra, adalimumab, and etanercept. Results demonstrated that although these treatments induce a significant reduction in pain metrics, this effect is not clinically relevant.[57]

5 | INTRA-ARTICULAR DRUG DELIVERY STRATEGIES IN OA

Despite the encouraging advances in the discovery of DMOADs, the translation of these drugs into the clinic is limited given the challenging pharmacokinetics of the joints. Free small molecule drugs and even proteins injected in the joint space are rapidly cleared via

lymphatic drainage and their retention time does not exceed few hours (Table 1). Also, most of these drugs have poor water solubility and require a delivery system in order to be administered via IA injections.[9,48,58] Multiple intra-articular drug delivery vehicles including hydrogels, liposomes, nanoparticles and microparticles have been formulated and will be discussed in the following sections (Figure 2).

5.1 | Hydrogels

Various viscosupplementation products, such as lightly cross-linked HA hydrogel formulations (Synvisc-ONE®, EUFLEXXA®, Gel-One® and MonoVisc®),[14] represent an attractive alternative to use as drug delivery vehicles. Several research groups have shown that drug-loaded HA hydrogel formulations can be used to reduce the frequency of IA injections compared to free drug.[65,66] However, the retention of HA cross-linked formulations is still a concern. Yoshioka et al. demonstrated that the commercially available cross-linked HA formulation Gel-One® cannot be detected in the synovial fluid of rabbit knee joints after Day 7, only 30% is retained in the synovial membrane at Day 7 and 3.3% at Day 28.[67] In an attempt to improve hydrogel intra-articular retention, the use of synthetic hydrogels has been explored. For example, poly(caprolactone-co-lactide)-poly(ethylene glycol)-poly(caprolactone-co-lactide) (PCLA-PEG-PCLA) hydrogel, used to deliver celecoxib to horse knees, showed that the drug could be detected at Day 28 in the synovial fluid, but more than 90% of it was cleared by Day 7.[68] Despite these advances, hydrogels serve as drug depots but are unable to control small molecule drug release rate because their mesh size is usually orders of magnitude larger than the loaded drugs.[69,70]

TABLE 1 Half-life of different molecules after intra-articular injection

Molecule	Half-life (h)	Molecular weight (Da)
Paracetamol[59]	1.10	151
Ibuprofen[60]	2.20	206
Naproxen[61]	1.60	230
Ketoprofen[61]	1.90	254
Diclofenac[59]	5.20	296
Cortisone[45]	1.46	360
Dexamethasone[44]	3.60	392
Methotrexate[62]	2.90	454
Hyaluronic acid[19]	13.20	6,000
IL-1Ra[63]	23.04	65,400
Bovine serum albumin[64]	15.12	66,000

5.2 | Liposomes

Liposomes can provide controlled release rates of both lipophilic and water-soluble drugs. Also, compared to crystalline drug suspensions formed by hydrophobic drugs upon IA injection, liposomes are less inflammatory.[71] Studies have shown that liposomes loaded with a model small molecule, such as the contrast agent iohexol, presented an IA half-life time of 134 hr whereas the free molecule was not detected after 3 hr.[72] However, compared to other drug delivery vehicles like polymeric particles, liposomes have limited long term stability.[73] Additionally, the elevated oxidative stress seen in OA joints[74] as well as the shear and compressive loads characteristic of the IA space can reduce liposomes stability and induce drug leakage or burst release.[69,73,75]

5.3 | Nanoparticles and microparticles

An alternative to overcome the mechanical instability of liposomes is the use of lipid or polymeric nanoparticles. These vehicles have been shown to be susceptible to microvascular and synovial macrophage-mediated drainage and can be retained in the joint space only for few weeks, depending on their size, charge and composition.[9,64,76,77] In fact, Partain et al. determined that particles of around 190 nm in diameter, composed of poly(ethylene glycol)-ploy(lactic acid) copolymer containing magnetic nanoparticles, can be retained for around

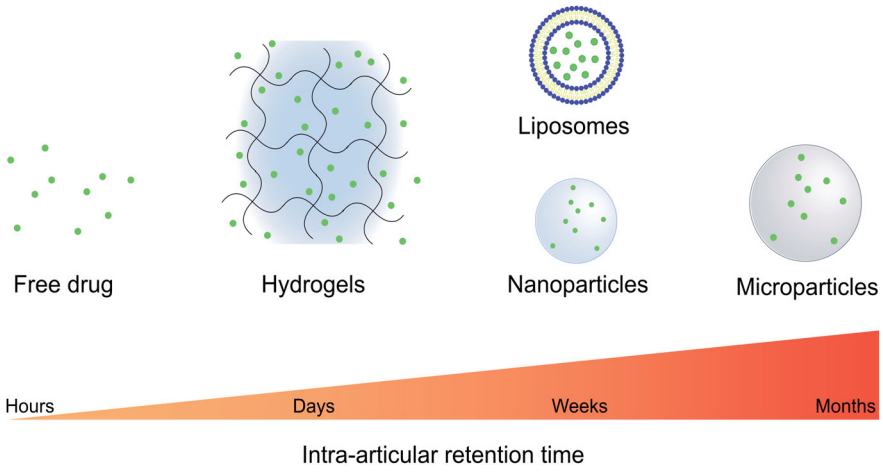

FIGURE 2 Drug delivery systems typically used for IA drug administration and their IA retention time. Free small molecule and macromolecule drugs are cleared from the joint space in few hours. The use of drug delivery vehicles increases drug IA retention time, typically in a size-dependent manner. Nano-scale vehicles such as nanoparticles and liposomes are generally retained up to a couple of weeks, whereas microparticles can be retained in the joint space up to a month. Hydrogels do not usually control the release rate of loaded drug molecules, thus present an IA retention time in the order of days

2 weeks after IA injection in a rat model of knee OA.[78] The use of larger particles that could better avoid lymphatic drainage and cell-mediated particles elimination (Figure 1) is a potential strategy to achieve IA drug sustained release over longer periods of time. In fact, polycaprolactone (PCL) microparticles with an average size of 16 μm were found to remain in the joint space of rats for up to a month.[79] Janssen et al. synthesized celecoxib-loaded polyester amide (PEA) microspheres with a mean particle size of 25 μm and were able to detect around 20% of the injected PEA 12 weeks after IA injection in Lewis rats.[80] Additionally, the company Flexion Therapeutics recently received FDA approval to commercialize ZILRETTA®, an IA formulation of 45 μm triamcinolone acetonide-loaded poly(lactic-co-glycolic) acid PLGA microparticles for pain management in OA patients. The associated clinical trials revealed persistent pain relief until 3 months posttreatment.[81,82] All together, these studies show the potential of microparticles to provide a sufficient IA retention time able to ensure drug bioactivity during a relevant therapeutic window.[9]

6 | TARGETING FOR IA DRUG DELIVERY

A wide variety of DMOADs are being studied for the treatment of OA and can be classified according to their function as analgesic, anti-inflammatory, cartilage-protective, or bone resorption inhibitors.[9] Depending on their function, these drugs act on specific biologic targets present in different tissues within the joint.[48] Studies have shown that nontissue specific delivery of these drugs may result in unwanted off-target effects. For example, the use of NSAIDs reduces proteoglycan secretion, thereby increasing cartilage degradation.[83] Other groups have shown that nerve growth factor (NGF) blockade for pain relief induced rapid OA progression and osteonecrosis in a phase III clinical trial.[84] Therefore, drugs that act on inflammatory and pain pathways should primarily target the synovium.[48] Likewise, drugs that induce chondrogenesis should be preferentially delivered to the articular cartilage in order to prevent adverse effects on the surrounding tissues. In fact, IA injection of TGF-β1[85] and the chondrogenic molecule kartogenin,[51,52,86-89] although beneficial for cartilage repair, increase synovium hyperplasia and induce the formation of cartilage-like tissues in ligaments and synovium.[86]

6.1 | Cartilage targeting

Cartilage extracellular matrix, primarily composed of collagen Type II and sulfated glycosaminoglycans (GAGs), presents a small pore size (60–200 nm) and high negative charge, which difficult the penetration of molecules into this tissue.[90,91] Therefore, the size and charge of drug delivery vehicles play an important role on cartilage targeting and penetration. Drug delivery systems of diverse compositions, ranging from few nanometers up to 100 nm in diameter have been shown to penetrate the articular cartilage matrix.[91-93] However, their retention is primarily controlled by their ability to bind to different components of this tissue.

One alternative to achieve cartilage targeting is to use ionic interactions between the negatively charged cartilage matrix and positively charged carriers.[90] For example, Cook Sangar et al. recently developed a cysteine-dense peptide (CDP-11R) that due to its high surface positive charge is able to accumulate in mice cartilaginous tissues after IV administration and into human articular cartilage explants in vitro.[94] Triamcinolone acetonide conjugated to CDP-11R peptide resulted in a dose-dependent reduction in rat paw inflammation after IV administration in a rat model of rheumatoid arthritis (RA).[94] Moreover, Geiger et al. used a positively charged, cartilage penetrating dendrimer to improve cartilage retention of insulin growth factor 1 (IGF-1), which resulted in significant cartilage protection and reduction of osteophyte formation compared to free IGF-1 in a rat model of OA.[95] Yan et al. developed cationic peptidic nanoparticles for IA delivery of NF-κB siRNA able to penetrate into human OA articular cartilage explants and be retained in the chondrocyte lacunae for at least 2 weeks. Additionally, IA delivery of NF-κB siRNA-conjugated cationic nanoparticles resulted in reduction of cartilage lesion length, chondrocyte apoptosis and synovitis in a mouse model of OA.[96] However, it is important to note that passive cartilage targeting based on electrostatic interactions is affected by the state of the disease. In fact, Vedadghavami et al. demonstrated that positively charged nano-carriers uptake and retention in articular cartilage explants with lower GAGs content were reduced due to a decrease in the cartilage net negative charge compared to healthy explants.[92] Additionally, Brown et al. demonstrated that reduced GAGs content as well as the presence of synovial fluid significantly reduce PLGA NPs retention into articular cartilage explants compared to healthy tissue and saline, respectively.[93]

Moreover, targeting cartilage extracellular matrix (ECM) components such as collagen Type II and aggrecan has gained attention as a promising strategy to target damaged areas of the articular cartilage (Figure 3). In fact, monoclonal anti-Type II collagen antibodies (MabCII) have been used in multiple drug delivery and diagnostics applications.[97-99] For example, Cho et al. demonstrated that liposomes functionalized with a collagen Type II monoclonal antibody are able to bind cartilage tissue proportionally to the severity of the disease in a mice model of OA after systemic administration.[99] Moreover, Bedingfield et al. used MabCII-functionalized polymeric NPs for cartilage-specific MMP13 siRNA delivery. These vehicles significantly reduced MMP13 expression and protected articular cartilage as measured via OARSI scores in a mouse model of OA after IA injection, compared to NPs functionalized with a negative control antibody.[100] Also, single-chain antibody variable fragment (scFv) specific to reactive oxygen species (ROS)-modified collagen II have been reported.[97]

More recently, the use of phage display technology has resulted in the discovery of tissue-specific peptides, which compared to larger proteins such as monoclonal antibodies, are easier to manufacture, less immunogenic, smaller in size and more stable.[73] Using this technology, Yanbin et al. discovered a cartilage affinity peptide (CAP: DWRVIIPPRPSA) able to specifically bind to rabbit chondrocytes and human chondrocytes isolated from a patient with OA. Compared to the scrambled peptide, conjugation of the CAP peptide to 50 nm polyethylenimine nanoparticles, a classical and efficient nonviral vector for

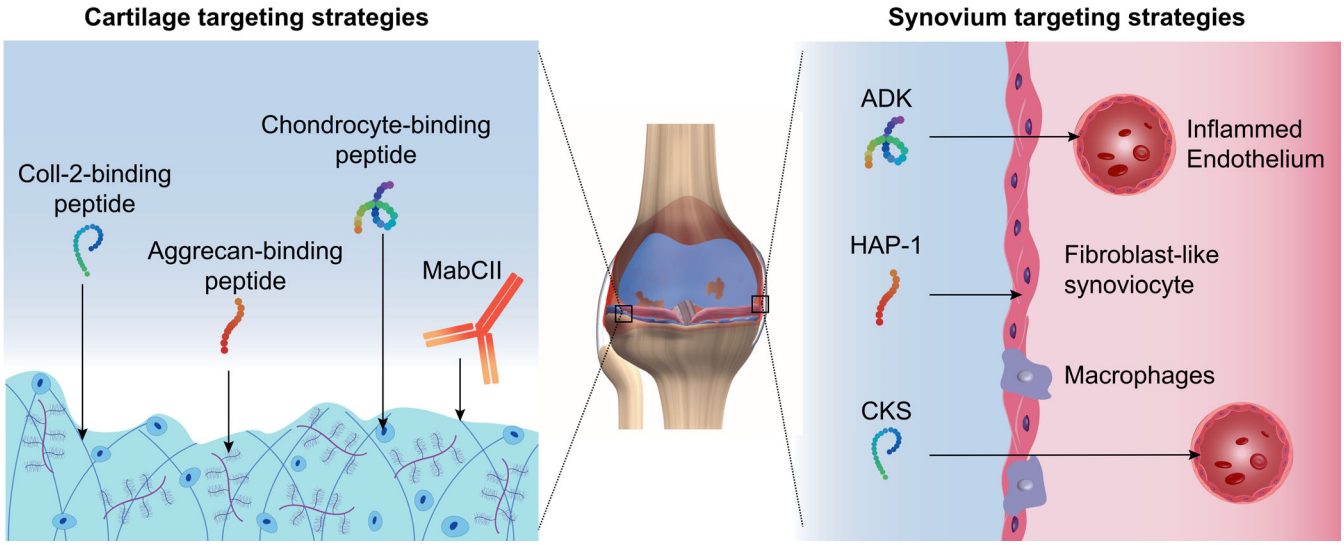

FIGURE 3 Active IA tissue targeting strategies. Targeting peptides binding articular chondrocytes[101] or cartilage ECM components, including collagen Type II (Coll-2)[103] and aggrecan,[102] have been reported. Anti-Coll-2 monoclonal antibodies (MabCII) have also been used for articular cartilage targeting.[97-99] Synovial membrane targeting can be achieved by the use of inflamed synovial endothelium-binding peptides (CKS: CKSTHDRLC,[107] ADK: CRNADKFPC[108]) or peptides targeting fibroblast-like synoviocytes (HAP-1: SFHQFARATLAS)[113]

gene therapy, resulted in particle binding and internalization into chondrocytes in vitro and 48 hr after IA injection into rabbit knee joints.[101] Later, Cheung et al. discovered two peptide sequences (RLDPTSYLRTFW and HDSQLEALIKFM) via phage display able to preferentially bind aggrecan in vitro. However, no scrambled control peptides were used and the ability of these sequences to bind cartilage in vivo was not assessed.[102] These aggrecan-binding and CAP peptides have not yet been used by other research groups for intra-articular drug delivery or diagnostics applications.

Rothenfluh et al. reported the ligand WYRGRL, a collagen Type II α1-targeting peptide. Functionalization of poly(propylene sulphide nanoparticles and subsequent IA injection in mice knees resulted in a 72-fold increase in cartilage-targeting ability compared to nanoparticles functionalized with the scrambled control.[103] In contrast to other reported peptides, this sequence has been successfully used in preclinical models for diagnostics and drug delivery applications.[12,91,103-106] In fact, the conjugation of this peptide to magnetic resonance imaging (MRI) contrast agents has allowed in vivo localization of cartilage hypertrophic changes in a rat model of OA.[104] Other researchers have coupled this ligand to near infra-red probes for in vivo imaging and detection of age-related decrease in collagen Type II in mice.[106] Furthermore, conjugation of this peptide to dexamethasone has proven to increase its retention into bovine articular cartilage explants and decreased the glycosaminoglycan depletion in an in vitro model of OA.[12]

6.2 | Synovial membrane targeting

Although drug delivery into the articular cartilage has been recognized as a key and very challenging aspect in the field, targeted delivery into the synovial membrane has gained interest as well. Originally, synovium targeting emerged as a strategy to minimize the secondary effects of systemic administration of NSAIDs and other anti-inflammatory therapeutics (Figure 3). Two peptides that bind to inflamed synovial vasculature[107,108] have been discovered via phage display and have shown promising targeting results after systemic administration in small animal models of rheumatoid arthritis.[109,110] The first peptide was discovered by screening the ability of peptides administered intravenously (IV) to specifically bind to the vasculature of human synovium grafted into immunodeficient mice.[107] The resulting peptide (CKS: CKSTHDRLC) was later used by Wythe et al. to formulate a fusion protein formed by the anti-inflammatory cytokine IL-4 and the synovium-targeting peptide, and demonstrated that this construct elicited a biological response specifically into human synovium grafts implanted into immunodeficient mice compared to the scrambled control.[109] To date, this peptide has not been used in preclinical models of OA. Another group reported the discovery of a peptide (ADK: CRNADKFPC) able to bind to inflamed synovial vasculature and showed that IV administration of ADK peptide in a rat model of adjuvant arthritis resulted in reduced inflammation scores, decreased T-cell trafficking and angiogenesis inhibition.[108] Additionally systemic administration of ADK-functionalized liposomes loaded with the immunomodulatory cytokine IL-27 resulted in in vivo targeting of arthritic joints and significant reduction in rat paw inflammation compared to nontargeting liposomes or free IL-27 in a rat model of rheumatoid arthritis.[110] Despite these results, the ADK peptide is also able to bind to inflamed skin[108] and the control scrambled sequence has not been characterized.

More recently, Katsumata et al. conjugated an anti-TNFα antibody to either a collagen-binding peptide[111] or a "promiscuous" ECM-binding peptide derived from placenta growth factor 2.[112] In both

studies, subcutaneous administration of the conjugate resulted in elevated retention and reduced paw inflammation compared to un-conjugated anti-TNFα antibodies.[111,112] Although Katsumata et al. demonstrated that these conjugates preferentially accumulate in the synovial membrane in vivo,[111] both of these peptides are able to bind to different types of collagen in vitro and exhibit significantly higher retention in OA human cartilage explants compared to un-conjugated anti-TNFα antibodies.[111,112] Even though it is unknown if these ECM-binding peptide conjugates are also retained in the articular cartilage in vivo, this strategy offers promising results in terms of specific drug delivery into inflamed joints.

A different approach for synovium targeting was proposed by Mi et al. who discovered a peptide (HAP-1: SFHQFARATLAS) that directly binds to synoviocytes.[113] HAP-1-functionalized liposomes loaded with prednisone[114] or an anti-inflammatory NF-κB-blocking peptide[115] showed promising results in terms of liposome localization into the arthritic joints and the reduction of rat paw inflammation after IV injection in a rat model of rheumatoid arthritis. Considering that synovium endothelium is not directly exposed to synovial fluid but synoviocytes are, the most promising strategy to target the synovial lining after IA injection could be HAP-1 peptide.

6.3 | Multitarget therapy

Current understanding of OA pathology indicates that it is a complex, multifactorial disease, which suggest that multitarget treatment may be a promising strategy to address the diverse mechanisms involved in OA progression. Although this idea has gained interest in the community, only few studies have explored the concept of multitarget therapy. One of the most investigated approaches is the use of dual-function lubricating drug-loaded nanoparticles.[116] Fan et al. developed HA nano-micelles containing the inti-inflammatory molecule, curcumin. These nano-micelles exhibited low friction coefficient and reduced paw inflammation by 30% in a rat model of rheumatoid arthritis.[117] Other researchers have focused on dual drug delivery to achieve multitarget therapies for OA treatment. Kang et al. developed chitosan-based thermoresponsive nanoparticles for independent delivery of kartogenin, a potent chondrogenic molecule, and diclofenac for pain and inflammation management.[118] These particles induced chondrogenic differentiation of mesenchymal stem cells in vitro, slowed OA progression and reduced the concentration of cyclooxygenase-2 in serum and synovial fluid in a rat model of post-traumatic OA compared to a solution of free drugs. However, the effect of combinatorial treatment compared to mono-therapy was not evaluated.[118] Moreover, Stone et al. demonstrated that IA combinatorial gene therapy using viral vectors expressing IL-1 receptor antagonist and lubricin induced the expression of anabolic and cartilage matrix genes, decreased the expression of catabolic and inflammatory mediators and provided significant cartilage protection compared to mono-therapy.[119] Despite the advances in the development of combinatorial therapies, the use of tissue-specific drug delivery vehicles for multitarget treatment of OA is yet to be explored.

7 | CONCLUSIONS AND FUTURE PERSPECTIVES

Current OA treatment strategies do not address the underlying joint degenerative processes and are ineffective at managing long-term pain. The lack of approved DMOADs has not only resulted in poor quality of life for OA patients, but has also made this disease a major cause of disability worldwide. Significant advances on elucidating OA etiology have moved the field forward in terms of developing promising DMOADs. However, much research is still needed in this regard. In addition to developing better DMOADs, there is an unmet need to design appropriate IA drug delivery vehicles that are able to increase drugs' IA retention time and directly release these molecules into the tissues of interest. Different biomaterials have been proposed in order to overcome the limitations related to IA drug administration including hydrogels, nanoparticles, liposomes and microparticles. To date, there is only one FDA-approved drug formulation that utilizes a biomaterial-based drug delivery system for IA injection in OA patients, which consist of triamcinolone acetonide-loaded PLGA microparticles.[82] Although microparticles generally present longer IA retention compared to other biomaterial-based formulations, extensive research on the use of different drug delivery vehicles, especially at a clinical level is still needed. Additionally, considering the complex nature of the disease, multitarget treatment strategies could represent a promising alternative to address the diverse underlying joint degenerative processes occurring in OA. In this regard, not only the development of appropriate IA drug delivery vehicles is imperative, but also the use of tissue-targeting strategies is essential. Future research on combinatorial drug delivery systems for the administration of therapeutic molecules with different IA tissue targets is still needed and could significantly contribute to the development of effective strategies for OA treatment.

ACKNOWLEDGMENTS

The authors acknowledge Laura Daniela Mancipe Castro for her support in the artwork production. This work was supported by the National Institute of Arthritis and Musculoskeletal and Skin Diseases of the National Institutes of Health under award numbers R01AR062920 and S10OD016264 and the Department of Defense PRMRP Grant (PR171379).

ORCID

Lina M. Mancipe Castro https://orcid.org/0000-0002-0722-9647
Andrés J. García https://orcid.org/0000-0001-6602-2518
Robert E. Guldberg https://orcid.org/0000-0002-0303-261X

REFERENCES

1. Kloppenburg M, Berenbaum F. Osteoarthritis year in review 2019: epidemiology and therapy. *Osteoarthr Cartil*. 2020;*28*:242-248. https://doi.org/10.1016/j.joca.2020.01.002.
2. Cisternas MG, Murphy L, Sacks JJ, Solomon DH, Pasta DJ, Helmick CG. Alternative methods for defining osteoarthritis and the impact on estimating prevalence in a US population-based survey. *Arthritis Care Res*. 2016;*68*:574-580.
3. Turkiewicz A, Petersson IF, Björk J, et al. Current and future impact of osteoarthritis on health care: a population-based study

with projections to year 2032. *Osteoarthr Cartil*. 2014;*22*: 1826-1832.
4. Chen D, Shen J, Zhao W, et al. Osteoarthritis: toward a comprehensive understanding of pathological mechanism. *Bone Res*. 2017;*5*: 16044.
5. Deshpande BR, Katz JN, Solomon DH, et al. Number of persons with symptomatic knee osteoarthritis in the United States: impact of race/ethnicity, age, sex, and obesity. *HHS Public Access Arthritis Care Res*. 2016;*68*:1743-1750.
6. Kotlarz H, Gunnarsson CL, Fang H, J a R. Insurer and out-of-pocket costs of osteoarthritis in the US: evidence from national survey data. *Arthritis Rheum*. 2009;*60*:3546-3553.
7. Zhang Y, Jordan JM. Epidemiology of osteoarthritis. *Clin Geriatr Med*. 2010;*26*:355-369.
8. Peat G, Mccarney R, Croft P. Knee pain and osteoarthritis in older adults: a review of community burden and current use of primary health care. *Ann Rheum Dis*. 2001;*60*:91-97.
9. Maudens P, Jordan O, Allémann E. Recent advances in intra-articular drug delivery systems for osteoarthritis therapy. *Drug Discov Today*. 2018;*23*:1761-1775.
10. Mora JC, Przkora R, Cruz-Almeida Y. Knee osteoarthritis: pathophysiology and current treatment modalities. *J Pain Res*. 2018;*11*:2189-2196.
11. Liu X, Machado GC, Eyles JP, Ravi V, Hunter DJ. Dietary supplements for treating osteoarthritis: a systematic review and meta-analysis. *Br J Sport Med*. 2018;*52*:167-175.
12. Formica FA, Barreto G, Zenobi-Wong M. Cartilage-targeting dexamethasone prodrugs increase the efficacy of dexamethasone. *J Control Release*. 2019;*295*:118-129.
13. Janssen M, Timur UT, Woike N, et al. Celecoxib-loaded PEA microspheres as an auto regulatory drug-delivery system after intra-articular injection. *J Control Release*. 2016;*244*:30-40.
14. Johal H, Devji T, Schemitsch EH, Bhandari M. Viscosupplementation in knee osteoarthritis: evidence revisited. *JBJS Rev*. 2016;*4*:1-11.
15. Jevsevar D, Donnelly P, Brown GA, Cummins DS. Viscosupplementation for osteoarthritis of the knee: a systematic review of the evidence. *J Bone Jt Surg*. 2015;*97*:2047-2060.
16. Rutjes AWS, Jiini P, da Costa BR, Trelle S, Eveline Niiesch SR. Background: viscosupplementation for osteoarthritis of the knee. *N Engl J Med*. 2015;*372*:2569-2570.
17. Goldring MB, Berenbaum F. Emerging targets in osteoarthritis therapy. *Curr Opin Pharmacol*. 2015;*22*:51-63.
18. Chevalier X, Eymard F, Richette P. Biologic agents in osteoarthritis: hopes and disappointments. *Nat Rev Rheumatol*. 2013;*9*:400-410.
19. Brown T, Fraser LU. Turnover of hyaluronan in synovial joints: elimination of labelled hyaluronan from the knee joint of the rabbit. *Exp Physiol*. 1991;*76*:125-134.
20. Blagojevic M, Jinks C, Jeffery A, Jordan KP. Risk factors for onset of osteoarthritis of the knee in older adults: a systematic review and meta-analysis. *Osteoarthr Cartil*. 2010;*18*:24-33.
21. Hootman JM, Helmick CG. Projections of US prevalence of arthritis and associated activity limitations. *Arthritis Rheum*. 2006;*54*:226-229.
22. Andriacchi TP, Favre J, Erhart-Hledik JC, Chu CR. A systems view of risk factors for knee osteoarthritis reveals insights into the pathogenesis of the disease. *Ann Biomed Eng*. 2015;*43*:376-387.
23. Loeser RF, Goldring SR, Scanzello CR, Goldring MB. Osteoarthritis: a disease of the joint as an organ. *Arthritis Rheum*. 2012;*64*:1697-1707.
24. Horisawa E, Kubota K, Tuboi I, et al. Size-dependency of DL-Lactide/Glycolide copolymer particulates for intra-articular delivery system on phagocytosis in rat Synovium. *Pharma*. 2002;*19*: 132-139.
25. Kapoor M, Martel-Pelletier J, Lajeunesse D, Pelletier JP, Fahmi H. Role of proinflammatory cytokines in the pathophysiology of osteoarthritis. *Nat Rev Rheumatol*. 2011;*7*:33-42.
26. Pontes-Quero GM, García-Fernández L, Aguilar MR, San Román J, Pérez Cano J, Vázquez-Lasa B. Active viscosupplements for osteoarthritis treatment. *Semin Arthritis Rheum*. 2019;*49*:171-183.
27. Qvist P, Bay-Jensen A-C, Christiansen C, Dam EB, Pastoureau P, Karsdal MA. The disease modifying osteoarthritis drug (DMOAD): is it in the horizon? *Pharmacol Res*. 2008;*58*:1-7.
28. Esser S, Bailey A. Effects of exercise and physical activity on knee osteoarthritis. *Curr Pain Headache Rep*. 2011;*15*:423-430.
29. Bliddal H, Leeds AR, Christensen R. Osteoarthritis, obesity and weight loss: Evidence, hypotheses and horizons - a scoping review. *Obes Rev*. 2014;*15*:578-586.
30. Brien S, Prescott P, Coghlan B, Bashir N, Lewith G. Review Systematic review of the nutritional supplement Perna Canaliculus (green-lipped mussel) in the treatment of osteoarthritis. *Q J Med*. 2008;*101*: 167-179.
31. Wandel S, Jüni P, Tendal B, et al. Effects of glucosamine, chondroitin, or placebo in patients with osteoarthritis of hip or knee: network meta-analysis. *Br Med J*. 2010;*341*:711.
32. Clegg DO, Reda DJ, Harris CL, et al. Glucosamine, chondroitin sulfate, and the two in combination for painful knee osteoarthritis. *N Engl J Med*. 2006;*354*:795-808.
33. Sawitzke AD, Shi H, Finco MF, et al. The effect of glucosamine and/-or chondroitin sulfate on the progression of knee osteoarthritis: a report from the glucosamine/chondroitin arthritis intervention trial. *Arthritis Rheum*. 2008;*58*:3183-3191.
34. AM AGIBA. Nutraceutical formulations containing glucosamine and chondroitin Sulphate in the treatment of osteoarthritis: emphasis on clinical efficacy and formulation challenges. *Int J Curr Pharm Res*. 2017;*9*:1.
35. Henrotin Y, Mathy M, Sanchez C, Lambert C. Chondroitin sulfate in the treatment of osteoarthritis: From in vitro studies to clinical recommendations. *Ther Adv Musculoskelet Dis*. 2010;*2*:335-348.
36. National Institute for Health and Care Excellence. *Osteoarthritis: Care and management in adults*, London, U.K.: National Institute for Health and Care Excellence; 2014.
37. McAlindon TE, Bannuru RR, Sullivan MC, et al. OARSI guidelines for the non-surgical management of knee osteoarthritis. *Osteoarthr Cartil*. 2014;*22*:363-388.
38. Pelletier JP, Martel-Pelletier J, Rannou F, Cooper C. Efficacy and safety of oral NSAIDs and analgesics in the management of osteoarthritis: Evidence from real-life setting trials and surveys. *Semin Arthritis Rheum*. 2016;*45*:S22-S27. https://doi.org/10.1016/j.semarthrit.2015.11.009.
39. Lin J, Zhang W, Jones A, care DMP. Efficacy of topical non-steroidal anti-inflammatory drugs in the treatment of osteoarthritis: meta-analysis of randomised controlled trials. *Br Med J*. 2004;*329*:1-6.
40. Smith SR, Deshpande BR, Collins JE, Katz JN, Losina E. Comparative pain reduction of oral non-steroidal anti-inflammatory drugs and opioids for knee osteoarthritis: systematic analytic review. *SR Osteoarthr Cartil*. 2016;*24*:962-972.
41. Krebs EE, Gravely A, Nugent S, et al. Effect of opioid vs nonopioid medications on pain-related function in patients with chronic back pain or hip or knee osteoarthritis pain the SPACE randomized clinical trial. *JAMA*. 2018;*319*:872-882.
42. Richards MM, Maxwell JS, Weng L, Angelos MG, Golzarian J. Intra-articular treatment of knee osteoarthritis: from anti-inflammatories to products of regenerative medicine. *Physician Sport Med*. 2016;*44*: 101-108.
43. Ayhan E, Kesmezacar H, Akgun I. Intraarticular injections (corticosteroid, hyaluronic acid, platelet rich plasma) for the knee osteoarthritis. *World J Orthop*. 2014;*5*:351-361.
44. Soma LR, Uboh CE, Liu Y, et al. Pharmacokinetics of dexamethasone following intra-articular, intravenous, intramuscular, and oral administration in horses and its effects on endogenous hydrocortisone. *J Vet Pharmacol Ther*. 2013;*36*(12):181-191. https://doi.org/10.1111/j.1365-2885.2012.01412.x
45. Peterson RE, Black RL, Bunim JJ. Disposition of intra-articularly injected cortisone and hydrocortisone. *Arthritis Rheum*. 1959;*2*: 433-439.

46. Berger RG, Yount WJ. Immediate "steroid flare" from intraarticular triamcinolone hexacetonide injection: case report and review of the literature. *Arthritis Rheum*. 2010;*33*:1284-1286. https://doi.org/10.1002/art.1780330833.
47. Butoescu N, Jordan O, Doelker E. Intra-articular drug delivery systems for the treatment of rheumatic diseases: A review of the factors influencing their performance. *Eur J Pharm Biopharm*. 2009;*73*:205-218.
48. Geiger BC. Alan J. Grodzinsky PTH. Designing drug delivery systems for articular Jointst. *Chem Eng Prog*. 2018;*114*:46-51.
49. Grothe K, Flechsenhar K, Paehler T, et al. IκB kinase inhibition as a potential treatment of osteoarthritis – results of a clinical proof-of-concept study. *Osteoarthr Cartil*. 2017;*25*:46-52.
50. Lohmander LS, Hellot S, Dreher D, et al. Intraarticular sprifermin (recombinant human fibroblast growth factor 18) in knee osteoarthritis: a randomized, double-blind, placebo-controlled trial. *Arthritis Rheumatol*. 2014;*66*:1820-1831.
51. Kang ML, Ko J-Y, Kim JE, Im G-I. Intra-articular delivery of kartogenin-conjugated chitosan nano/ microparticles for cartilage regeneration. *Biomaterials*. 2014;*35*:9984-9994.
52. Mohan G, Magnitsky S, Melkus G, et al. Kartogenin treatment prevented joint degeneration in a rodent model of osteoarthritis: a pilot study. *J Orthop Res*. 2016;*34*:1780-1789.
53. Ono Y, Ishizuka S, Knudson CB, Knudson W. Chondroprotective effect of Kartogenin on CD44-mediated functions in articular cartilage and chondrocytes. *Cartilage*. 2014;*5*:172-180.
54. Hee Jeon O, Kim C, Laberge R-M, et al. Local clearance of senescent cells attenuates the development of post-traumatic osteoarthritis and creates a pro-regenerative environment. *Nat Med*. 2017;*23*:775-783.
55. Xia C, Chen P, Mei S, Ning L, Lei C, Wang J, Zhang J, Ma J, Fan S. Photo-crosslinked HAMA hydrogel with cordycepin encapsulated chitosan microspheres for osteoarthritis treatment. *Oncotarget*. 2017;*8*(2):2835-2849.
56. Robinson WH, Lepus CM, Wang Q, et al. Low-grade inflammation as a key mediator of the pathogenesis of osteoarthritis. *Nat Rev Rheumatol*. 2016;*12*:580-592.
57. Persson MSM, Sarmanova A, Doherty M, Zhang W. Meta-analysis conventional and biologic disease-modifying anti-rheumatic drugs for osteoarthritis: a meta-analysis of randomized controlled trials. *Rheumatology*. 2018;*57*:1830-1837.
58. Kavanaugh TE, Werfel TA, Cho H, Hasty KA, Duvall CL. Particle based Technologies for Osteoarthritis Detection and Therapy. *Drug Deliv Transl Res*. 2016;*6*:132-147.
59. Owen S, Francis H, Roberts M. Disappearance kinetics of solutes from synovial fluid after intra- articular injection. *Br J Clin Pharmacol*. 1994;*38*:349-355.
60. Elmquist WF, Chan KKH. RJS. Synovial mean transit time of diclofenac and other nonsteroidal antiinflammatory drugs. *Pharm Res*. 1994;*11*:1689-1697.
61. Simkin PA, Wu MP, Foster DM. Articular pharmacokinetics of protein-bound Antirheumatic agents. *Clin Pharmacokinet*. 1993;*25*:342-350.
62. Wigginton SM, Chu BCF, Weisman MH, Howell SB. Methotrexate pharmacokinetics after intraarticular injection in patients with rheumatoid arthritis. *Arthritis Rheum*. 1980;*23*:119-122.
63. Whitmire RE, Wilson DS, Singh A, Levenston ME, Murthy N, García AJ. Self-assembling nanoparticles for intra-articular delivery of anti-inflammatory proteins. *Biomaterials*. 2012;*33*:7665-7675.
64. Singh A, Agarwal R, Diaz-Ruiz CA, et al. Nano-engineered particles for enhanced intra-articular retention and delivery of proteins. *Adv Heal Mater*. 2014;*3*:1562-1567.
65. Palmieri B, Rottigni V, Iannitti T. Preliminary study of highly cross-linked hyaluronic acid-based combination therapy for management of knee osteoarthritis-related pain. *Drug des Devel Ther*. 2013;*7*:7-12.
66. Park CW, Ma KW, Jang SW, Son M, Kang MJ. Comparison of Piroxicam pharmacokinetics and anti-inflammatory effect in rats after intra-articular and intramuscular administration. *Biomol Ther (Seoul)*. 2014;*22*:260-266.
67. Yoshioka K, Yasuda Y, Kisukeda T, Nodera R, Tanaka Y, Miyamoto K. Pharmacological effects of novel cross-linked hyaluronate, Gel-200, in experimental animal models of osteoarthritis and human cell lines. *Osteoarthr Cartil*. 2014;*22*:879-887.
68. Petit A, Redout EM, Van De Lest CH, et al. Sustained intra-articular release of celecoxib from in situ forming gels made of acetyl-capped PCLA-PEG-PCLA triblock copolymers in horses. *Biomaterials*. 2015;*53*:426-436.
69. Samad A, Sultana Y, Aqil M, Sultana Y, Aqil M. Liposomal drug delivery systems: an update review. *Curr Drug Deliv*. 2007;*4*:297-305.
70. Xu X, Jha AK, Harrington DA, Farach-Carson MC, Jia X. Hyaluronic acid-based hydrogels: from a natural polysaccharide to complex networks. *Soft Matter*. 2012;*8*:3280-3294.
71. Akbarzadeh A, Rezaei-Sadabady R, Davaran S, et al. Liposome: classification, preparation, and applications. *Nanoscale Res Lett*. 2013;*8*:1-9.
72. Edwards SHR, Cake MA, Spoelstra G, Read RA. Biodistribution and clearance of intra-articular liposomes in a large animal model using a radiographic marker. *J Liposome Res*. 2007;*17*:249-261.
73. Kamaly N, Xiao Z, Valencia PM, Radovic-Moreno AF, Farokhzad OC. Targeter polymeric therapeutic nanoparticles: design, development and clinical translation. *Chem Soc Rev*. 2012;*29*:1883-1889.
74. Paździor M, Kiełczykowska M, Kurzepa J, Luchowska-kocot D, Kocot J, Musik I. The oxidative stress in knee osteoarthritis patients. An attempt of evaluation of possible compensatory effects occurring in the disease development. *Medicina*. 2019;*55*:150.
75. Natsume T, Yoshimoto M. Membrane permeability and stability of liposomes suspended in shear flow. *J Dispers Sci Technol*. 2013;*34*:1557-1562.
76. Pradal J, Maudens P, Gabay C, Seemayer CA, Jordan O, Allémann E. Effect of particle size on the biodistribution of nano- and microparticles following intra-articular injection in mice. *Int J Pharm*. 2016;*498*:119-129.
77. Morgen M, Tung D, Boras B, et al. Nanoparticles for improved local retention after intra-articular injection into the knee joint. *Pharm Res*. 2013;*30*:257-268.
78. Partain BD, Unni M, Rinaldi C, Allen KD. The clearance and biodistribution of magnetic composite nanoparticles in healthy and osteoarthritic rat knees. *J Control Release*. 2020;*321*:259-271.
79. Arunkumar P, Indulekha S, Vijayalakshmi S, Srivastava R. Synthesis, characterizations, in vitro and in vivo evaluation of Etoricoxib-loaded poly (Caprolactone) microparticles-a potential intra-articular drug delivery system for the treatment of osteoarthritis. *Aust J Biol Sci*. 2016;*27*:303-316.
80. Maarten Janssen, Ufuk Tan Timur, Nina Woike, Tim J.M. Welting, Guy Draaisma, Marion Gijbels, Lodewijk W. van Rhijn, George Mihov, Jens Thies PJE. Celecoxib-loaded PEA microspheres as an auto regulatory drug-delivery system after intra-articular injection. *J Control Release* 2016;*244*:30–40.
81. Flexion Therapeutics. ZILRETTA® (triamcinolone acetonide extended-release injectable suspension). [cited 2019 Jan 18]. Available from: https://flexiontherapeutics.com/our-product/
82. Conaghan PG, Hunter DJ, Cohen SB, et al. Effects of a single intra-articular injection of a microsphere formulation of triamcinolone Acetonide on knee osteoarthritis pain. *J Bone Jt Surg*. 2018;*100*:666-677.
83. Suh J-K, Muzzonigro TS, Fu FH. Injury and repair of articular cartilage: related scientific issues. *Oper Tech Orthop*. 1997;*7*:270-278.
84. Hochberg MC, Tive LA, Abramson SB, et al. When is osteonecrosis not osteonecrosis?: adjudication of reported serious adverse joint events in the Tanezumab clinical development program. *Arthritis Rheumatol*. 2016;*68*:382-391.

85. Bakker AC, Van De Loo FAJ, Van Beuningen HM, et al. Overexpression of active TGF-beta-1 in the murine knee joint: evidence for synovial-layer-dependent chondro-osteophyte formation. *Osteoarthr Cartil*. 2001;*9*:128-136.
86. Zhang J, Wang JHC. Kartogenin induces cartilage-like tissue formation in tendon-bone junction. *Bone Res*. 2014;*2*:12-17.
87. Shi D, Xu X, Ye Y, et al. Photo-cross-linked scaffold with Kartogenin-encapsulated nanoparticles for cartilage regeneration. *ACS Nano*. 2016;*10*:1292-1299.
88. Kang M-L, Jeong S-Y, Im G-I. Hyaluronic acid hydrogel functionalized with self-assembled micelles of Amphiphilic PEGylated Kartogenin for the treatment of osteoarthritis. *Tissue Eng Part A*. 2017;*23*:630-639.
89. Li X, Ding J, Zhang Z, et al. Kartogenin-incorporated Thermogel supports stem cells for significant cartilage regeneration. *ACS Appl Mater Interfaces*. 2016;*8*:5148-5159.
90. Bajpayee AG, Grodzinsky AJ. Cartilage-targeting drug delivery: can electrostatic interactions help? [internet]. *Nat Rev Rheumatol*. 2017;*13*:183-193.
91. Brown SB, Wang L, Jungels RR, Sharma B. Effects of cartilage-targeting moieties on nanoparticle biodistribution in healthy and osteoarthritic joints. *Acta Biomater*. 2020;*101*:469-483.
92. Vedadghavami A, Wagner EK, Mehta S, He T, Zhang C, Bajpayee AG. Cartilage penetrating cationic peptide carriers for applications in drug delivery to avascular negatively charged tissues. *Acta Biomater*. 2019;*93*:258-269.
93. Brown S, Pistiner J, Adjei IM, Sharma B, Crayton Pruitt J. Nanoparticle properties for delivery to cartilage: The implications of disease state, synovial fluid, and off-target uptake. *Mol Pharm*. 2019;*16*:469-479.
94. Cook Sangar ML, Girard EJ, Hopping G, et al. A potent peptide-steroid conjugate accumulates in cartilage and reverses arthritis without evidence of systemic corticosteroid exposure. *Sci Transl Med*. 2020;*12*:1041.
95. Geiger BC, Wang S, Padera RF, Grodzinsky AJ, Hammond PTNANOMEDICINE. Cartilage-penetrating nanocarriers improve delivery and efficacy of growth factor treatment of osteoarthritis. *Sci Transl Med*. 2018;*10*:eaat8800.
96. Yan H, Duan X, Pan H, et al. Suppression of NF-κB activity via nanoparticle-based siRNA delivery alters early cartilage responses to injury. *PNAS*. 2016;*113*:E6199-E6208. https://doi.org/10.1073/pnas.1608245113.
97. Hughes C, Faurholm B, Dell'Accio F, et al. Human single-chain variable fragment that specifically targets arthritic cartilage. *Arthritis Rheum*. 2010;*62*:1007-1016.
98. Cho H, Pinkhassik E, David V, Stuart JM, Hasty KA. Detection of early cartilage damage using targeted nanosomes in a post-traumatic osteoarthritis mouse model. *Nanomedicine*. 2015;*11*:939-946.
99. Cho H, Kim BJ, Park S-H, Hasty KA, Min B-H. Noninvasive visualization of early osteoarthritic cartilage using targeted nanosomes in a destabilization of the medial meniscus mouse model. *Int J Nanomedicine*. 2018;*13*:1215-1224.
100. Sean K Bedingfield, Fang Yu, Danielle D. Liu, Meredith A. Jackson, Lauren E. Himmel, Hongsik Cho, Juan M. Colazo, Leslie J. Crofford, Karen A. Hasty Craig L. Duvall. Matrix-targeted nanoparticles for MMP13 RNA interference blocks post-traumatic osteoarthritis; 2020;1–54.
101. Pi Y, Zhang X, Shi J, et al. Targeted delivery of non-viral vectors to cartilage in vivo using a chondrocyte-homing peptide identified by phage display. *Biomaterials*. 2011;*32*:6324-6332.
102. Cheung CSF, Lui JC, Baron J. Identification of chondrocyte-binding peptides by phage display. *J Orthop Res*. 2013;*31*:1053-1058.
103. Rothenfluh DA, Bermudez H, O'neil CP, Hubbell JA. Biofunctional polymer nanoparticles for intra-articular targeting and retention in cartilage. *Nat Mater*. 2008;*7*:248-254.
104. Hu H-Y, Lim N-H, Juretschke H-P, et al. In vivo visualization of osteoarthritic hypertrophic lesions. *Chem Sci*. 2015;*6*:6256-6261.
105. Chen H, Qin Z, Zhao J, et al. Cartilage-targeting and dual MMP-13/pH responsive theranostic nanoprobes for osteoarthritis imaging and precision therapy. *Biomaterials*. 2019;*225*:119520.
106. Yi W, Zhou H, Li A, et al. A NIR-II fluorescent probe for articular cartilage degeneration imaging and osteoarthritis detection. *Biomater Sci*. 2019;*7*:1043-1051.
107. Lee L, Buckley C, Blades MC, Panayi G, George AJT. Identification of synovium-specific homing peptides by in vivo phage display selection. *Arthritis Rheum*. 2002;*46*:2109-2120.
108. Yang Y-H, Rajaiah R, Ruoslahti E, Moudgil KD. Peptides targeting inflamed synovial vasculature attenuate autoimmune arthritis. *Proc Natl Acad Sci U S A*. 2011;*108*:12857-12862.
109. Wythe SE, Dicara D, Taher TEI, et al. Targeted delivery of cytokine therapy to rheumatoid tissue by a synovial targeting peptide. *Ann Rheum Dis*. 2013;*72*:129-135.
110. Meka RR, Venkatesha SH, Moudgil KD. Peptide-directed liposomal delivery improves the therapeutic index of an immunomodulatory cytokine in controlling autoimmune arthritis. *J Control Release*. 2018;*286*:279-288.
111. Katsumata K, Ishihara J, Mansurov A, et al. Targeting inflammatory sites through collagen affinity enhances the therapeutic efficacy of anti-inflammatory antibodies. *Sci Adv*. 2019;*5*:eaay1971.
112. Katsumata K, Ishihara J, Fukunaga K, et al. Conferring extracellular matrix affinity enhances local therapeutic efficacy of anti-TNF-α antibody in a murine model of rheumatoid arthritis. *Athritis Res Ther*. 2019;*21*:1-10. https://doi.org/10.1186/s13075-019-2075-8.
113. Mi Z, Lu X, Mai JC, et al. Identification of a synovial fibroblast-specific protein transduction domain for delivery of apoptotic agents to hyperplastic synovium. *Mol Ther*. 2003;*8*:295-305.
114. Vanniasinghe AS, Manolios N, Schibeci S, et al. Targeting fibroblast-like synovial cells at sites of inflammation with peptide targeted liposomes results in inhibition of experimental arthritis. *Clin Immunol*. 2014;*151*:43-54.
115. You C, Zu J, Liu X, et al. Synovial fibroblast-targeting liposomes encapsulating an NF-κB-blocking peptide ameliorates zymosan-induced synovial inflammation. *J Cell Mol Med*. 2018;*22*:2449-2457.
116. Ji X, Zhang H. Current strategies for the treatment of early stage osteoarthritis. *Front Mech Eng*. 2019;*5*:57.
117. Fan Z, Li J, Liu J, Jiao H, Liu B. Anti-inflammation and joint lubrication dual effects of a novel hyaluronic acid/curcumin nanomicelle improve the efficacy of rheumatoid arthritis therapy. *ACS Appl Mater Interfaces*. 2018;*10*:23595-23604.
118. Kang ML, Kim JE, Il IG. Thermoresponsive nanospheres with independent dual drug release profiles for the treatment of osteoarthritis. *Acta Biomater*. 2016;*39*:65-78.
119. Stone A, Grol MW, Merry RZC, et al. Combinatorial Prg4 and Il-1ra gene therapy protects against hyperalgesia and cartilage degeneration in post-traumatic osteoarthritis. *Hum Gene Ther*. 2019;*30*:225-235.

How to cite this article: Mancipe Castro LM, García AJ, Guldberg RE. Biomaterial strategies for improved intra-articular drug delivery. *J Biomed Mater Res*. 2020;1–11. https://doi.org/10.1002/jbm.a.37074

ACS Biomaterials SCIENCE & ENGINEERING

pubs.acs.org/journal/abseba

Article

Articular Cartilage- and Synoviocyte-Binding Poly(ethylene glycol) Nanocomposite Microgels as Intra-Articular Drug Delivery Vehicles for the Treatment of Osteoarthritis

Lina M. Mancipe Castro, Abigail Sequeira, Andrés J. García,* and Robert E. Guldberg*

Cite This: https://dx.doi.org/10.1021/acsbiomaterials.0c00960

Read Online

ACCESS | Metrics & More | Article Recommendations | Supporting Information

ABSTRACT: Intra-articular (IA) injection is an attractive route of administration for the treatment of osteoarthritis (OA). However, free drugs injected into the joint space are rapidly cleared and many of them can induce adverse off-target effects on different IA tissues. To overcome these limitations, we designed nanocomposite 4-arm-poly(ethylene glycol)-maleimide (PEG-4MAL) microgels, presenting cartilage- or synoviocyte-binding peptides, containing poly-(lactic-*co*-glycolic) acid (PLGA) nanoparticles (NPs) as an IA small molecule drug delivery system. Microgels containing rhodamine B (model drug)-loaded PLGA NPs were synthesized using microfluidics technology and exhibited a sustained, near zero-order release of the fluorophore over 16 days *in vitro*. PEG-4MAL microgels presenting synoviocyte- or cartilage-targeting peptides specifically bound to rabbit and human synoviocytes or to bovine articular cartilage *in vitro*, respectively. Finally, using a rat model of post-traumatic knee OA, PEG-4MAL microgels were shown to be retained in the joint space for at least 3 weeks without inducing any joint degenerative changes as measured by EPIC-μCT and histology. Additionally, all microgel formulations were found trapped in the synovial membrane and significantly increased the IA retention time of a model small molecule near-infrared (NIR) dye compared to that of the free dye. These results suggest that peptide-functionalized nanocomposite PEG-4MAL microgels represent a promising intra-articular vehicle for tissue-localized drug delivery and prolonged IA drug retention for the treatment of OA.

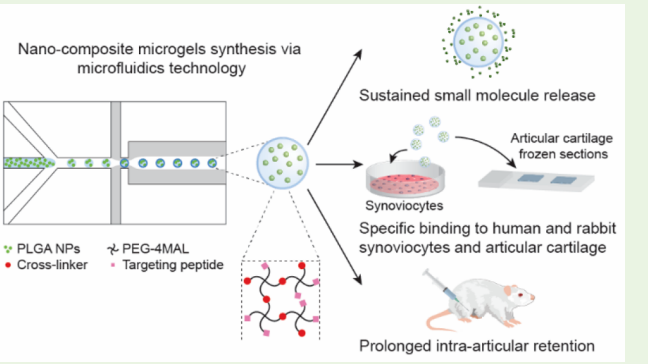

KEYWORDS: *microgels, tissue-binding, intra-articular, drug delivery, osteoarthritis*

1. INTRODUCTION

Osteoarthritis (OA) is a progressive joint degenerative disease that affects approximately 303 million people in the world[1] and 30.8 million adults in the U.S.[2] There are no FDA-approved disease modifying OA drugs (DMOADs).[3] OA treatment is limited to weight management and physical therapy,[4] systemic pain management using non-steroidal anti-inflammatory drugs (NSAIDs), cyclooxygenase inhibitors, and weak opioids, whose long-term use has been associated with adverse effects on the gastrointestinal, renal, and circulatory systems,[5,6] and visco-supplementation injections of hyaluronic acid.[7] Nevertheless, these management approaches do not address the underlying joint degeneration and have limited long-term benefits.[4,8,9]

Intra-articular (IA) injection offers an attractive route of drug administration, which can reduce systemic off-target effects and allow for a higher local drug concentration while using lower doses compared to those of systemic delivery.[3] However, free drugs injected in the IA space are rapidly cleared, which leads to insufficient retention times and effective concentrations for drugs to elicit a therapeutic effect.[10] For example, the IA half-life time of small molecule drugs (<1 kDa) is less than 5 h[11] and that of larger molecules such as proteins does not exceed 24 h.[12,13] Although recently discovered DMOADs have demonstrated promising results in preclinical models of OA, their translation into the clinic has been hindered, in part due to the lack of IA drug delivery vehicles able to support long-term treatment.[3]

Extensive research has led to the development of novel DMOADs that act on different joint tissues.[3] However, non-tissue specific drug delivery may result in unwanted off-target effects. For example, drugs-targeting processes occurring in the synovial membrane such as NSAIDs have been related to reduced proteoglycan secretion and increased cartilage degradation.[14] Similarly, nerve growth factor (NGF) blockade for pain relief resulted in rapid OA progression and osteonecrosis in a phase III clinical trial.[15] Likewise, drugs

Received: June 28, 2020
Accepted: August 11, 2020
Published: August 11, 2020

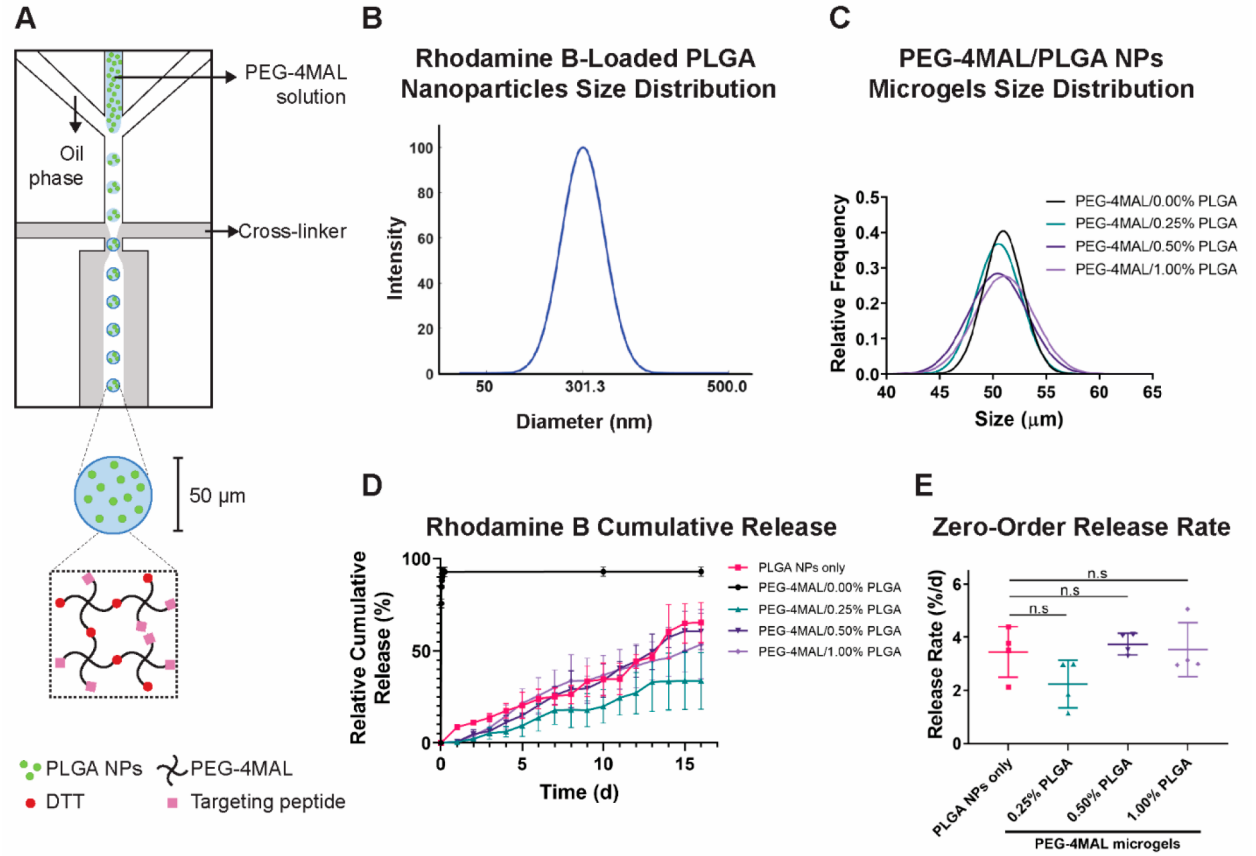

Figure 1. Nanocomposite PEG-4MAL/PLGA NP microgels synthesis and characterization. (A) Schematic of microgel fabrication. PEG-4MAL was functionalized with targeting peptides (1.0 mM) and mixed with PLGA NPs prior to microgels synthesis *via* microfluidics technology. (B) Rhodamine-B-loaded PLGA NP size distribution. (C) Encapsulation of PLGA NPs into PEG-4MAL microgels did not affect microgel size ($p > 0.99$). (D) Rhodamine B release profile from empty microgels, nanocomposite microgels, and PLGA NPs. Rhodamine B rapidly diffuses out of empty PEG-4MAL microgels, whereas microgels containing PLGA NPs and PLGA NPs alone exhibited a zero-order release. (E) Nanocomposite PEG-4MAL microgels presented a rhodamine B release rate comparable to PLGA NPs alone ($p = 0.107$).

that induce chondrogenesis such as TGF-β and kartogenin increase synovium hyperplasia and formation of cartilage-like tissues in ligaments and synovial membrane.[16,17]

To overcome these limitations, targeting strategies have been used to confer the delivery vehicle with the ability to bind articular cartilage[18−22] or synovial membrane.[23−29] Targeting peptides that bind the inflamed synovial vasculature[28,29] or fibroblast-like synoviocytes have been identified.[25] In particular, the HAP-1 peptide (SFHQFARATLAS), which targets fibroblast-like synoviocytes, has been conjugated to drug-loaded liposomes, demonstrating encouraging results in rat models of adjuvant- and zymosan-induced arthritis.[26,27] On the contrary, active cartilage targeting has been achieved *via* antitype II collagen (Coll-2) monoclonal antibodies[18−20] and Coll-2-targeting peptides.[22] Rothenfluh et al. reported the peptide WYRGRL (WYR), which specifically binds to Coll-2 α1 chain[22] and has shown efficient cartilage binding in a variety of diagnostic and drug delivery applications.[5,30−33]

Despite advances on tissue targeting, only nano-sized carriers have been used for IA tissue-localized drug delivery.[19−22,26−28] Even though the use of nanoparticles (NPs) may be advantageous for intra-cartilage and intracellular drug delivery, recent studies have shown that the use of targeting moieties does not improve IA drug carrier retention. Brown et al. demonstrated that cartilage-targeting poly(lactic-*co*-glycolic) acid (PLGA)-based NPs effectively penetrate the articular cartilage when conjugated with the targeting peptide WYR or to positively charged moieties. However, the use of these cartilage-targeting strategies did not improve NPs IA retention compared to that of non-targeting control NPs.[30] In general, particles larger than a few microns in diameter present better IA retention than NPs.[3] Nevertheless, the use of larger particles may not always be beneficial. Polymeric microparticles resulting from joint arthroplasty implant wear are associated with articular cartilage and meniscus degradation and synovitis.[34] Liggins et al. demonstrated that PLGA particles between 1 and 20 μm in size induced higher proteoglycan depletion and synovial cellular infiltration than larger particles (30−100 μm) in a rabbit model of antigen-induced arthritis.[35] These observations raise concerns regarding the use of solid polymeric microparticles for long-term IA delivery. Therefore, there is an unmet need to develop safe intra-articular drug delivery systems with tissue-localized delivery capabilities and prolonged IA drug retention times.

Synthetic microgels, micron-sized hydrogel particles, offer attractive chemical and mechanical properties for the development of intra-articular drug delivery vehicles. In particular 4-arm-poly(ethylene glycol)-maleimide (PEG-4MAL) microgels allow for efficient incorporation of biological ligands and have been used for cell encapsulation and protein delivery applications.[36−38] However, their use as small molecule intra-articular drug carriers has not been explored. Here, we

https://dx.doi.org/10.1021/acsbiomaterials.0c00960
ACS Biomater. Sci. Eng. XXXX, XXX, XXX−XXX

developed nanocomposite PEG-4MAL microgels containing poly(lactic-*co*-glycolic) acid (PLGA) NPs and functionalized with HAP-1- and WYR-targeting peptides as synoviocyte-binding and articular cartilage surface-binding intra-articular small molecule delivery vehicles. We evaluated these systems for their ability to support the sustained release of model small molecule drugs and bind to synoviocytes and articular cartilage *in vitro*. Additionally, the IA retention of PEG-4MAL microgels and a loaded model small molecule were evaluated in a rat model of OA. Finally, the IA localization of peptide-functionalized microgels was evaluated and their effect on articular cartilage and synovial membrane structure were investigated.

2. MATERIALS AND METHODS

2.1. Materials. The reagents and peptides used in this work are described in the Supporting Information.

2.2. PLGA Nanoparticles Synthesis and Characterization. PLGA NPs containing model small molecules were synthesized by an oil-in-water single emulsion method. PLGA (210 mg) was dissolved in 6 mL of dichloromethane (DCM) and mixed with 1 mL of a solution of either rhodamine B or cyanine 7 (Cy7) in DCM (1 mg/mL). The mixture was added to 50 mL of 1% poly(vinyl alcohol) (PVA) in distilled water and sonicated for 3 min (A = 100%, VibraCell Ultrasonic Processor, VCX 130 PB). The emulsion was added to 50 mL of 1% PVA and magnetically stirred for 4 h. PLGA NPs were washed with distilled water three times *via* centrifugation at 16 000*g* for 10 min, lyophilized, and stored at −20 °C. Nanoparticles size was determined using dynamic light scattering (Brookhaven 90 Plus Particle Size Analyzer, Brookhaven Instruments, Holtsville, NY).

2.3. Preparation PEG-4MAL/PLGA NPs Composite Microgels and Characterization. PEG microgels were synthesized using microfluidics technology as described elsewhere with minor modifications.[36] The aqueous phase was composed of PBS with Ca^{2+} and Mg^{2+} ($PBS^{+/+}$) and Optiprep (2:1) with 20 mM HEPES, and the oil phase contained mineral oil with 2% SPAN 80. Prior to microgel formation, PEG-4MAL macromer was reacted with cartilage- (WYR), synoviocyte- (HAP-1), or integrin- (RGD) binding peptides or their respective scrambled controls (WYRsc, HAP-1sc, RDG) at room temperature and pH 7.0 for 10 min and mixed with an aqueous suspension of PLGA NPs. The final PEG-4MAL concentration was 6% w/v, and it contained 1.0 mM peptide and either 0, 0.25, 0.50, or 1.00% w/v PLGA NPs. Cross-linker emulsion was prepared using a solution of dithiothreitol (DTT) in aqueous phase (30 mg/mL) mixed with oil phase at a 1:14 ratio. Microgels were synthesized using PDMS flow-focusing devices with a nozzle size of 46.5 ± 0.5 μm (Figure 1A) and washed five times with a 1% bovine serum albumin (BSA) solution in $PBS^{+/+}$ *via* centrifugation (1000*g* for 5 min). Size distribution of PEG-4MAL microgels was determined *via* microscopy image analysis using ImageJ. Further microgels characterization methods are described in the Supporting Information.

2.4. Rhodamine B *in Vitro* Release. PEG-4MAL microgels containing different rhodamine-B-loaded PLGA NPs concentrations (0, 0.25, 0.50, and 1.00% w/v) were prepared as described before (n = 4 independent runs, 27 μL of PEG-4MAL macromer precursor solution were used to prepare each batch). Empty microgels were loaded with a rhodamine B solution (5 μg/mL) by incubation and physical entrapment. PLGA NPs alone (1.35 mg/mL) were used as a control. Samples were then incubated at 4 °C with constant stirring in a total volume of 200 μL of 1% BSA. At each time point, microgel samples were centrifuged at 1000*g* for 5 min and 150 μL of supernatant were taken for rhodamine B release measurements *via* spectrophotometry ($\lambda_{ex}/\lambda_{em}$: 553/627 nm) and replaced with fresh 1% BSA solution. For PLGA NPs only, a centrifugation speed of 16 000*g* was used to ensure appropriate separation. The encapsulated rhodamine content in PLGA NPs was measured after extraction in methanol (1 mg/mL) at 4 °C. Relative cumulative release profiles were analyzed using a zero-order curve fit.

2.5. HAP-1-Functionalized PEG-4MAL Microgel-Binding Assay. To evaluate the ability of HAP-1 peptide-functionalized PEG-4MAL microgels to specifically bind to synovial cells, rabbit and human synoviocytes (HIG-82 and SW982), mouse myoblasts (C2C12), and mouse preosteoblasts (MC3T3-E1) were cultured in a 24-well plate at an initial seeding density of 100 000 cells/well for 1 day to achieve over 95% confluency. C2C12 and MC3T3-E1 cell lines were used as negative controls to assess microgel binding specificity. Cells were stained using CellTracker Green according to the manufacturer's instructions. PEG-4MAL microgels (19 000 microgels/mL, 500 μL/well) containing rhodamine-B-loaded PLGA NPs and functionalized with either 1.0 mM HAP-1, HAP-1sc, RGD, or RDG (n = 4 wells per group) were incubated for 30 min with the different cell lines in growth media (Ham's F12 media supplemented with 10% fetal bovine serum (FBS)). The integrin-binding peptide RGD was used as positive control. Unbound microgels were washed three times using growth media, and then, 10 images per well were taken at random positions using confocal microscopy and bound microgels were manually quantified.

2.6. WYR-Functionalized PEG-4MAL Microgel Binding Assay. The ability of WYR-conjugated PEG-4MAL microgels to bind to articular cartilage was evaluated using 10 μm thick fresh bovine cartilage frozen sections. Sections (∼1 cm^2, n = 3) were stained with DAPI and incubated for 30 min with 100 μL of WYR or WYRsc-functionalized microgels suspended in growth media (19 000 microgels/mL). Samples were washed twice using growth media, and a minimum of 7 randomly located images per sample were taken using confocal microscopy to quantify bound microgels. To assess for the specificity of the cartilage-targeting peptide and confirm that it does not bind to synoviocytes, a microgels-binding assay was conducted using the HIG-82 cells monolayer platform as described in section 2.5.

2.7. Surgical Induction of OA in Lewis Rats. All animal experiments were performed following Georgia Tech's Institutional Animal Care and Use Committee (IACUC) approval. Male Lewis rats (250−300 g) were subjected to unilateral medial meniscus transection (MMT) as previously described.[39]

2.8. Peptide-Functionalized PEG-4MAL/PLGA NPs Microgel *in Vivo* Intra-Articular Retention. HAP-1 and WYR peptides were conjugated to Cy7-NHS ester prior to microgel formation following the manufacturer's instructions. Three weeks after MMT procedure, rats received 50 μL bilateral injections of the following formulations in sterile saline: (1) free sulfo-Cy7 dye (negative control), (2) Cy7-WYR-functionalized microgels, or (3) Cy7-HAP-1-functionalized microgels (530 000 microgels/mL, n = 9). Microgel formulations contained 0.5% w/v PLGA NPs. Rats were scanned before and immediately after injection and on days 1, 3, 5, 7, 10, 13, 16, 19, and 26 post-injection using an *in vivo* imaging system (PerkinElmer IVIS Spectrum CT). At day 26, rats were euthanized and legs harvested to assess knee joint health and OA progression (Figure 4A).

2.9. Assessment of the Medial Tibial Articular Cartilage and Synovial Membrane Thickness. Harvested tissues were fixed in 10% neutral buffered formalin for 3 days and then stored in PBS without Ca^{2+} and Mg^{2+} ($PBS^{-/-}$). Cartilage degradation and osteophyte formation were measured *via* equilibrium partitioning of ionic contrasting agent microcomputed tomography (EPIC μ-CT).[40] Dissected tibias (n = 6) were incubated in 37.5% Conray contrast agent for 40 min at room temperature. Samples were scanned in a Scanco μCT40 (45 kVp, 177 μA, 8 W, 16 μm resolution), and images were contoured and analyzed for cartilage attenuation, lesion volume, roughness, and calcified osteophyte volume.[40,41] Three samples per group were decalcified for 10 days, and then, knee joints were dissected leaving the knee cap intact, embedded in paraffin, and sectioned through the coronal plane (5 μm thick sections). Samples were then stained using Toluidine Blue and synovial membrane thickness was measured using ImageJ.

2.10. *In Vivo* Localization of Nanocomposite Microgels. Peptide-functionalized microgels (HAP-1, HAP-1sc, WYR, and WYRsc) were injected into rat knees 2 weeks after surgical induction of OA (50 μL/injection, 530 000 microgels/mL, n = 4). Animals were

https://dx.doi.org/10.1021/acsbiomaterials.0c00960
ACS Biomater. Sci. Eng. XXXX, XXX, XXX−XXX

euthanized 2 weeks after IA injections, and knees were collected. Tissues were fixed in 10% neutral buffered formalin for 3 days, decalcified for 10 days, and embedded in optimal cutting temperature compound (OCT) and sectioned through the midcoronal plane. For each sample, three sections (15 μm thick) were collected and stained with hematoxylin and eosin (H&E) for microgels localization.

2.11. Small Molecule Cargo *in Vivo* Intra-Articular Retention. The near-infrared dye Cy7, used as model small molecule drug, was loaded into PLGA NPs as described in section 2.2. Microgels functionalized with WYR, WYRsc, HAP-1, and HAP-1sc peptides, containing 0.5% w/v Cy7-loaded PLGA NPs, were injected into the knee joints of male Lewis rats (50 μL/injection, 530 000 microgels/mL) at 3 weeks after surgical induction of OA (n = 7). Sulfo-Cy7 free dye and Cy7-loaded PLGA NPs (no microgels) were used as controls. Rats were scanned before and immediately after injection and on days 1, 3, 5, 7, 10, 13, 16, 19, and 26 post-injection using an *in vivo* imaging system (PerkinElmer IVIS Spectrum CT).

3. STATISTICAL METHODS

All data are reported as mean ± standard deviation. Data obtained from the rhodamine B release assay was fitted using either zero- or first-order models, and the corresponding curve fits were compared for their goodness of fit using the Akaike's Information Criterion (AIC). Data acquired from the *in vivo* microgels and Cy7 tracking studies were fitted to a one-phase exponential decay, and curve fit parameters were then compared among groups. Outlier analysis was performed using a maximum false discovery rate of 1% prior to statistical analysis. Normally distributed data that presented equal variances was analyzed *via* one-way ANOVA. All other data that did not present a Gaussian distribution or homoscedasticity was subjected to a logarithmic transformation. If the transformation resulted in normally distributed data with equal variances, a one-way ANOVA was applied. If the logarithmic transformation only corrected for data non-normality, a Welch's ANOVA was used on the transformed data. A p-value <0.05 was considered significant. All analyses were performed using Prism (GraphPad Software, San Diego, CA).

4. RESULTS

4.1. Microfluidic Polymerization Produces PEG-4MAL/PLGA NP Microgels. Small-molecule-loaded PLGA NPs exhibited a mean size of 338 ± 91 nm (Figure 1 B) and contained 3 μg of rhodamine B per milligram of PLGA (encapsulation efficiency 63%). The microfluidic technology generates PLGA-NP-loaded PEG-4MAL microgels with tight size distribution (Figure 1 C). All formulations presented a mean size between 50.4 and 51.4 μm with a coefficient of variation (CV) below 6.5% (Table 1). PLGA NP encapsulation did not significantly affect microgels mean size (p > 0.99). PLGA NP content per microgel followed a Poisson distribution for formulations containing 0.25% w/v PLGA NPs, whereas higher PLGA NP concentrations (0.50 and 1.00% w/v) led to a bimodal distribution with most microgels containing 10% or 90% of their cross-sectional area filled with PLGA NPs (Figure S2). This phenomenon is more pronounced in the 1.00% w/v PLGA NP group and can be attributed to the NP hydrophobic nature, which leads to nanoparticle aggregation as its concentration increases in the precursor PEG-4MAL solution.

Table 1. PLGA-NPs-Loaded Microgels Size and Coefficient of Variance (CV %)

PLGA NPs (% w/v)	diameter mean ± SD (μm)	CV (%)
0.00	51.0 ± 2.7	5.20
0.25	50.4 ± 2.2	4.38
0.50	50.9 ± 3.3	6.44
1.00	51.4 ± 3.3	6.48

4.2. Rhodamine B *in Vitro* Release Is Controlled by PLGA NPs. Rhodamine B was used as a model small molecule (MW = 479.02 Da). When encapsulated into empty PEG-4MAL microgels by simple physical entrapment, over 80% rhodamine B was released within the first hour, consistent to our previous studies using other small molecules loaded into PEG-4MAL microgels.[36] In contrast, PLGA alone or microgels containing rhodamine-B-loaded PLGA NPs exhibited a sustained release over 16 days (Figure 1D), which followed a zero-order release kinetics model (AIC test, > 99% compared to first-order model). PLGA NPs alone presented an initial burst release (10.0 ± 2.8% by day 1) followed by a zero-order profile, characteristic of PLGA particulate systems.[42,43] In contrast, nanocomposite microgels did not exhibit an initial burst release (p < 0.0001 compared to PLGA NPs only at day 1), which typically occurs due to rapid diffusion of molecules loaded at the surface of these systems.[43] We attribute this difference to the multiple washing steps involved in microgels synthesis, which can remove the rhodamine B molecules at the surface of PLGA NPs. The release rate of rhodamine B from PLGA NPs alone was comparable to the rates observed for microgels containing different concentrations of PLGA NPs (p = 0.107) (Figure 1E). This result indicates that the release rate of small molecules, like rhodamine B, is mainly controlled by the encapsulated PLGA NPs and not by the hydrogel itself.

4.3. HAP-1-Functionalized PEG-4MAL Microgels Bind Synoviocytes. Microgels functionalized with synoviocyte-targeting peptide were evaluated for their ability to specifically bind to rabbit (HIG-82) and human (SW982) synovial cell lines (Figure 2A). Positive control microgels functionalized with RGD bound to all evaluated cell types at a higher level compared to that of its scrambled control RDG (p < 0.0025) (Figure 2B). Moreover, HAP-1-functionalized PEG-4MAL microgels bound to rabbit and human synoviocytes to the same level as RGD microgels (p > 0.59) but in a specific manner, as evidenced by their lower binding capacity to C2C12 and MC3T3-E1 cells (p < 0.0008 compared to RGD). Also, HAP-1sc presented a binding level comparable to those of RDG negative control microgels in all cell types (p > 0.49). These results demonstrate that HAP-1 peptide confers nanocomposite PEG-4MAL/PLGA NPs microgels with the ability to bind specifically to rabbit and human synoviocytes.

4.4. WYR-Functionalized PEG-4MAL Microgels Bind Articular Cartilage. WYR peptide binds specifically to the collagen type II α1 chain.[22] Therefore, a collagen-type-II-rich system such as bovine articular cartilage was used to assess WYR-functionalized PEG-4MAL microgels binding (Figure 3A). WYR-presenting microgels bound to bovine cartilage fresh frozen sections to a greater extent than scrambled peptide control microgels (p = 0.0015) (Figure 3B). To investigate whether this formulation also binds to synoviocytes, a HIG-82 cell monolayer platform was used and WYR-presenting microgel binding was compared to positive control peptide (RGD, HAP-1) microgel formulations (Figure 3C). WYR-presenting microgels exhibited significantly lower binding levels to rabbit synoviocytes compared to those of HAP-1- and RGD-functionalized microgels (p < 0.025). Furthermore, their binding levels were comparable to those of negative control peptide-presenting microgels, including RDG, HAP-1sc, and WYRsc (p > 0.93) (Figure 3D). These results

https://dx.doi.org/10.1021/acsbiomaterials.0c00960
ACS Biomater. Sci. Eng. XXXX, XXX, XXX−XXX

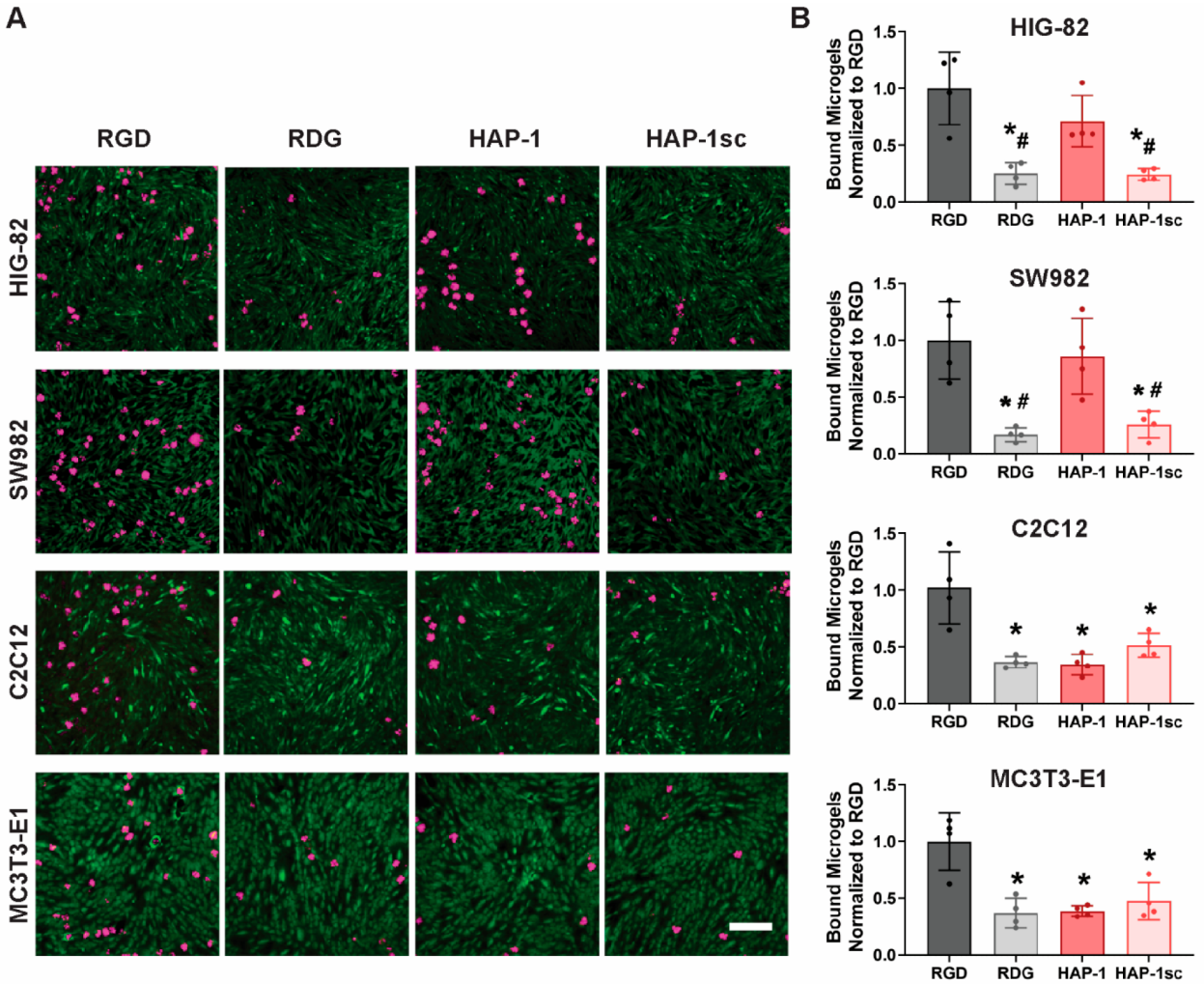

Figure 2. HAP-1-functionalized PEG-4MAL/PLGA NP microgels bind synoviocytes. (A) Confocal images of peptide-functionalized microgels (magenta) bound to rabbit (HIG-82) and human (SW982) synoviocytes, mouse myoblasts (C2C12), and mouse preosteoblasts (MC3T3-E1) stained with Cell Tracker Green. Scale bar 200 μm. (B) RGD-functionalized microgels bound to HIG-82, SW982, C2C12, and MC3T3-E1 cell lines at a higher level than RDG microgels. HAP-1-functionalized PEG microgels bound to rabbit and human synoviocytes to the same extent as RGD-functionalized microgels and is specific for synovial cells lines as demonstrated by its low binding to C2C12 and MC3T3-E1 cells. Mean ± SD, $^{*}p < 0.05$ compared to RGD, $^{\#}p < 0.05$ compared to HAP-1.

demonstrate that WYR-functionalized PEG-4MAL microgels specifically bind to articular cartilage but not to synoviocytes.

4.5. PEG-4MAL/PLGA NP Microgels Have Increased *in Vivo* Intra-Articular Retention. An *in vivo* tracking study was conducted to determine the IA retention of HAP-1- and WYR-functionalized microgels compared to that of a free small molecule near-infrared dye (Cy7) in healthy and OA rat joints. Radiant efficiency data resulting from IVIS imaging (Figure 4B) demonstrate that Cy7 free dye is cleared faster than the microgel formulations (Figure 4C) in healthy and OA joints, exhibiting a half-life time of 0.14 ± 0.04 and 0.21 ± 0.06 days, respectively (Figure 4D). In contrast, nanocomposite microgels exhibited a significant increase in the intra-articular half-life time compared to free dye control in MMT knees (HAP-1, 6.03 ± 4.76 days, $p < 0.0005$; WYR, 2.48 ± 0.70 days, $p < 0.006$) and healthy joints (HAP-1, 3.37 ± 2.82 days, $p < 0.0056$; WYR, 4.70 ± 1.78 days, $p < 0.0003$). These findings demonstrate that peptide-functionalized PEG-4MAL nanocomposite microgels are retained in the knee space for a significantly longer period of time compared to free small molecules such as Cy7. WYR-functionalized microgels in both healthy and diseased joints exhibited an increase in radiant efficiency at day 1 compared to day 0 (Figure 4C). This increase in fluorescence can be attributed to a self-quenching effect characteristic of cyanine dyes.[44] This phenomenon was more pronounced in WYR- than HAP-1-presenting microgels, probably due to a higher degree of Cy7 aggregation in WYR peptide molecules compared to that in HAP-1 (Figure S3). Because of this self-quenching increase in radiant efficiency, one-phase exponential decay curve fit of WYR-conjugated PEG-4MAL microgels did not include values from the day 0 time point.

We next examined the size stability of WYR-functionalized microgels in the IA space to assess any microgel degradation due to joint motion and other *in vivo* effects. Microgel size was reduced by day 14 as evidenced by the presence of smaller, irregular hydrogel fragments (Figure S4). We attribute this reduction in size to mechanical forces in the joint breaking up microgels. Nevertheless, 40% of the retrieved microgels was found intact at day 21, demonstrating that PEG-4MAL nanocomposite microgels are retained in the rat knee joint for at least 3 weeks.

https://dx.doi.org/10.1021/acsbiomaterials.0c00960
ACS Biomater. Sci. Eng. XXXX, XXX, XXX−XXX

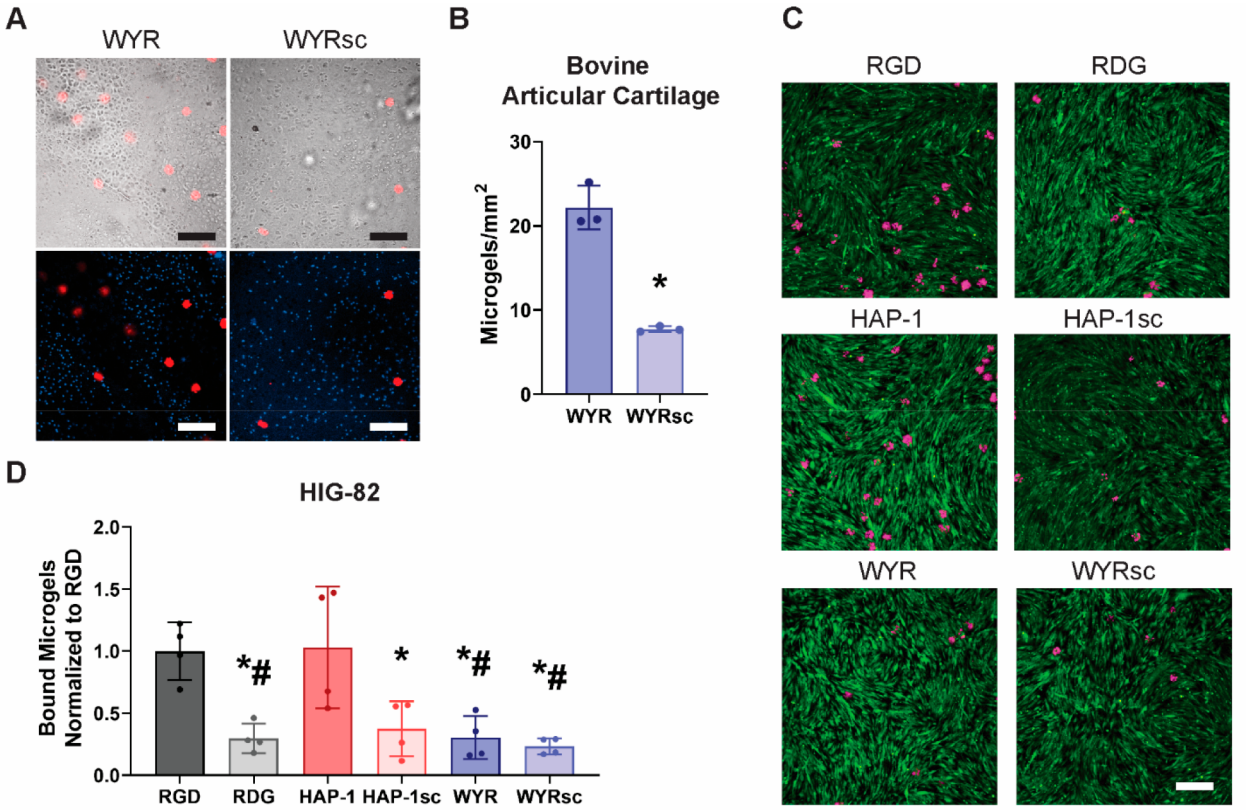

Figure 3. WYR-functionalized PEG microgels bind articular cartilage. (A) Confocal images of PEG-4MAL microgels (red) bound to bovine articular cartilage sections stained with DAPI (blue). Scale bar 200 μm. (B) WYR-functionalized microgels bind to bovine cartilage sections to a higher level than the scrambled control WYRsc-presenting microgels. Mean ± SD, $n = 3$, $^{*}p < 0.05$. (C) Confocal images of PEG-4MAL microgels (magenta) bound to rabbit synoviocytes stained with Cell Tracker Green. Scale bar 200 μm. (D) Binding of WYR-functionalized PEG-4MAL microgels to synoviocytes is significantly lower those of than RGD- and HAP-1-functionalized microgels. Mean ± SD, $n = 4$, 8 images per well, $^{*}p < 0.05$ compared to HAP-1, $^{\#}p < 0.05$ compared to RGD.

4.6. Microgels Do Not Negatively Impact Cartilage Structure. EPIC-μCT was used to evaluate whether peptide-functionalized nanocomposite PEG-4MAL microgels affected articular cartilage integrity (Figure 5A). We have previously shown that the MMT model induces a higher degree of articular cartilage damage in the medial third of the medial tibial plateau;[39] therefore, parameters such as cartilage attenuation and surface roughness were evaluated in this region. As expected, animals subjected to surgical induction of OA presented significant cartilage damage compared to naïve joints as evidenced by a significant increase in tissue attenuation ($p < 0.0001$) (Figure 5D), an indication of proteoglycan depletion, an increase in surface roughness ($p < 0.0001$) (Figure 5E), and the presence of calcified osteophytes ($p < 0.0001$) (Figure 5G). Additionally, animals in the MMT groups presented full thickness articular cartilage lesions (Figure 5F). WYR- and HAP-1-functionalized PEG-4MAL microgels did not induce any cartilage degenerative changes compared to free Cy7 dye in healthy joints and did not worsen OA progression in MMT animals. In this experiment, the free dye group was considered the negative control, given that free Cy7 dye is cleared from the joint in less than 5 h (Figure 4D), and to the best of our knowledge, this does not negatively affect the knee joint. Although injection of WYR-functionalized PEG-4MAL microgels did not induce a significant reduction in lesion volume compared to free dye and HAP-1-functionalized microgels in MMT rats (Figure 5F), one of the animals did not exhibit any cartilage lesions and three of them presented smaller lesions than HAP-1 and free dye treated rats. This is an interesting observation because cartilage damage seen in the rat MMT model at 6 weeks post-surgery is usually characterized by the development of full-thickness lesions.[45] This observation provides a basis for future evaluation of WYR-functionalized PEG-4MAL nanocomposite microgels and their effect on OA progression. Additionally, synovial membrane thickness as a marker of inflammation was measured *via* histology image analysis (Figure 5B). Synovium thickness was not affected either by the progression of the disease or the presence of microgels in the intra-articular space (Figure 5C). Overall, these results demonstrate that IA injection of peptide-functionalized PEG-4MAL microgels containing PLGA NPs does not result in detectable cartilage damage or synovial membrane thickening in healthy joints and does not accelerate the progression of OA following meniscal injury.

4.7. Microgels Accumulate in the Synovial Membrane. Histological analysis of H&E-stained samples revealed that 2 weeks after injection all PEG-4MAL microgel formulations accumulate in the synovial membrane (Figure 6). This result is consistent with prior work showing that micron-sized materials injected in the IA space are trapped in the synovial membrane and induce local hypercellularity.[46,47] Therefore, it is not surprising that no gross differences in microgel accumulation into the synovial membrane were observed among formulations. Analysis of microgel localization in other areas of the joint such as the synovial fluid or the

https://dx.doi.org/10.1021/acsbiomaterials.0c00960
ACS Biomater. Sci. Eng. XXXX, XXX, XXX−XXX

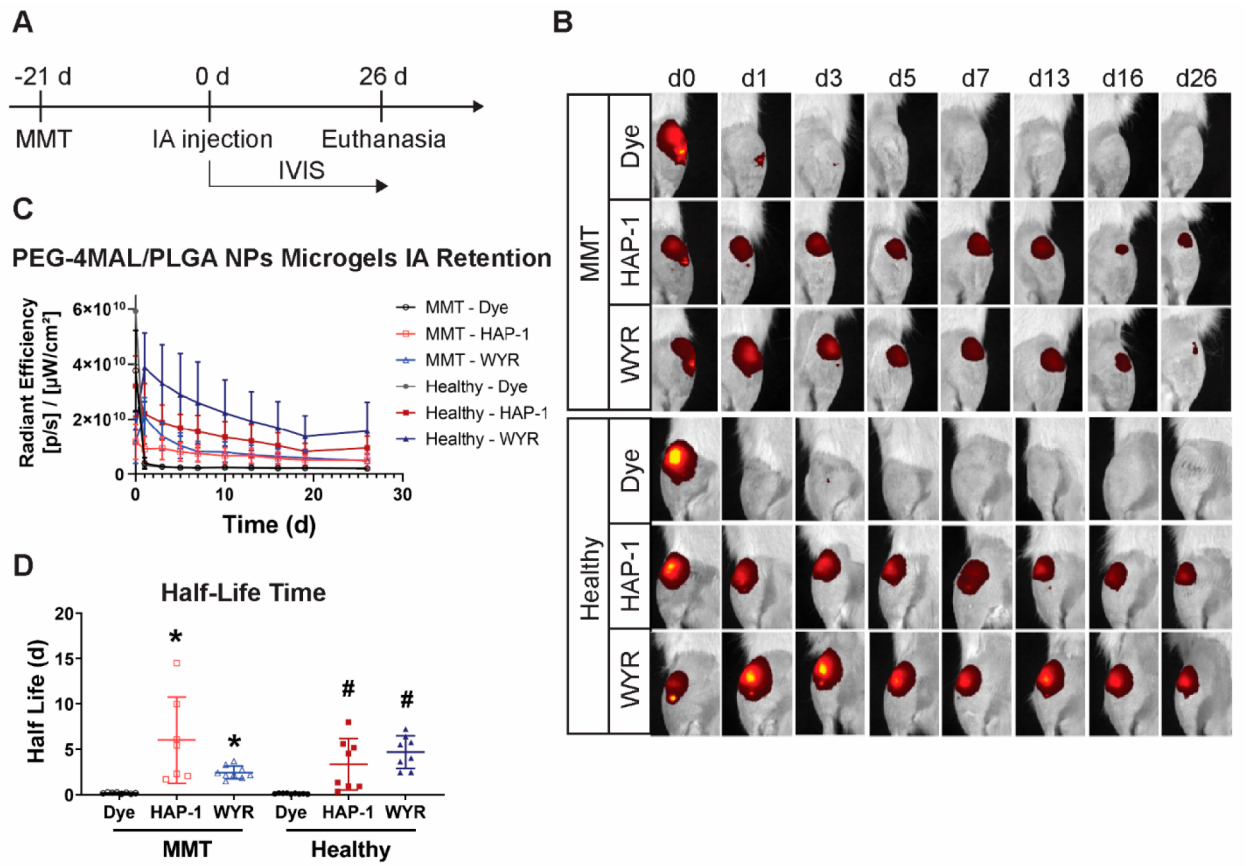

Figure 4. *In vivo* retention of peptide-functionalized PEG-4MAL nanocomposite microgels. (A) Rats received MMT surgery in the left joint; and 21 days after OA induction, they were injected bilaterally with Cy7 or WYR- or HAP-1-functionalized PEG-4MAL microgels. (B) IVIS images of healthy and OA rat knees show that free Cy7 dye is cleared from the joints faster than nanocomposite microgels. (C) Radiant efficiency of the different formulations as a function on time (mean ± SD, $n = 9$). (D) Half-life time obtained from one-phase exponential decay curve fit shows that nanocomposite PEG-4MAL microgels present a significantly higher retention time compared to free dye (mean ± SD, $n = 9$, $^{*}p < 0.05$ compared to dye in MMT joints, $^{\#}p < 0.05$ compared to dye in healthy joints).

articular cartilage surface was not technically feasible. Hence, it was not possible to determine the ability of WYR-functionalized microgels to bind to the articular cartilage *in vivo*. The development of quantitative, three-dimensional techniques would be necessary to further evaluate the fate of peptide-functionalized microgels within the joint.

4.8. Small Molecule Cargo *in Vivo* Intra-Articular Retention. We investigated the IA retention of a model small molecule encapsulated in the nanocomposite PEG-4MAL microgels, which are retained in the IA space for at least 3 weeks (Figure 4 and Figure S4). Comparable to our previous studies, IA injection of the NIR dye Cy7, used as a model small molecule, resulted in a short IA half-life time (0.25 ± 0.07 days) (Figure 7A,B). The steady state value obtained from a one-phase exponential decay demonstrates that free Cy7 dye is eliminated from the joint space (0.5 ± 0.2%), whereas PLGA NPs alone or encapsulated into any PEG-4MAL microgels formulation exhibited higher steady state values compared to that of free dye ($p < 0.0001$) (Figure 7C). PLGA NPs alone and WYR-functionalized PEG-4MAL microgels did not improve the Cy7 IA half-life time over that of free dye ($p = 0.0652$ and 0.0583, respectively) (Figure 7B). Additionally, the area under the curve (AUC) values, used as an overall metric of Cy7 IA retention, demonstrated that all PLGA NPs alone and nanocomposite PEG-4MAL microgel formulations presented a significantly larger AUC compared to that of free dye ($p < 0.022$) (Figure 7D). All together, these results suggest that nanocomposite PEG-4MAL microgels increase Cy7 retention in the joint.

5. DISCUSSION

Osteoarthritis has become one of the leading causes of disability in the world,[48] and still, there is no FDA-approved treatment to effectively slow down the progression of the disease.[3] Multiple DMOAD candidates have shown promising results in preclinical studies, but their translation into the clinic has been limited in part due to the lack of appropriate IA drug delivery systems.[49] In particular, small molecule drugs (<1 kDa) that are rapidly cleared from the joint space could greatly benefit from appropriate IA drug delivery vehicles.

Although microparticles composed of several materials have been used as IA drug delivery vehicles, to the best of our knowledge, this is the first report of nanocomposite microgels as intra-articular drug delivery vehicles. Compared to free nanosize carriers, the nanocomposite microgels presented in this study offer significant improvements in terms of IA retention. Nano-sized vehicles, such as polymeric NPs, are subjected to cell-mediated clearance and lymphatics drainage[50] and are retained in the IA space for around a week,[49] which can explain why PLGA NPs alone failed to improve the IA half-life time of the model small molecule Cy7 (Figure 7B). In contrast, our nanocomposite PEG-4MAL microgel system acts

https://dx.doi.org/10.1021/acsbiomaterials.0c00960
ACS Biomater. Sci. Eng. XXXX, XXX, XXX−XXX

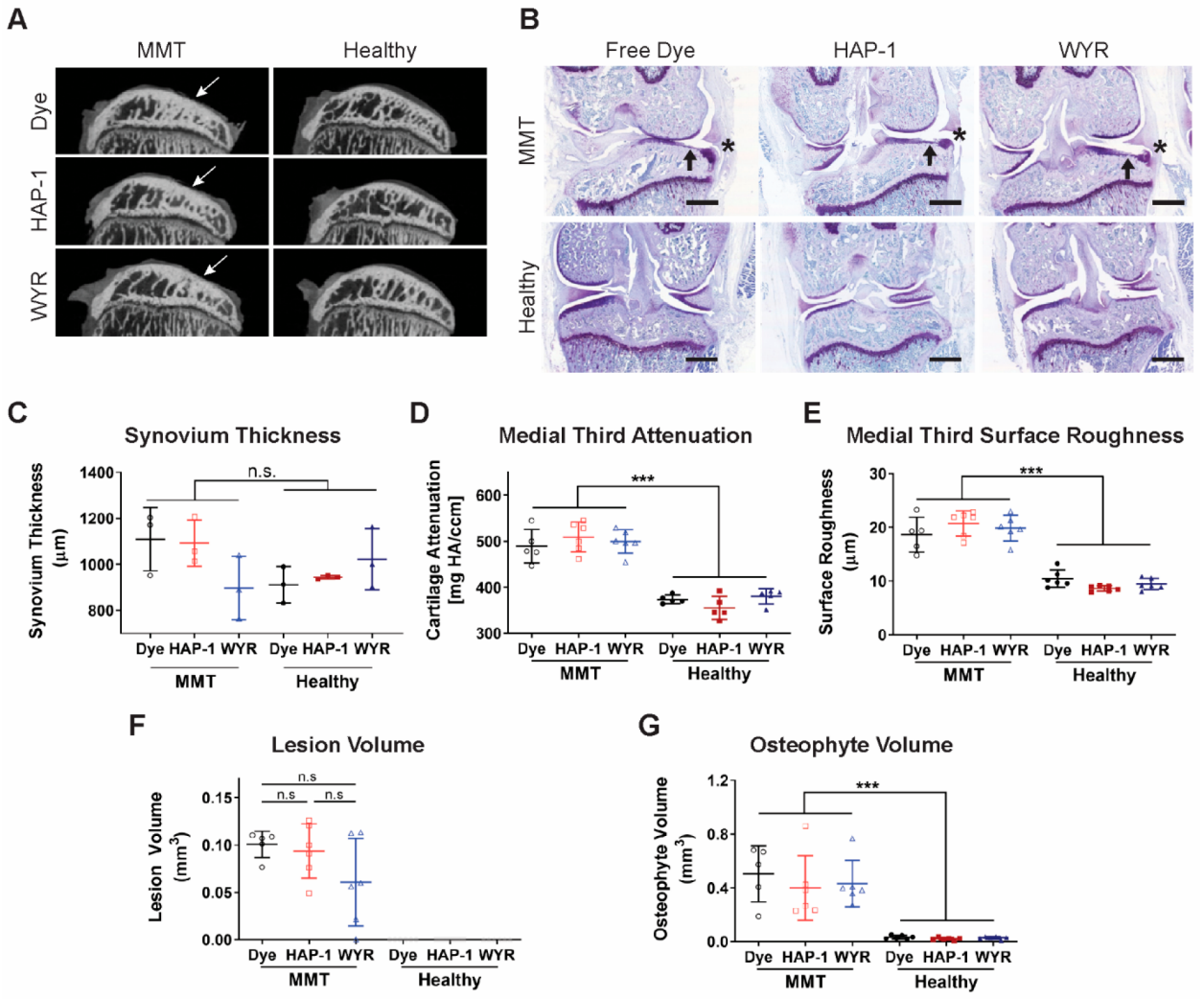

Figure 5. Effects of peptide-functionalized PEG-4MAL nanocomposite microgels on cartilage degradation, osteophyte formation, and synovial membrane thickness. (A) EPIC-μCT images of the medial tibial plateau (sagittal view) show full-thickness cartilage lesions in MMT animals (white arrows) and intact articular cartilage in all naïve groups. (B) Coronal rat knee sections stained with toluidine blue indicate the presence of cartilage lesions (black arrows) and osteophytes (asterisk). Scale bar 2 mm. (C) Synovial membrane thickness (mean ± SD, $n = 3$, $p > 0.13$). (D–G) Cartilage degradation and osteophyte formation metrics obtained *via* EPIC-μCT demonstrate that WYR- and HAP-1-functionalized PEG-4MAL nanocomposite microgels do not induce damage in naïve joints and do not worsen OA progression compared to the free dye negative control (mean ± SD, $n = 6$). (D) Medial third attenuation significantly increased in all MMT groups, indicating a higher degree of proteoglycan depletion in diseased joints (***$p < 0.0001$). 9E) Cartilage fibrillations were present in all MMT groups, as evidenced by an increase in articular cartilage surface roughness (***$p < 0.0001$). (F) Animals that received surgical induction of OA presented full-thickness cartilage lesions whose volume was not different among injected formulations ($p > 0.13$). (G) MMT surgery induces calcified osteophyte formation compared to healthy joints (***$p < 0.0001$).

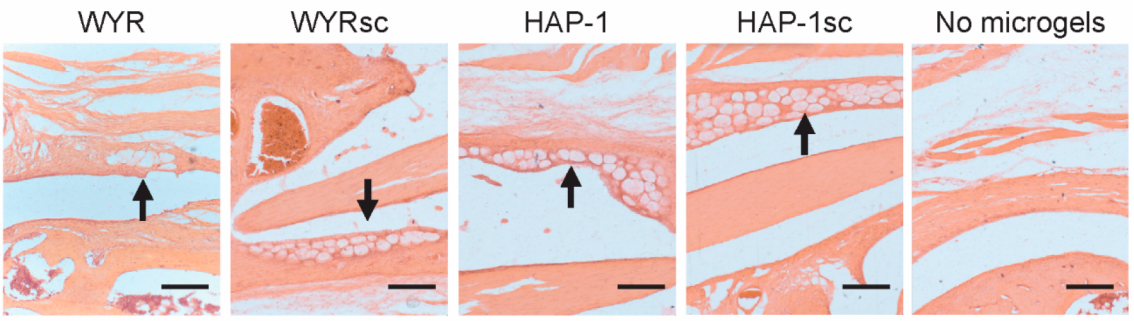

Figure 6. *In vivo* localization of peptide-functionalized PEG-4MAL nanocomposite microgels. Representative images of the synovial membrane 2 weeks after IA administration of PEG-4MAL microgels. Black arrows denote the accumulation of peptide-functionalized microgels within the synovial membrane, which appear as circular white pockets (scale bar 200 μm).

https://dx.doi.org/10.1021/acsbiomaterials.0c00960
ACS Biomater. Sci. Eng. XXXX, XXX, XXX−XXX

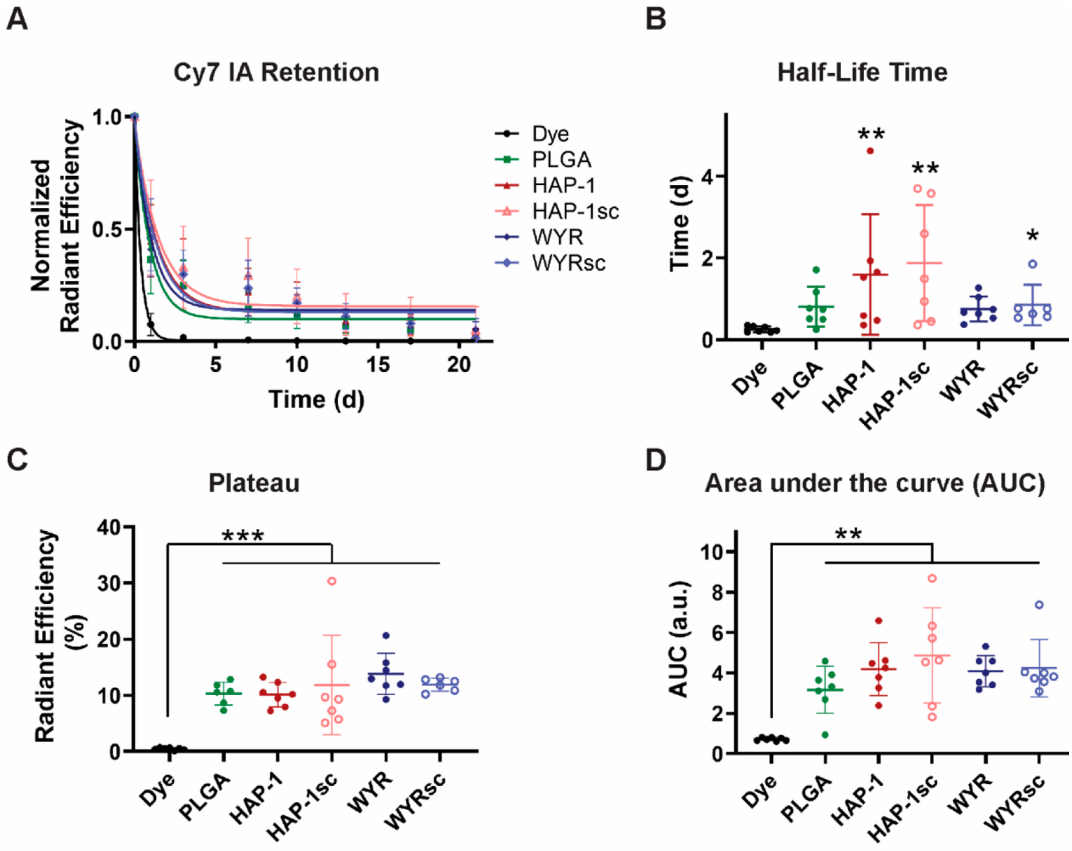

Figure 7. Intra-articular Cy7 retention time of Cy7-loaded peptide-functionalized PEG-4MAL microgels. (A) Cy7 retention profile for free dye control, PLGA NPs alone, and peptide-functionalized nanocomposite PEG-4MAL microgels (mean ± SD, n = 7, data normalized to radiant efficiency measured immediately after injection). (B) IA half-life of Cy7 dye was increased using HAP-1, HAP-1sc, and WYRsc microgels (n = 7, *p < 0.05, **p < 0.002 compared to free dye). (C) Steady state radiant efficiency values demonstrate that free dye is eliminated from the rat knee joints whereas PLGA NPs and nanocomposite PEG-4MAL microgels increased the IA retention of Cy7 (n = 7, ***p < 0.0001). (D) Area under the curve (AUC) indicates that nanocomposite microgels can significantly increase model small molecule IA retention compared to free dye control (n = 7, **p < 0.002).

as a nanoparticle depot, which could extend their IA retention for at least 3 weeks. Additionally, we demonstrated that peptide-functionalized PEG-4MAL microgel formulations accumulate in the synovial membrane. Even though the incorporation of synoviocyte-binding peptides into PEG-4MAL microgels did not seem to increase their accumulation in the synovial lining compared to scrambled peptide controls, microgels accumulation into this tissue may help improve the IA retention of loaded small molecules as observed in Figure 7. We hypothesize that microgels accumulation into the synovial membrane may help protect these structures from the IA compression and shear stresses and therefore improve their cargo IA retention time. Similar to our microgels, solid polymeric microparticles exhibit higher IA retention times compared to NPs.[3,50] However, solid polymeric microparticles resulting from IA implant wear, as well as PLGA NPs below 20 μm in diameter, have been shown to promote synovial cell infiltration and proteoglycan loss,[34,35] raising concerns regarding the use of solid microparticles as intra-articular drug delivery vehicles. The use of a softer, water-swollen material such as PEG-4MAL microgels may be advantageous in terms of joint health after long-term exposure to these carriers. In fact, Holyoak et al. recently demonstrated that bulk PEG-4MAL hydrogels containing drug-loaded PLGA NPs acting as "mechanical pillows" can protect the joint from cartilage degradation and osteophyte formation after IA injection in a mouse model of knee OA.[51] These findings align with the results presented in this study, where no microgels-induced articular cartilage damage or significant synovial membrane thickening was observed. Importantly, in contrast to the bulk hydrogels proposed by Holyoak et al., our approach supports the possibility of developing tissue-specific treatment strategies for the treatment of OA, an important feature that could minimize drugs' adverse off-target effects.

An advantage of the proposed PEG-4MAL nanocomposite microgels is the modular design that permits independent control over the hydrogel and the encapsulated NPs properties. This could allow for better control of microgel IA retention and stability. Our results demonstrate that WYR-functionalized microgels are subjected to mechanical degradation (Figure S4), which may have a negative impact on the loaded small molecules' IA retention time. This can be observed in Figure 7B, where WYR-presenting microgels were the only formulation that did not improve IA half-life time of the model small molecule Cy7 compared to the free dye control. This limitation could be addressed by changing the macromer molecular weight and/or concentration to optimize the microgels mechanical properties, while independently enhancing the small molecule release rate by tuning the encapsulated NPs properties. Moreover, the modular design of our nanocomposite microgels allows for the incorporation of other functionalities. In the present study, we conjugated

https://dx.doi.org/10.1021/acsbiomaterials.0c00960
ACS Biomater. Sci. Eng. XXXX, XXX, XXX−XXX

tissue-targeting peptides to promote microgel binding to articular cartilage and synoviocytes. Intra-articular tissue targeting has been explored to detect cartilage lesions, enhance NPs IA retention, and increase drug bioavailability into tissues of interest such as the articular cartilage.[18,19,22,25,26,32] Additionally, a better understanding of the off-target effects of some promising drug candidates[3,14−16,52−57] has evidenced the necessity of developing IA tissue-targeting drug delivery vehicles. Here, we showed that cartilage- (WYR) and synoviocyte-targeting (HAP-1) peptides can be conjugated to nanocomposite PEG-4MAL microgels to promote specific binding to articular cartilage and synovial cell lines *in vitro* and *in vivo* binding to synovial membrane and may support microgels binding to the articular cartilage.

One limitation of the microgel drug delivery vehicles is that their size may not be ideal for direct intra-cartilage drug delivery applications. In particular, cartilage extracellular matrix presents a small mesh size (60−200 nm) and high negative charge, which impair the penetration of molecules and particles into this tissue.[30,58] However, IA pharmacokinetics modeling suggests that cartilage-binding, non-penetrating particles, such as those presented in this study, may increase intra-cartilage drug concentrations compared to those of non-penetrating particles that do not present any cartilage-binding mechanism.[58] Therefore, we hypothesize that WYR-functionalized PEG-4MAL microgels could improve the effectiveness of conventional non-targeting drug delivery vehicles for OA treatment by localizing them to the articular cartilage surface. Furthermore, we expect that these microgels will enhance the therapeutic efficacy of cartilage targeting drugs by preferentially binding and delivering their cargo into damaged areas of the articular cartilage. In this regard, the proposed WYR-functionalized PEG-4MAL microgels are expected to exhibit different binding patterns as the disease progresses, probably exhibiting an optimal binding in moderate cases of OA where Coll-2 is exposed in cartilage fibrillations and lesions but not fully degraded to subchondral bone, as occurs in severe OA cases.[59]

Finally, we used PLGA NPs to fabricate nanocomposite PEG-4MAL microgels. This specific polymeric system may not be ideal to achieve efficient loading and delivery of many DMOAD candidates, which may be more compatible with liposomes, lipid NPs, or other polymeric NPs formulations.[3] Microfluidic synthesis of PEG-4MAL nanocomposite microgels could allow for the encapsulation of multiple types of particulate drug delivery vehicles. In fact, preliminary studies conducted in our laboratory suggest that solid lipid NPs and gold NPs could be effectively loaded into PEG-4MAL microgels. Additionally, our research group has previously demonstrated that PEG-based microgels are effective methods for protein and cell delivery.[36−38] The modular design of the proposed microgels offers a range of possibilities for the IA delivery of multiple types of therapeutics including synthetic small molecules, macromolecules, cells, and their combinations. Therefore, we expect our tissue-binding nanocomposite PEG-4MAL microgels to facilitate the clinical translation of DMOAD candidates as well as support the development of multitarget, combinatorial therapeutic strategies for OA treatment.

6. CONCLUSIONS

We synthesized cartilage- and synoviocyte-binging nanocomposite PEG-4MAL microgels for improved IA small molecule drug delivery. Microgels containing PLGA NPs exhibited sustained delivery of a model small molecule. Additionally, tethering of tissue-targeting peptides to PEG-4MAL microgels provided specific binding to articular cartilage and synoviocytes *in vitro*. Moreover, nanocomposite PEG-4MAL microgels were retained in the IA space for at least 3 weeks without inducing degenerative changes in the articular cartilage or promoting synovial membrane thickening. Synoviocyte-targeting PEG-4MAL microgels localized to the synovial membrane in the joint and improved the intra-articular retention time of a model small molecule. These results support the application of tissue-binding, nanocomposite PEG-4MAL microgels as promising IA drug delivery systems for OA treatment.

■ ASSOCIATED CONTENT

Supporting Information

The Supporting Information is available free of charge at https://pubs.acs.org/doi/10.1021/acsbiomaterials.0c00960.

Discussions of materials and methods used, PLGA NP distribution within PEG-4MAL microgels, and WYR-functionalized PEG-4MAL/PLGA NPs microgel *in vivo* stability and figures of chemical structures, representative confocal images, PLGA NP encapsulation into PEG-4MAL microgels, self-quenching effect, and microgel area histogram at different time points (PDF)

■ AUTHOR INFORMATION

Corresponding Authors

Andrés J. García − *Parker H. Petit Institute for Bioengineering and Biosciences and George W. Woodruff School of Mechanical Engineering, Georgia Institute of Technology, Atlanta, Georgia 30332, United States*; Email: andres.garcia@me.gatech.edu

Robert E. Guldberg − *Phil and Penny Knight Campus for Accelerating Scientific Impact, University of Oregon, Eugene, Oregon 97403-6231, United States*; Email: guldberg@uoregon.edu

Authors

Lina M. Mancipe Castro − *Parker H. Petit Institute for Bioengineering and Biosciences and George W. Woodruff School of Mechanical Engineering, Georgia Institute of Technology, Atlanta, Georgia 30332, United States*; orcid.org/0000-0002-0722-9647

Abigail Sequeira − *School of Chemical and Biomolecular Engineering, Georgia Institute of Technology, Atlanta, Georgia 30332, United States*

Complete contact information is available at: https://pubs.acs.org/10.1021/acsbiomaterials.0c00960

Funding

L.M.M.C. and A.J.G. received funding from the Department of Defense PRMRP Grant (PR171379). Also, the National Institute of Arthritis and Musculoskeletal and Skin Diseases of the National Institutes of Health, under award numbers R01AR062920 and S10OD016264, provided funding for A.J.G. All other authors have no sponsored funding to report for this project.

Notes

The authors declare no competing financial interest.

https://dx.doi.org/10.1021/acsbiomaterials.0c00960
ACS Biomater. Sci. Eng. XXXX, XXX, XXX−XXX

■ ACKNOWLEDGMENTS

The authors acknowledge Casey Vantucci, Gilad Doron, Fabrice Bernard, Marissa Ruehle and Brett Klosterhoff for their assistance with surgeries and Dr. Nick Willett for his guidance throughout the development of this work.

■ REFERENCES

(1) Kloppenburg, M.; Berenbaum, F. Osteoarthritis Year in Review 2019: Epidemiology and Therapy. *Osteoarthr. Cart.* **2020**, *28*, 242−248.

(2) Lawrence, R. C.; Felson, D. T.; Helmick, C. G.; Arnold, L. M.; Choi, H.; Deyo, R. A.; Gabriel, S.; Hirsch, R.; Hochberg, M. C.; Hunder, G. G.; Jordan, J. M.; Katz, J. N.; Kremers, H. M.; Wolfe, F. Estimates of the Prevalence of Arthritis and Other Rheumatic Conditions in the United States, Part II. *Arthritis Rheum.* **2008**, *58* (1), 26−35.

(3) Maudens, P.; Jordan, O.; Allémann, E. Recent Advances in Intra-Articular Drug Delivery Systems for Osteoarthritis Therapy. *Drug Discovery Today* **2018**, *23* (10), 1761−1775.

(4) Mora, J. C.; Przkora, R.; Cruz-Almeida, Y. Knee Osteoarthritis: Pathophysiology and Current Treatment Modalities. *J. Pain Res.* **2018**, *11*, 2189−2196.

(5) Formica, F. A.; Barreto, G.; Zenobi-Wong, M. Cartilage-Targeting Dexamethasone Prodrugs Increase the Efficacy of Dexamethasone. *J. Controlled Release* **2019**, *295*, 118−129.

(6) Janssen, M.; Timur, U. T.; Woike, N.; Welting, T. J. M.; Draaisma, G.; Gijbels, M.; van Rhijn, L. W.; Mihov, G.; Thies, J.; Emans, P. J. Celecoxib-Loaded PEA Microspheres as an Auto Regulatory Drug-Delivery System after Intra-Articular Injection. *J. Controlled Release* **2016**, *244*, 30−40.

(7) Johal, H.; Devji, T.; Schemitsch, E. H.; Bhandari, M. Viscosupplementation in Knee Osteoarthritis: Evidence Revisited. *JBJS Rev.* **2016**, *4* (4), 1−11.

(8) Jevsevar, D.; Donnelly, P.; Brown, G. A; Cummins, D. S Viscosupplementation for Osteoarthritis of the Knee: A Systematic Review of the Evidence. *J. Bone Jt. Surg.* **2015**, *97*, 2047−2060.

(9) Hunter, D. J. Viscosupplementation for Osteoarthritis of the Knee. *N. Engl. J. Med.* **2015**, *372* (26), 2569−2570.

(10) Brown, T.; Laurent, U.; Fraser. Turnover of Hyaluronan in Synovial Joints: Elimination of Labelled Hyaluronan from the Knee Joint of the Rabbit. *Exp. Physiol.* **1991**, *76* (1), 125−134.

(11) Larsen, C.; Østergaard, J.; Larsen, S. W.; Jensen, H.; Jacobsen, S.; Lindegaard, C.; Andersen, P. H. Intra-Articular Depot Formulation Principles: Role in the Management of Postoperative Pain and Arthritic Disorders. *J. Pharm. Sci.* **2008**, *97* (11), 4622−4654.

(12) Whitmire, R. E.; Wilson, D. S.; Singh, A.; Levenston, M. E.; Murthy, N.; García, A. J. Self-Assembling Nanoparticles for Intra-Articular Delivery of Anti-Inflammatory Proteins. *Biomaterials* **2012**, *33* (30), 7665−7675.

(13) Singh, A.; Agarwal, R.; Diaz-Ruiz, C. A.; Willett, N. J.; Wang, P.; Lee, L. A.; Wang, Q.; Guldberg, R. E.; García, A. J. Nano-Engineered Particles for Enhanced Intra-Articular Retention and Delivery of Proteins. *Adv. Healthcare Mater.* **2014**, *3* (10), 1562−1567.

(14) Suh, J.-K.; arøen, A.; Muzzonigro, T. S.; Disilvestro, M.; Fu, F. H. Injury and Repair of Articular Cartilage: Related Scientific Issues. *Oper. Technol. Orthop.* **1997**, *7* (4), 270−278.

(15) Hochberg, M. C.; Tive, L. A.; Abramson, S. B.; Vignon, E.; Verburg, K. M.; West, C. R.; Smith, M. D.; Hungerford, D. S. When Is Osteonecrosis Not Osteonecrosis?: Adjudication of Reported Serious Adverse Joint Events in the Tanezumab Clinical Development Program. *Arthritis Rheumatol.* **2016**, *68* (2), 382−391.

(16) Bakker, A. C.; Van De Loo, F. A. J.; Van Beuningen, H. M.; Sime, P.; Van Lent, P. L. E. M.; Van Der Kraan, P. M.; Richards, C. D.; Van Den Berg, W. B. Overexpression of Active TGF-Beta-1 in the Murine Knee Joint: Evidence for Synovial-Layer-Dependent Chondro-Osteophyte Formation. *Osteoarthr. Cartil.* **2001**, *9*, 128−136.

(17) Zhang, J.; Wang, J. H.-C. Kartogenin Induces Cartilage-like Tissue Formation in Tendon− Bone Junction. *Bone Res.* **2014**, *2* (1), 1−10.

(18) Hughes, C.; Faurholm, B.; Dell'Accio, F.; Manzo, A.; Seed, M.; Eltawil, N.; Marrelli, A.; Gould, D.; Subang, C.; Al-Kashi, A.; De Bari, C.; Winyard, P.; Chernajovsky, Y.; Nissim, A. Human Single-Chain Variable Fragment That Specifically Targets Arthritic Cartilage. *Arthritis Rheum.* **2010**, *62* (4), 1007−1016.

(19) Cho, H.; Pinkhassik, E.; David, V.; Stuart, J. M.; Hasty, K. A. Detection of Early Cartilage Damage Using Targeted Nanosomes in a Post-Traumatic Osteoarthritis Mouse Model. *Nanomedicine* **2015**, *11*, 939−946.

(20) Cho, H.; Kim, B. J.; Park, S.-H.; Hasty, K.; Min, B.-H. Noninvasive Visualization of Early Osteoarthritic Cartilage Using Targeted Nanosomes in a Destabilization of the Medial Meniscus Mouse Model. *Int. J. Nanomed.* **2018**, *13*, 1215−1224.

(21) Pi, Y.; Zhang, X.; Shi, J.; Zhu, J.; Chen, W.; Zhang, C.; Gao, W.; Zhou, C.; Ao, Y. Targeted Delivery of Non-Viral Vectors to Cartilage in Vivo Using a Chondrocyte-Homing Peptide Identified by Phage Display. *Biomaterials* **2011**, *32* (26), 6324−6332.

(22) Rothenfluh, D. A.; Bermudez, H.; O'neil, C. P.; Hubbell, J. A. Biofunctional Polymer Nanoparticles for Intra-Articular Targeting and Retention in Cartilage. *Nat. Mater.* **2008**, *7*, 248−254.

(23) Lee, L.; Buckley, C.; Blades, M. C.; Panayi, G.; George, A. J. T.; Pitzalis, C. Identification of Synovium-Specific Homing Peptides by In Vivo Phage Display Selection. *Arthritis Rheum.* **2002**, *46* (8), 2109−2120.

(24) Yang, Y.-H.; Rajaiah, R.; Ruoslahti, E.; Moudgil, K. D. Peptides Targeting Inflamed Synovial Vasculature Attenuate Autoimmune Arthritis. *Proc. Natl. Acad. Sci. U. S. A.* **2011**, *108* (31), 12857−12862.

(25) Mi, Z.; Lu, X.; Mai, J. C.; Ng, B. G.; Wang, G.; Lechman, E. R.; Watkins, S. C.; Rabinowich, H.; Robbins, P. D. Identification of a Synovial Fibroblast-Specific Protein Transduction Domain for Delivery of Apoptotic Agents to Hyperplastic Synovium. *Mol. Ther.* **2003**, *8* (2), 295−305.

(26) You, C.; Zu, J.; Liu, X.; Kong, P.; Song, C.; Wei, R.; Zhou, C.; Wang, Y.; Yan, J. Synovial Fibroblast-Targeting Liposomes Encapsulating an NF-KB-Blocking Peptide Ameliorates Zymosan-Induced Synovial Inflammation. *J. Cell. Mol. Med.* **2018**, *22* (4), 2449−2457.

(27) Vanniasinghe, A. S.; Manolios, N.; Schibeci, S.; Lakhiani, C.; Kamali-Sarvestani, E.; Sharma, R.; Kumar, V.; Moghaddam, M.; Ali, M.; Bender, V. Targeting Fibroblast-like Synovial Cells at Sites of Inflammation with Peptide Targeted Liposomes Results in Inhibition of Experimental Arthritis. *Clin. Immunol.* **2014**, *151* (1), 43−54.

(28) Wythe, S. E.; Dicara, D.; Taher, T. E. I.; Finucane, C. M.; Jones, R.; Bombardieri, M.; Man, Y. K. S.; Nissim, A.; Mather, S. J.; Chernajovsky, Y.; Pitzalis, C. Targeted Delivery of Cytokine Therapy to Rheumatoid Tissue by a Synovial Targeting Peptide. *Ann. Rheum. Dis.* **2013**, *72*, 129−135.

(29) Meka, R. R.; Venkatesha, S. H.; Moudgil, K. D. Peptide-Directed Liposomal Delivery Improves the Therapeutic Index of an Immunomodulatory Cytokine in Controlling Autoimmune Arthritis. *J. Controlled Release* **2018**, *286*, 279−288.

(30) Brown, S. B.; Wang, L.; Jungels, R. R.; Sharma, B. Effects of Cartilage-Targeting Moieties on Nanoparticle Biodistribution in Healthy and Osteoarthritic Joints. *Acta Biomater.* **2020**, *101*, 469−483.

(31) Hu, H.-Y.; Lim, N.-H.; Juretschke, H.-P.; Ding-Pfennigdorff, D.; Florian, P.; Kohlmann, M.; Kandira, A.; Peter Von Kries, J.; Saas, J.; Rudolphi, K. A.; Wendt, K. U.; Nagase, H.; Plettenburg, O.; Nazare, M.; Schultz, C. In Vivo Visualization of Osteoarthritic Hypertrophic Lesions. *Chem. Sci.* **2015**, *6*, 6256−6261.

(32) Chen, H.; Qin, Z.; Zhao, J.; He, Y.; Ren, E.; Zhu, Y.; Liu, G.; Mao, C.; Zheng, L. Cartilage-Targeting and Dual MMP-13/PH Responsive Theranostic Nanoprobes for Osteoarthritis Imaging and Precision Therapy. *Biomaterials* **2019**, *225*, 119520.

(33) Yi, W.; Zhou, H.; Li, A.; Yuan, Y.; Guo, Y.; Li, P.; Qi, B.; Xiao, Y.; Yu, A.; Hu, X. A NIR-II Fluorescent Probe for Articular Cartilage

https://dx.doi.org/10.1021/acsbiomaterials.0c00960
ACS Biomater. Sci. Eng. XXXX, XXX, XXX−XXX

Degeneration Imaging and Osteoarthritis Detection. *Biomater. Sci.* **2019**, *7*, 1043−1051.
(34) Park, D. Y.; Min, B. H.; Kim, D. W.; Song, B. R.; Kim, M.; Kim, Y. J. Polyethylene Wear Particles Play a Role in Development of Osteoarthritis via Detrimental Effects on Cartilage, Meniscus, and Synovium. *Osteoarthr. Cartil.* **2013**, *21* (12), 2021−2029.
(35) Liggins, R.T.; Cruz, T.; Min, W.; Liang, L.; Hunter, W.L.; Burt, H.M. Intra-Articular Treatment of Arthritis with Microsphere Formulations of Paclitaxel: Biocompatibility and Efficacy Determinations in Rabbits. *Inflammation Res.* **2004**, *53* (8), 365−372.
(36) Headen, D. M.; Aubry, G.; Lu, H.; García, A. J. Microfluidic-Based Generation of Size-Controlled, Biofunctionalized Synthetic Polymer Microgels for Cell Encapsulation. *Adv. Mater.* **2014**, *26* (19), 3003−3008.
(37) Foster, G. A.; Headen, D. M.; González-García, C.; Salmerón-Sánchez, M.; Shirwan, H.; García, A. J. Protease-Degradable Microgels for Protein Delivery for Vascularization. *Biomaterials* **2017**, *113*, 170−175.
(38) Headen, D. M.; García, J. R.; García, A. J. Parallel Droplet Microfluidics for High Throughput Cell Encapsulation and Synthetic Microgel Generation. *Microsystems Nanoeng.* **2018**, *4* (17076), 1−9.
(39) Thote, T.; Lin, A.S.P.; Raji, Y.; Moran, S.; Stevens, H.Y.; Hart, M.; Kamath, R.V.; Guldberg, R.E.; Willett, N.J. Localized 3D Analysis of Cartilage Composition and Morphology in Small Animal Models of Joint Degeneration. *Osteoarthr. Cartil.* **2013**, *21*, 1132−1141.
(40) Xie, L.; Lin, A. S. P.; Levenston, M. E.; Guldberg, R. E. Quantitative Assessment of Articular Cartilage Morphology via EPIC-MCT. *Osteoarthr. Cartil.* **2009**, *17* (3), 313−320.
(41) Reece, D. S.; Thote, T.; Lin, A. S. P.; Willett, N. J.; Guldberg, R. E. Contrast Enhanced MCT Imaging of Early Articular Changes in a Pre-Clinical Model of Osteoarthritis. *Osteoarthr. Cartil.* **2018**, *26* (1), 118−127.
(42) Fredenberg, S.; Wahlgren, M.; Reslow, M.; Axelsson, A. The Mechanisms of Drug Release in Poly(Lactic-Co-Glycolic Acid)-Based Drug Delivery Systems - A Review. *Int. J. Pharm.* **2011**, *415*, 34−52.
(43) Fu, Y.; Kao, W. J. Drug Release Kinetics and Transport Mechanisms of Non-Degradable and Degradable Polymeric Delivery Systems. *Expert Opin. Drug Delivery* **2010**, *7* (4), 429−444.
(44) Zhegalova, N. G.; He, S.; Zhou, H.; Kim, D. M.; Berezin, M. Y. Minimization of Self-Quenching Fluorescence on Dyes Conjugated to Biomolecules with Multiple Labeling Sites via Asymmetrically Charged NIR Fluorophores. *Contrast Media Mol. Imaging* **2014**, *9* (5), 355−362.
(45) Tsai, L. C.; Cooper, E. S.; Hetzendorfer, K. M.; Warren, G. L.; Chang, Y. H.; Willett, N. J. Effects of Treadmill Running and Limb Immobilization on Knee Cartilage Degeneration and Locomotor Joint Kinematics in Rats Following Knee Meniscal Transection. *Osteoarthr. Cartil.* **2019**, *27* (12), 1851−1859.
(46) Bédouet, L.; Pascale, F.; Moine, L.; Wassef, M.; Ghegediban, S. H.; Nguyen, V.-N.; Bonneau, M.; Labarre, D.; Laurent, A. Intra-Articular Fate of Degradable Poly(Ethyleneglycol)-Hydrogel Microspheres as Carriers for Sustained Drug Delivery. *Int. J. Pharm.* **2013**, *456*, 536−544.
(47) Willett, N. J.; Thote, T.; Lin, A. S.; Moran, S.; Raji, Y.; Sridaran, S.; Stevens, H. Y.; Guldberg, R. E. Intra-Articular Injection of Micronized Dehydrated Human Amnion/Chorion Membrane Attenuates Osteoarthritis Development. *Arthritis Res. Ther.* **2014**, *16* (1), R47.
(48) Chen, D.; Shen, J.; Zhao, W.; Wang, T.; Han, L.; Hamilton, J. L.; Im, H.-J. Osteoarthritis: Toward a Comprehensive Understanding of Pathological Mechanism. *Bone Res.* **2017**, *5* (16044), 1−13.
(49) Brown, S.; Kumar, S.; Sharma, B. Intra-Articular Targeting of Nanomaterials for the Treatment of Osteoarthritis. *Acta Biomater.* **2019**, *93*, 239−257.
(50) Pradal, J.; Maudens, P.; Gabay, C.; Seemayer, C. A.; Jordan, O.; Allémann, E. Effect of Particle Size on the Biodistribution of Nano- and Microparticles Following Intra-Articular Injection in Mice. *Int. J. Pharm.* **2016**, *498*, 119−129.
(51) Holyoak, D. T.; Wheeler, T. A.; van der Meulen, M. C.; Singh, A. Injectable Mechanical Pillows for Attenuation of Load-Induced Post-Traumatic Osteoarthritis. *Regen. Biomater.* **2019**, *6*, 211−219.
(52) Geiger, B. C.; Grodzinsky, A. J.; Hammond, P. Designing Drug Delivery Systems for Articular Jointst. *Chem. Eng. Prog.* **2018**, *114* (5), 46−51.
(53) Kang, M. L.; Ko, J.-Y.; Kim, J. E.; Im, G.-I. Intra-Articular Delivery of Kartogenin-Conjugated Chitosan Nano/ Microparticles for Cartilage Regeneration. *Biomaterials* **2014**, *35*, 9984−9994.
(54) Zhang, J.; Wang, J. H. C. Kartogenin Induces Cartilage-like Tissue Formation in Tendon-Bone Junction. *Bone Res.* **2014**, *2* (1), 12−17.
(55) Shi, D.; Xu, X.; Ye, Y.; Song, K.; Cheng, Y.; Di, J.; Hu, Q.; Li, J.; Ju, H.; Jiang, Q.; Gu, Z. Photo-Cross-Linked Scaffold with Kartogenin- Encapsulated Nanoparticles for Cartilage Regeneration. *ACS Nano* **2016**, *10*, 1292−1299.
(56) Li, X.; Ding, J.; Zhang, Z.; Yang, M.; Yu, J.; Wang, J.; Chang, F.; Chen, X. Kartogenin-Incorporated Thermogel Supports Stem Cells for Significant Cartilage Regeneration. *ACS Appl. Mater. Interfaces* **2016**, *8*, 5148−5159.
(57) Mohan, G.; Magnitsky, S.; Melkus, G.; Subburaj, K.; Kazakia, G.; Burghardt, A. J.; Dang, A.; Lane, N. E.; Majumdar, S. Kartogenin Treatment Prevented Joint Degeneration in a Rodent Model of Osteoarthritis: A Pilot Study. *J. Orthop. Res.* **2016**, *34* (10), 1780−1789.
(58) Bajpayee, A. G.; Grodzinsky, A. J. Cartilage-Targeting Drug Delivery: Can Electrostatic Interactions Help? *Nat. Rev. Rheumatol.* **2017**, *13* (3), 183−193.
(59) Loeser, R. F.; Goldring, S. R.; Scanzello, C. R.; Goldring, M. B. Osteoarthritis: A Disease of the Joint as an Organ. *Arthritis Rheum.* **2012**, *64* (6), 1697−1707.

https://dx.doi.org/10.1021/acsbiomaterials.0c00960
ACS Biomater. Sci. Eng. XXXX, XXX, XXX−XXX

Title

Biomaterial encapsulation of human mesenchymal stromal cells modulates paracrine signaling response and enhances efficacy for treatment of established osteoarthritis

Authorship

Jay M. McKinney[1,2,3], Krishna A. Pucha[1], Thanh N. Doan[1,2], Lanfang Wang[4], Laura D. Weinstock[5,6], Benjamin T. Tignor[3], Kelsey L. Fowle[3], Rebecca D. Levit[4], Levi B. Wood[3,5,6*†], Nick J. Willett[1,2,3,5*†]

† Equally contributing senior authors.

[1]Research Division, VA Medical Center, Atlanta, GA
[2]Department of Orthopaedics, Emory University, Atlanta, GA
[3]Wallace H. Coulter Department of Biomedical Engineering, Georgia Institute of Technology and Emory University, Atlanta, GA
[4]Department of Medicine, Division of Cardiology, Emory University, Atlanta, GA
[5]Parker H. Petit Institute for Bioengineering and Bioscience, Georgia Institute of Technology, Atlanta, GA
[6]George W. Woodruff School of Mechanical Engineering, Georgia Institute of Technology, Atlanta, GA

*** Correspondence**

Nick J. Willett
Research Division, VA Medical Center
1670 Clairmont Rd
Decatur, GA 30033

Levi B. Wood
Georgia Institute of Technology
315 Ferst Dr. NW
Atlanta, GA 30332

Abstract

Mesenchymal stromal cells (MSCs) have shown promise as a treatment for osteoarthritis (OA); however, effective translation has been limited by numerous factors ranging from high variability and heterogeneity of hMSCs, to suboptimal delivery strategies, to poor understanding of critical quality and potency attributes. The objective of the current study was to assess the effects of biomaterial encapsulation in alginate microcapsules on human MSC (hMSC) secretion of immunomodulatory cytokines in an OA microenvironment and therapeutic efficacy in treating established OA. Lewis rats underwent Medial Meniscal Transection (MMT) surgery to induce OA. Three weeks post-surgery, after OA was established, rats received intra-articular injections of either encapsulated hMSCs or controls (saline, empty capsules, or non-encapsulated hMSCs). Six weeks post-surgery, microstructural changes in the knee joint were quantified using contrast enhanced microCT. Encapsulated hMSCs attenuated progression of OA including articular cartilage degeneration (swelling and cartilage loss) and subchondral bone remodeling (thickening and hardening). A multiplexed immunoassay panel (41 cytokines) was used to profile the *in vitro* secretome of encapsulated and non-encapsulated hMSCs in response to IL-1□, a key cytokine involved in OA. Non-encapsulated hMSCs showed an indiscriminate increase in all cytokines in response to IL-1□ while encapsulated hMSCs showed a highly targeted secretory response with increased expression of some pro-inflammatory (IL-1β, IL-6, IL-7, IL-8), anti-inflammatory (IL-1RA), and chemotactic (G-CSF, MDC, IP10) cytokines. These data show that biomaterial encapsulation using alginate microcapsules can modulate hMSC paracrine signaling in response to OA cytokines and enhance the therapeutic efficacy of the hMSCs in treating established OA.

Introduction

Osteoarthritis (OA) is the most common chronic disease of synovial joints and is defined pathologically by degeneration of articular cartilage consisting of proteoglycan loss, chondrocyte hypertrophy, matrix fibrillation, surface erosion and lesion formation, and eventually full-thickness loss of articular cartilage resulting in bone-on-bone contact.[1,2] OA currently impacts over 242 million people worldwide and incidence is expected to increase with rising global life expectancy.[3,4] OA was long viewed as a degenerative disease resulting from normal body wear and tear, but the general understanding of the underlying mechanisms of OA has now expanded and it is now viewed as a multifactorial disorder that also consists of low-grade chronic inflammation.[5-7] OA inflammation is part of a positive feedback loop that can activate chondrocytes, synoviocytes, subchondral bone cells, and other joint resident cells to secrete an array of cytokines, chemokines, and catabolic enzymes in OA.[8] This process leads to dysregulated homeostasis of inflammatory factors including enhanced pro-inflammatory cytokine secretion [tumor necrosis factor (TNF)-α, interleukin (IL)-6, and IL-1β], which can lead to increased catabolism of the articular cartilage and increased matrix metalloproteinases (MMP) production.[9,10] Furthermore, imbalances in anti-inflammatory cytokines [IL-1 receptor antagonist (IL-1RA), IL-4, IL-10, and IL-13] lead to attenuated chondroprotective effects and further exacerbation of OA.[11-13] Chemokines further amplify this feedback system by stimulating neovascularization and the influx of inflammatory cells which further propagate the inflammatory response.[10,14] Clinically, dysregulation of inflammatory cytokine balance has been shown to have a significant correlation with increased levels of knee pain.[15] These findings have motivated the development of therapeutics that modulate the OA inflammatory disease state. Mesenchymal stromal cells (MSCs) are a promising treatment for targeting OA as they possess immunomodulatory and anti-inflammatory properties in addition to the capacity to regenerate numerous tissue types.

MSCs can be isolated from most human tissues and organs and are defined by characteristic cell surface markers and multilineage differentiation capabilities.[16,17] While these cells do have the ability to differentiate into chondrogenic, osteogenic, and adipogenic lineages, there has been increasing interest in the paracrine signaling capabilities of MSCs as a means for their therapeutic effect in OA.[18-21] MSC secreted factors can create a regenerative niche through numerous mechanisms, including the recruitment of additional stem and progenitor cells along with immunomodulatory effects. MSCs have the capacity to secrete an array of immunosuppressive factors [indoleamine-pyrrole 2,3-dioxygenase(IDO), TNFα-stimulated gene-6(TSG6), nitric oxide (NO), IL-10, galectins, prostaglandin E_2 (PGE2), and transforming growth factor (TGF)-*β*] to modulate the local inflammatory environment.[22,23] These MSC paracrine mechanisms also maintain the capacity to regulate inflammatory cell action through suppression of T-cells (proliferation and chemotaxis) and of B-cells (differentiation and chemotaxis) to further aid in modulating the inflammatory response.[23-25] MSCs often act as sensors of the local environment and their secretome changes in response to local environmental signals; one promising approach for providing a control point for the MSC secretome is through the use of three-dimensional (3D) biomaterial constructs to deliver MSCs.

Material-based strategies have been shown to have a substantial impact on the immunomodulatory and regenerative properties of MSCs.[26,27] The 3D environment constructed by biomaterials is well documented as a major determinant affecting MSC fate and function, and these 3D environments better replicate *in vivo* environments and cellular responses relative to two-dimensional (2D) culture systems.[28-30] While the effects of a 3D microenvironment on MSCs has been readily studied, prior research has often focused on the effects of material-based strategies on MSC proliferation and differentiation. Encapsulation of MSCs within bulk hydrogels is a widely used strategy which can mimic native environments and allow for matrix-based signals to the cells.[30] Biomaterial encapsulation of MSCs has been shown to increase multipotency and rates of proliferation.[27-29] Initial work on the effects of hydrogel encapsulation

on MSC immunomodulation demonstrated reduced MSC secretion of pro-inflammatory cytokines (TNF-α) and enhanced secretion of anti-inflammatory cytokines (PGE-2).[31] Many of these same signals can be provided by cellular encapsulation in micro-sized hydrogel capsules which additionally allow for shorter diffusion distances for biochemical signals and a minimally invasive injectable means of administration.[32] Furthermore, microencapsulation of MSCs has shown enhanced potential for suppressing proinflammatory activity of macrophages and suppressing the proliferation of peripheral blood mononuclear cells (PBMCs).[33-35] The role biomaterials play in modulating MSC paracrine activities in the chronic inflammatory environment of OA remains understudied, especially *in vivo*.

In the current study, sodium alginate cellular encapsulation was used to modulate the paracrine signaling properties of human MSCs (hMSCs). Alginate is a heteropolysaccharide which is used in many biomedical applications; it is highly tailorable and can be modified to yield variable levels of biodegradability, mechanical strength, and cellular affinity, among numerous other properties.[36] In previous work we utilized an alginate microencapsulation system with 1% ultrapure low viscosity sodium alginate crosslinked with $BaCl_2$ to create microcapsules approximately 150 μm in diameter.[18,37,38] These studies demonstrated that this encapsulation system permits molecules < 80 kDa to diffuse in and out while preventing the MSCs from integrating with the host tissue.[37] Furthermore, in an OA rat model we showed that encapsulated hMSC viability following intra-articular injection was ~ 9 days while non-encapsulated hMSC remained viable for ~ 7 days.[18] We also demonstrated that intra-articular injection of encapsulated hMSCs ameliorated the onset of post traumatic OA.[18] To further explore the utility of this encapsulation system, it was used in the current study to analyze the therapeutic efficacy of encapsulated hMSC in established OA.

While pre-clinical OA studies have shown MSC treatment can be chondroprotective (attenuating cartilage breakdown), MSCs have yet to translate into a consistently reliable and effective clinical therapy.[39] A distinct gap in the pre-clinical literature is that the majority of the work studying MSC efficacy in OA focuses on preventing disease development; however, in clinical scenarios, patients that are treated with cell therapies typically have already developed OA when they seek treatment.[22] There is a fundamental difference in the local environment, and likely the necessary therapeutic mechanism of action, between an injured joint prior to OA development (but primed to develop OA) and a joint where OA is established. Thus, there is a substantial gap in our understanding of the therapeutic efficacy of MSCs in delaying further disease progression once OA is established. The objective of the current study was to assess the effects of biomaterial encapsulation in alginate microcapsules on hMSC secretion of immunomodulatory cytokines in an OA microenvironment and therapeutic efficacy in treating established OA.

Materials and methods

Cell culture

Bone marrow derived hMSCs, obtained from the Emory Personalized Cell Therapy Core (EPIC) facility at Emory University, were cultured in complete minimum essential medium Eagle-α modification (α-MEM; 12561; Gibco, Carlsbad, CA, USA) supplemented with 10% heat-inactivated fetal bovine serum (FBS; S11110H; Atlanta Biologicals, Lawrenceville, GA, USA), 2 mM L-glutamine (SH3003401; HyClone, Logan, UT, USA), and 100 μg/mL penicillin/streptomycin (P/S; B21110; Atlanta Biologicals, Lawrenceville, GA, USA), and sub-cultured at 80% confluency. The three criteria for hMSC designation – tri-lineage differentiation, surface marker phenotyping, and adherence to plastic – were confirmed in a previous study.[18] Briefly, differentiation was confirmed for chondrogenesis, adipogenesis, and osteogenesis; hMSC phenotyping confirmed cells were positive for MSC markers, including CD73, CD90, and CD105, and negative for hematopoietic markers, including CD45, CD34, CD11b, CD79A, and

HLA-DR; expansion of hMSCs relied on adherence to plastic tissue culture plates up to passage 4.

Cell encapsulation

An electrostatic encapsulator was used to encapsulate 5×10^5 cells/mL hMSCs (passage 4) suspended in 2% ultrapure low viscosity sodium alginate LVG (UP-LVG; 4200006; PRONOVA™ UP LVG; NovaMatrix, Sandvika, Norway) using the following parameters: 0.2 µm nozzle, 2.5 mL/h flow rate, and 7 kV voltage. Capsules were gelled in 50 mM $BaCl_2$ and subsequently washed two times with 0.9% saline (NaCl), and re-suspended to the appropriate dose in complete α-MEM (*in vitro* hMSC culture model) or saline (*in vivo* MMT model). A Live/Dead™ Viability/Cytotoxicity kit (L3224; Invitrogen, Carlsbad, CA, USA) was used to assess encapsulated hMSC viability. The average diameter of encapsulated hMSC microspheres was 144 ± 16 µm, as previously quantified.[18] Empty capsules were manufactured using the same procedure, without the addition of hMSCs, and yielded similar size.

In vivo MMT model

All animal care and experiments were conducted in accordance with the institutional guidelines and approved by the Atlanta Veteran Affairs Medical Center (VAMC) with experimental procedures approved by the Atlanta VAMC Institutional Animal Care and Use Committee (IACUC). Weight-matched (300-350 g) male Lewis rats (strain code: 004; Charles River, Wilmington, MA, USA) were used for the medial meniscal transection (MMT) model used to induce OA in the current study.[40] Briefly, animals were anesthetized under isoflurane and injected subcutaneously with 1 mg/kg sustained-release (SR) buprenorphine (ZooPharm, Windsor, CO, USA). The skin over the medial aspect of the left femoro-tibial joint was sterilized, and a blunt dissection was used to expose the medial collateral ligament (MCL) and transect it to expose the meniscus. A full-thickness cut was made through the meniscus at its narrowest point followed by soft tissue re-approximation and closure using 4.0 Vicryl sutures and wound clips for skin closure. Sham surgery involved MCL transection, with no transection of the meniscus, followed by closure of the skin. Intra-articular injections were performed at three weeks post-surgery, the time point in the MMT model corresponding to the presentation of OA-associated cartilage degeneration and osteophyte formation.[40,41] Intra-articular injections were performed using a 25-gauge needle and included: hanks balanced salt solution (HBSS; MMT/Saline; n = 7), empty sodium alginate capsules in HBSS (MMT/Empty Caps; n = 7), 5×10^5 non-encapsulated hMSC in HBSS (MMT/hMSC; n = 8) and 5×10^5 encapsulated hMSC in HBSS (MMT/Encap hMSC; n=7). Rats in the MMT/Encap hMSC were injected within two hours of hMSC encapsulation (cells were stored at 4°C until injection). Sham (n = 6) animals did not receive any injection post-surgery. At six weeks post-surgery, animals were euthanized by CO_2 inhalation. Left hind limbs were collected and fixed in 10% neutral buffered formalin for a two-day minimum before further sample preparation.

microCT analysis of articular joint parameters

Prior to scanning, all muscle and connective tissue from collected hind limbs was removed, the femur was disarticulated from the tibia, and all peripheral connective tissue surrounding the joint was removed to expose the articular cartilage of the medial tibial plateau. Tibiae were immersed in 30% (diluted in PBS) hexabrix 320 contrast reagent (NDC 67684-5505-5, Guerbet, Villepinte, France) at 37°C for 30 minutes before being scanned.[42] All samples were scanned using equilibrium partitioning of an ionic contrast agent based micro-computed tomography (EPIC-µCT; microCT) through the use of a Scanco µCT 40 (Scanco Medical, Brüttisellen, Switzerland) using the following parameters: 45 kVp, 177 µA, 200 ms integration time, isotropic 16 µm voxel size, and ~27 min scan time.[42] Scans were read out as 2D tomograms which were subsequently orthogonally transposed to yield 3D reconstructions for all scanned samples. All

microCT parameters (articular cartilage, osteophyte, and subchondral bone) were evaluated as previously described.[43,44] For cartilage parameters, thresholding of 110 - 435 mg hydroxyapatite per cubic centimeter (mg HA/cm^3) was used to isolate the cartilage from the surrounding air and bone. Furthermore, for bone parameters, thresholds of 435 - 1200 mg HA/cm^3 were implemented to isolate bone from the overlying cartilage. Coronal sections were both evaluated along the full length of the cartilage surface (total) and in third (medial, central, and lateral) regions of the medial tibial condyle. For articular cartilage, volume, thickness, and attenuation parameters were quantified. Attenuation is inversely related to sulfated glycosaminoglycans (sGAG) content.[42] In OA, sGAG concentration in articular cartilage decreases due to degradation, creating a gradient which leads to an increased hexabrix concentration in the cartilage. High hexabrix and low sGAG levels (increased sGAG loss) correspond to a higher attenuation value. In addition to microCT analysis of articular cartilage, osteophyte volumes found on the most medial aspect of the medial tibial plateau were evaluated for their cartilaginous and mineralized portions. Additionally, subchondral bone was evaluated for volume, thickness, and attenuation (indirect measure of bone mineral density) along the total, medial, central, and lateral regions, similar to the approach used for articular cartilage analysis.

Surface roughness of articular cartilage

Articular cartilage surface roughness and exposed bone surface area (full thickness lesion surface area) were quantified using a custom MATLAB script, *SurfaceRoughness* function.[45] Briefly, coronal sections from the Scanco µCT 40 were exported as 2D TIFF images and imported into MATLAB R2016a (MathWorks, Natick, MA, USA). A custom code created a 3D surface with these images by scanning section images sequentially and consolidating them. This 3D surface was fitted along a computationally generated 3D polynomial surface, unique for each sample imported, which was fourth order along the ventral-dorsal axis and second order along the medial-lateral axis. Surface roughness was quantified as the root mean square of differences between the 3D surface created with the exported TIFF images and the polynomial fitted surface. Exposed bone (full thickness lesion surface area) was quantified as root mean square of area where the difference between the 3D cartilage surface and 3D bone surface was ≤ three pixels (i.e. no presence of any articular cartilage). Threshold values of 110 - 435 mg HA/cm^3 were used to separate cartilage from air and the underlying subchondral bone and threshold values of 435 - 1200 mg HA/cm^3 were used to isolate bone from overlying cartilage (matching microCT thresholds). All MATLAB analyses were performed along the total surface and in regions (medial, central, lateral) of the medial tibial plateau, similar to the microCT analyses.

Histology

To prepare bone samples for sectioning, tibiae were decalcified in Immunocal (SKU-1414-32; StatLab, McKinney, TX, USA) for 14-21 days. Dehydrated samples were processed into paraffin-embedded blocks, sectioned at 5 µm thickness and stained. Hematoxylin and eosin (H&E; Fisherbrand™ 517-28-2, Waltham, MA, USA), and Safranin O and fast green (Saf-O; Electron Microscopy Sciences® 20800, Hatfield, PA, USA) were used to stain all study samples in accordance with manufacturer protocols. For all samples, a single representative image was selected for H&E and Saf-O (serial sections).

In vitro hMSC cytokine analysis model

Passage 4 hMSCs, matching donor with *in vivo* MMT model, were utilized *in vitro*. Non-encapsulated hMSCs were sub-cultured to 80% confluency in complete α-MEM medium in 12-well plates and cultured at 37°C, 5% CO_2. For encapsulated hMSCs, immediately following encapsulation and washing, cells were placed in treatment medium (unstimulated or stimulated) in 12-well plates at 37°C, 5% CO_2. Unstimulated media (+CTRL) contained complete α-MEM

medium only and stimulated media (+IL-1β) contained 20 ng/mL IL-1β (FHC05510, Promega, Madison, WI, USA) in complete α-MEM medium. IL-1β was used to model the OA inflammatory environment in the current study as it is a major pro-inflammatory modulator in OA.[9] IL-1β concentration (and group sample size) were selected based on prior experiments and preliminary data.[46,47] Stimulated and unstimulated media were added to non-encapsulated and encapsulated hMSCs at day 0 (n=6) followed by a 24-hour stimulation period with media collection at the end point for stimulation for the four study groups. Additional filtering steps were implemented in order to remove encapsulated hMSCs by passing collected media through a 9 μm filter. Samples were stored at -80°C until Luminex analysis was performed. Loaded samples (2.03 μL) were determined to be within the linear range of detection of the MAGPIX (MAGPIX-XPON4.1-CEIVD; EMD Millipore Corporation, Burlington, MA, USA) system. Cytokines were quantified using a bead based multiplex immunoassay, Luminex Cytokine/Chemokine 41 Plex Kit (HCYTMAG-60K-PX41; EMD Millipore Corporation, Burlington, MA, USA). Median fluorescent intensity values were read out using Luminex xPONENT software V4.3 in the MAGPIX system. Background subtraction was performed on non-stimulated and stimulated conditions using read out values from media only and 20 ng/mL IL-1β supplemented media, respectively.

Partial Least Squares Regression (PLSR)

Partial least squares discriminant analysis (PLSDA) was performed in MATLAB (Mathworks, Natick, MA, USA) using a function written by Cleiton Nunes (Mathworks File Exchange).[48] This approach accounts for the multivariate nature of the data without overfitting.[49,50] Prior to inputting the data into the algorithm, all cytokines were z-scored [(observed - mean) / standard deviation]. For articular cartilage, osteophyte, and subchondral bone *in vivo* analyses, total and medial microCT parameters were used as the independent variables and the five separate treatment groups were used as the outcome variables. For cytokine analysis of the *in vitro* cell culture model, cytokine measurements were used as the independent variables and the four individual treatment groups were used as the outcome variable. Latent variables (LV) in a multidimensional space (dimensionality varied by number of independent input variables) were defined and the two primary LVs were used for orthogonal rotation to best separate groups in the new plane defined by LV1 and LV2 (Fig. 1a). In the *in vitro* cell culture model orthogonality between encapsulated hMSCs (LV1 horizontal axis) and non-encapsulated hMSCs (LV2 vertical access) was confirmed via dot product (LV1 • LV2 = -1.059 x 10-16 ~ 0). Loadings plots were generated from this analysis and display the relative importance of input variables (microCT parameters or cytokines) in contributing to the final composite values (scores) for each sample (Fig. 1b&c). Error bars on each cytokine (in the loadings plots) were computed by PLSR model regeneration using iterative (1000 iterations) leave one out cross validation (LOOCV). To further confirm significant differences between groups assessed in PLSDA, the true differences in centroids (center of mass) of all groups were compared against the differences computed by a random distribution obtained by permuting the group labels 100 times. For each test, true group assignment showed $p_{permute}<0.05$ compared to the randomly permuted distribution, further confirming the validity of the data.

Statistics

All data is presented as mean ± standard deviation (SD). Significance for all microCT parameters was determined with one-way ANOVA with post hoc Tukey honest test for articular cartilage and subchondral bone parameters. Bonferroni correction was used for post hoc analysis for the exposed bone and osteophyte parameters due to their nonparametric nature. For all PLSDA scores plots, significance was determined with one-way ANOVA and post hoc Tukey honest test. To determine significant differences between encapsulated hMSCs in unstimulated (+CTRL) and stimulated (+IL-1β) conditions, two tailed t-tests were used with

Bonferroni correction to account for the independent analysis of multiple groups. Statistical significance was set at $p < 0.05$. All data were analyzed using the *R stats*, *ggsignif*, and *ggpubr* packages in R (The R Foundation, Vienna, Austria).

Results and discussion

Qualitative analysis of the therapeutic efficacy of encapsulated hMSCs

While MSCs have been readily studied in the context of OA, the major focus of previous research has targeted delaying OA development.[22,51] To address this gap in knowledge, the effect of MSCs in delaying further disease progression of established OA was assessed in the current study. This approach provides added clinical relevance since clinical OA is more commonly diagnosed based on progressive disease phenotypes, including joint space narrowing and osteophyte development, as pain is commonly associated with these more established manifestations of the disease leading patients to seek medical treatment.[52,53] The rat MMT OA model was used as an OA phenotype manifests by the 3 week timepoint and further progression is observed at the six week timepoint; encapsulated hMSC treatment was administered at three weeks post-surgery, once OA had already been established, and the effects of the treatment were evaluated at the six week endpoint.[44] At the time of injection, encapsulated hMSC viability was 96.4 ± 2.1%. Encapsulation was leveraged in the current study to assess its effects on modulating the paracrine response of hMSCs in established OA.

Histology (H&E and Saf-O) was performed on tibiae to qualitatively assess the effects of encapsulated hMSC therapeutics on OA progression (Fig. 2a-j). Representative histological images of the Sham group showed consistent proteoglycan staining and a smoothness along the entire medial articular cartilaginous surface and no presence of osteophyte development on the most medial aspect of the joint (Fig. 2a&f). All MMT conditions showed proteoglycan loss (loss of Saf-O staining), loss of chondrocytes (lack of hematoxylin staining in certain regions of the articular cartilage layer), presence of fibrillations in the articular cartilage layer, and the development of osteophytes (Fig. 2b-e&g-j). While all MMT conditions did show variable levels of cartilage damage, the MMT/Encap group showed qualitatively less cartilage degeneration and surface roughness, relative to all other MMT conditions (Fig. 2e&j). Furthermore, while all MMT conditions showed osteophytes developing on the marginal edges of the joint, the MMT/hMSC and MMT/Encap hMSC group showed qualitatively larger areas relative to the MMT/Saline and MMT/Empty Caps group (Fig. 2d-e&i-j). Representative cartilage surface renderings were generated for each sample from each group using microCT captured images (samples matched with representative histology; Fig. 2k-o). Analysis of cartilage surface roughness was performed by subtracting individual 3D polynomial surfaces from the corresponding cartilage surface renderings (generated by custom MATLAB algorithm). All MMT conditions exhibited changes in articular cartilage structure as can be visualized with the development of elevations (red regions) and depressions (blue regions) relative to the Sham group. Furthermore, the MMT/Encap hMSC showed qualitatively attenuated cartilage surface roughness relative to other MMT groups (Fig. 2k-o). Together, these metrics demonstrated that with encapsulated hMSC treatment there was qualitatively less cartilage degeneration when compared to the other MMT groups.

Encapsulated hMSCs attenuated cartilage degeneration in established OA

For quantitative analysis, microCT was employed to study the articular cartilage, osteophytes, and subchondral bone regions of rat tibiae, as previously described.[43,44] MicroCT analysis of OA phenotypes has been demonstrated to be comparable to histopathology – the gold standard reference for OA characterization – when assessed in 2D and more sensitive than histopathology when used to assess 3D parameters.[43]

Detailed analysis of the articular cartilage was performed on various morphological parameters for both the total and segmented regions (medial, central, and lateral) of the medial

tibial condyle (Fig. 3&S1). Previous studies have demonstrated that OA development in the MMT model is largely localized to the medial plateau and specifically the medial 1/3 region of the articular cartilage.[44] For total cartilage volume, all MMT conditions showed elevated cartilage volume relative to Sham (Fig. 3a). Treatment with MMT/Encap hMSCs attenuated the MMT induced increase in cartilage volume that was found in the MMT/Saline and MMT/Empty Caps groups. However, no significant difference was found between MMT/Encap hMSC and MMT/hMSC alone, suggesting a milder effect of non-encapsulated cells relative to the encapsulated hMSCs. For medial cartilage volume analysis, significant increases in volume were yielded for the MMT/Saline, MMT/Empty Caps, and MMT hMSC groups. The MMT/Encap hMSC group did not show significant increases in cartilage volume relative to Sham (Fig. 3b). Cartilage thickness yielded similar outcomes to the volume parameter as no significant difference for cartilage thickness were found between the MMT/Encap hMSC group relative to the Sham group for both total and medial analysis (Fig. 3c&d). Furthermore, for the medial thickness parameter there were no significant differences noted between MMT/Encap hMSC and MMT/hMSC, further demonstrating the mild therapeutic effect of the non-encapsulated hMSCs. Cartilage attenuation, which permits the indirect quantification of proteoglycan content, yielded a single significant difference between Sham and MMT/hMSC for total analysis (Fig. 3e). While the medial analysis did discern differences between the Sham and all MMT conditions, there were no differences found between the MMT conditions as they all demonstrated increased attenuation (decreased proteoglycan content) relative to the Sham group (Fig. 3f). Additional analysis of the articular cartilage surface was performed using a custom MATLAB script to quantify surface roughness and exposed bone surface area (full thickness lesion surface area).

Surface roughness analysis of the articular cartilage surface provides a quantitative measure of changes that may arise from matrix fibrillation, erosion and lesion formation, and full-thickness cartilage loss (exposed bone surface area). All MMT conditions showed significantly increased surface roughness relative to Sham for analysis of the total tibial plateau (Fig. 3g). For medial surface roughness analysis, the MMT/Saline, MMT/Empty Caps, and MMT/hMSC groups showed significantly increased surface roughness compared to Sham but no difference was detected between MMT/Encap hMSC and Sham (Fig. 3h). Additionally, treatment with MMT/Encap attenuated the surface roughness to a level significantly lower than the other MMT conditions for both total and medial analyses (Fig. 3g&h). To further characterize changes to articular cartilage, exposed bone surface area was quantified. The total surface area of exposed bone was significantly different between the MMT/hMSC group and the Sham group (Fig. 3i). For medial analysis of exposed bone, both MMT/Saline and MMT/hMSC showed a significant increase relative to Sham (Fig. 3j). Additionally, incidence of exposed bone was assessed by group: MMT/Encap hMSC had the least number of samples with exposed bone (4/7), followed by MMT/Empty Caps (5/7), MMT/Saline (6/7), and MMT/hMSC (8/8). Fisher's exact test was performed for contingency analysis of exposed bone groups. MMT/Encap hMSC showed no significant difference from Sham, whereas all other MMT groups were significantly different from Sham (0/6; Fig. S2a). For the analysis of incidence of exposed bone on the medial aspect of the joint, increased exposed bone incidence was found in both MMT/Saline (5/7) and MMT/hMSC (8/8) groups relative to Sham (0/6; Fig. S2b). No significant differences were found between Sham and MMT/Encap hMSC (3/7) or MMT/Empty Caps (4/7) groups (Fig. S2b).

To assess the overall effect of encapsulated hMSCs on MMT induction, factoring in all articular cartilage parameters (total and medial) as model inputs, PLSDA was implemented to identify new axes which better separate the data with respect to the identity of the treatment group (Sham and MMT groups). LV1 separated out groups by severity of cartilage damage with the Sham and MMT/Encap hMSC groups separating to the left from the MMT/Saline, MMT/Empty Caps, and MMT/hMSC groups, on the right (Fig. 3k). A one-way ANOVA of the

LV1 scores demonstrated that all MMT conditions had significantly higher scores (increased damage) than the Sham; while the MMT/Encap hMSC group was significantly lower than the other MMT groups (Fig. 3l). However, MMT/Encap hMSC also demonstrated a higher LV1 score compared to the Sham, suggesting increased cartilage damage (Fig. 3l). Overall, these metrics reveal that encapsulated hMSCs provided a positive therapeutic protective effect on articular cartilage in established OA.

Articular cartilage degeneration, the primary outcome of OA, manifests with proteoglycan loss, resulting in increased water concentration in cartilage (swelling), superficial cartilage matrix fibrillation, erosion and lesion formation, and eventually full-thickness loss of articular cartilage resulting in bone-on-bone contact.[2,54] Further development of these articular cartilage phenotypes was attenuated with encapsulated hMSC treatment and not found with hMSCs or alginate (empty capsules) alone. Specifically, encapsulated hMSCs attenuated further articular cartilage swelling (volume and thickness) and delayed the further development of matrix fibrillations and erosion and lesion formation (surface roughness). Additionally, there was lower incidence of full thickness cartilage loss (exposed bone) after treatment with encapsulated hMSCs. These findings suggest that while encapsulated hMSCs elicit a positive therapeutic effect in delaying further articular cartilage degeneration, this treatment did not fully restore articular cartilage to a similar state as the Sham control (regenerative effect). There was still significant cartilage proteoglycan loss (attenuation), cartilage swelling, and full thickness cartilage loss; these levels were comparable to previous reports of the disease state at the three week time point (i.e. the time point of the encapsulated hMSC intervention).[18,43-45,55] While encapsulated hMSCs may not necessarily have any restorative properties that can reverse established disease damage, this treatment does have disease modifying potential that still provides high clinical translatability.

Encapsulated hMSCs had a minimal therapeutic effect on subchondral bone remodeling in established OA

Subchondral bone, which is the bone layer immediately underlying articular cartilage, has been observed to harden and thicken during the progression of OA (sclerosis), especially at later stages of the disease.[53,56-58] Subchondral bone sclerosis, along with joint space narrowing, is one of the most common phenotypes observed in clinical OA via standard x-ray diagnostic imaging.[52,53,57]

Detailed analysis of subchondral bone was performed on various morphological parameters for both the total and segmented regions (medial, central, and lateral) of the medial tibial condyle (Fig. 4&S3). Previous work with the rat MMT model at three weeks post-surgery has shown that there is increased incidence of subchondral bone remodeling in the medial 1/3 region.[59] Subchondral bone volume, for both total and medial regions, showed MMT/Saline, MMT/Empty Caps, and MMT/hMSC groups were significantly elevated relative to Sham (Fig. 4a&b). For the subchondral bone thickness parameter, all MMT conditions demonstrated significantly increased values relative to Sham (Fig. 4c&d). Total attenuation was not significantly different between MMT/Encap hMSC and Sham or between MMT/hMSC and Sham (Fig. 4e). The other two MMT conditions (MMT/Saline and MMT/Empty Caps) had a significant increase in attenuation values relative to the Sham group, indicating increased bone mineral density (hardening) of the subchondral bone (Fig. 4e). However, the analysis of attenuation for the medial 1/3 plateau showed significantly higher values for all MMT groups compared to Sham (Fig. 4f).

Cumulative analysis of the efficacy of encapsulated hMSCs on the subchondral bone layer in OA (accounting for volume, thickness, and attenuation parameters) was analyzed with PLSDA. LV1 separated out all study groups by levels of subchondral bone remodeling with Sham separating out on the left from all MMT groups on the right (Fig. 4g). This finding was further confirmed with ANOVA on LV1 scores which demonstrated that there were no

cumulative significant differences between respective MMT conditions (Fig. 4h). Consideration of all these findings suggests encapsulated hMSCs yield a minimal therapeutic effect on subchondral bone in OA as this therapeutic yielded less bone thickening (volume) and hardening (attenuation). These disease modifying effects were similar to those found for articular cartilage analyses as further disease development from the time point of intervention was attenuated. Furthermore, encapsulated hMSCs again did not provide a restorative effect as there was still significant subchondral bone thickening (thickness) and bone hardening (medial 1/3 attenuation).

Encapsulated hMSCs augmented osteophyte development in OA

One of the major associated phenotypes in OA is the development of tissues that form along the marginal edges of joints, known as osteophytes.[60] These formations are the most common radiographic finding of OA in the clinic and therefore are a key consideration in studying therapeutics for this disease.[57,58,61] Osteophytes consist of cartilaginous and mineralized portions, as they undergo an endochondral-like ossification process in formation, both of which were quantified in the current study in addition to a total osteophyte parameter (consisting of a combination of both cartilaginous and mineralized osteophytes).[60]

MicroCT analysis was implemented to quantitatively assess osteophyte volumes. Mineralized osteophyte volume was significantly greater in all MMT conditions relative to the Sham group (Fig. 5a). Furthermore, MMT/Encap hMSC and MMT/hMSC, which were not found to be different from one another, had significantly higher osteophyte volumes than the other two MMT conditions (Fig. 5a). Analysis of the other major osteophyte component (cartilaginous osteophytes) showed significantly higher volumes for all MMT groups relative to Sham (Fig. 5b). The MMT/Encap hMSC group also demonstrated increased cartilaginous osteophyte volumes relative to the MMT/hMSC and MMT/Empty Caps groups (Fig. 5b). Qualitative representation of these cartilaginous osteophytes can be viewed in the Saf-O histological images (Fig. 2f-j). Total osteophytes, a summation of mineralized and cartilaginous osteophytes, demonstrated similar findings to those for the individual parameters (Fig. 5c). A key difference identified was between MMT/Encap hMSC and MMT/hMSC, with the encapsulated condition demonstrating a significantly higher total osteophyte volume.

To assess the overall effect of encapsulated hMSCs on both cartilaginous and mineralized osteophytes, PLSDA established an LV1 that separated Sham to the left, and all MMT groups to the right based on increasing osteophyte volumes (Fig. 5d). ANOVA of LV1 scores displayed that all MMT conditions were significantly higher (increased volume) than Sham and that MMT/Encap hMSC was significantly higher than all other MMT conditions (Fig. 5e). Importantly, these results indicate that hMSCs, particularly the encapsulated hMSCs, potentiated osteophyte volumes relative to other MMT conditions that did not receive treatment. Even though increased osteophyte volumes have generally been viewed as an adverse outcome in OA, their development has been shown to occur independently of changes in articular cartilage morphology.[62] Furthermore, osteophytes have been shown to increase motion segment resistance to both bending and compression forces, suggesting that osteophyte formation may reverse some of the mechanical stimuli that cause them to form, in a possible compensatory and protective role.[63]

Biomaterial encapsulation of hMSCs induced a targeted paracrine response

The overall finding from the MMT study demonstrated a therapeutic effect of encapsulated hMSCs in preventing further cartilage degeneration in established OA. Another major finding drawn from the MMT study is the role that biomaterial encapsulation has in modulating the paracrine response of hMSCs *in vivo*. While the same cells (matched donor), administered at the same dose, were used for encapsulated and non-encapsulated therapeutic conditions, the two groups yielded differing levels of therapeutic efficacy. The encapsulated

hMSCs elicited a more potent therapeutic effect compared to the non-encapsulated hMSCs which yielded a mild therapeutic effect in established OA. Specifically, non-encapsulated hMSCs demonstrated attenuation of increases in cartilage degeneration (volume and thickness) and subchondral bone remodeling (attenuation). These non-encapsulated hMSCs also yielded augmented osteophyte volumes, comparable to those yielded by encapsulated hMSCs. This led to the hypothesis that there would be significant differences in the secretome response to an OA microenvironment between non-encapsulated hMSCs and encapsulated hMSCs. Numerous studies have shown that biomaterials can alter MSC function, survival, and mechanotransduction; there is limited understanding of the effects encapsulation has on MSC cytokine expression which the current study sought to explore.[18,37,38,64] To assess the effects of biomaterial encapsulation on the secreted cytokines from hMSCs in a simulated OA microenvironment, an *in vitro* cell culture model was used where the media was supplemented with the primary OA cytokine IL-1β. Cell viability immediately following encapsulation was 97.1 ± 3.1%, after which cells were plated. Cells were either conditioned in media alone (+CTRL) or stimulated with IL-1β in media (+IL-1β).[9,47,65]

Following treatment with or without IL-1β for 24 hours, media was collected and assessed for 41 immunomodulatory cytokines and chemokines (Fig. 6a). Background subtraction was performed for both non-stimulated and stimulated conditions; all cytokine values only show the cytokine levels resulting from hMSC paracrine expression. Both non-encapsulated and encapsulated hMSCs were responsive to IL-1β stimulation when compared to CTRL conditions. For non-encapsulated hMSCs, IL-1β stimulation yielded indiscriminate upregulation of all measured cytokines, compared to the non-encapsulated hMSC control (+CTRL). In contrast, IL-1β stimulation of encapsulated hMSCs yielded a more targeted response with distinct qualitative increases in six cytokines: IL-1β, IL-1RA, IL-7, IL-8, Granulocyte Colony Stimulating Factor (G-CSF), and IL-6, relative to the encapsulated hMSC control (+CTRL). PLSDA revealed LV1 and LV2 axes that separated differentially modulated cellular paracrine responses with encapsulated hMSC conditions separating on LV1 (+IL-1β separated left and +CTRL separated right) and non-encapsulated hMSCs separating along LV2 (+CTRL at the bottom and + IL-1β at the top of the axis; Fig. 6b). Significant separation of latent variable scores was confirmed with t-tests of both LVs, with Bonferroni correction applied, for encapsulated and non-encapsulated hMSCs on the LV1 and LV2 axes, respectively (Fig. 6c&d).

To assess the effects of IL-1β stimulation on encapsulated cells, PLSDA was conducted on the encapsulated data alone (Fig. 7a). From LV1, the separation between CTRL to the left and IL-1β to the right can be easily observed. LV1 consisted of a profile of cytokines that correlated with the CTRL group (blue) or IL-1β treated cells (red; Fig. 7b). To determine which cytokines yielded differences in cytokine expression (Encap hMSC + CTRL vs. Encap hMSC + IL-1β), univariate analysis was performed on all cytokines that were upregulated with IL-1β stimulation (shown in red; Fig. 7b). Of the 18 cytokines that showed upregulation with IL-1β stimulation, eight were found to be significantly elevated, including the pro-inflammatory cytokines IL-1β, IL-6, IL-7 and IL-8, the anti-inflammatory cytokine IL-1RA and the chemokines G-CSF, macrophage derived chemokine (MDC; CCL-12), and interferon gamma-induced protein 10 (IP10; CXCL-10; Fig. 7c-j). These *in vitro* findings demonstrate a more modulated, and targeted response of encapsulated hMSCs when compared to the expression profile of non-encapsulated hMSCs, which yielded increased expression of all cytokines.

The roles that cytokines play in OA pathology have been well documented, including a critical role for cytokines in osteophyte development.[13] Previous studies have demonstrated that osteophyte growth is driven by cytokine release and not by mechanical forces on the joint capsule.[66-68] However, a limitation of this study was that one of the major cytokines implicated in osteophyte development, TGF-β, was not part of the 41-plex cytokine panel. While previous studies have demonstrated that hMSCs yield an anti-inflammatory and regulatory paracrine expression profile in various disease states, the current study demonstrated increased pro-

inflammatory cytokine secretion.[69,70] Of note, IL-6 has been shown to decrease collagen II production and is implicated as a critical cytokine in subchondral bone remodeling in OA.[13,71] Additionally, IL-7 has been demonstrated to increase production of MMP-13 and IL-8 has been shown to recruit additional neutrophils and further type II collagen degradation in OA.[72,73] Even though these cytokines have been previously reported to be involved in OA pathogenesis when chronically elevated, it is important to note that encapsulated hMSCs yielded a more targeted response when compared to non-encapsulated hMSCs treated with IL-1β (Fig. 6a). Non-encapsulated hMSCs yielded increased expression of numerous other cytokines implicated in the OA inflammatory cascade (TNFα, IFNγ, IL-17).[71] Furthermore, it is important to draw the distinction between the chronic nature of the OA inflammatory environment and the acute response induced by the hMSC secretome. To resolve chronic inflammation, an acute event is needed to bring in immune cells and activate different inflammatory cascades to resolve and induce a pro-regenerative response.[74] This mechanism is common in other chronic inflammatory environments and wound healing environments where acute inflammatory events are necessary to resolve chronic inflammation and transition to pro-regenerative immune responses to regulate inflammation.[75-77] Furthermore, the pro-inflammatory cytokines that showed increased expression in the current study (IL-6, IL-7, IL-8) have been implicated as significant mediators in wound healing and similar diseases that involve resolution of inflammatory events.[78-80] Additionally, when looking at the duration of hMSC viability from our previous study, we observed that the hMSCs are only viable for the first ~9 days post-injection, thus the hMSCs likely respond to the local environment to help induce a local endogenous response which could have longer lasting therapeutic effects, particularly if it promoted the resolution of chronic inflammation.[18]

While encapsulated hMSCs elicited a pro-inflammatory response in the current study, they also secreted anti-inflammatory cytokines and chemokines which may have therapeutic potential. Specifically, the anti-inflammatory cytokine IL-1RA has been studied extensively in the context of OA with pre-clinical studies demonstrating a protective capacity on articular cartilage.[81,82] Furthermore, a number of chemokines were increased (G-CSF, MDC, IP10) when stimulated with IL-1β, which would suggest that hMSCs could induce a response to recruit native stem and immune cells to the injury site. While the role of G-CSF has not been documented in OA, this cytokine is known to mobilize MSCs from bone marrow and has been found to promote cartilage repair in a pre-clinical full cartilage defect rabbit model.[83,84] MDC (CCL-12), which is understudied in OA, has been shown to recruit memory T cells in patients with OA.[85] The cytokine IP10 (CXCL-10) was also upregulated by encapsulated hMSCs. IP10 has been shown in previous studies to be specifically involved in recruitment of synovial macrophages in OA.[86] While the cytokines of interest in the current study were categorized based on their most commonly identified pro-inflammatory, anti-inflammatory, or chemotactic nature it is important to note that cytokines are well known to have varying roles and can be both cell and context dependent.[87] Most notably IL-6, which has both pro-inflammatory and anti-inflammatory potential.[88,89] While the present secretome assessment does not provide a direct link between specific cytokines and therapeutic efficacy *in vivo*, there were a number of potential cytokines that may be implicated in the therapeutic efficacy of hMSCs in OA. Further study of these specific cytokines, as well as their up-stream regulators and downstream targets, will provide new insights into the mechanisms involved in OA that may be therapeutically targeted with hMSCs. Additional investigation is merited to determine what characteristics of biomaterial encapsulation yielded this modulated response and whether further tailoring the biomaterial properties could further enhance the therapeutic efficacy of the hMSCs. This could include further study into the effects of the niche constructed by a 3D microporous hydrogel system (e.g. chemical composition, lack of peptide modification, pore size, topography) on hMSC paracrine function as all these properties have been demonstrated to directly impact the secretome of these cells.[90-92]

Conclusions

In the current study, bone marrow derived hMSCs were encapsulated in sodium alginate microcapsules to study the effects of biomaterial encapsulation on the modulation of the paracrine signaling response and therapeutic efficacy of these cells in an OA microenvironment. The therapeutic potential of this cellular treatment was assessed in a pre-clinical rat model (MMT) of established OA, which is relevant because patients commonly seek treatment once OA is more readily evident and they have developed a more advanced stage of the disease. Encapsulation of hMSCs demonstrated a positive therapeutic effect by delaying further development of the disease; specifically, encapsulated hMSC treatment attenuated further cartilage degeneration and subchondral bone sclerosis. Though the encapsulated hMSCs provided a disease modifying protective effect, the treatment did not regenerate or restore the cartilage or subchondral bone back to levels comparable to Sham operated controls. These data suggest that the timing of hMSC treatment in the OA disease progression will be critical, as this treatment protected the integrity of the remaining tissue and thus suggests that treatment during earlier disease stages (when there is still tissue to protect) may have longer and more potent therapeutic effects. Though protective effects were observed on the cartilage and subchondral bone, encapsulated hMSCs yielded increased osteophyte volumes which have been identified as an unwanted phenotype for restoring joint function. The immunomodulatory potential of biomaterial encapsulation on hMSC function demonstrated a targeted paracrine response to a simulated OA microenvironment while non-encapsulated hMSCs showed an indiscriminate upregulation of all cytokines in the cytokine panel. While expression of numerous anti-inflammatory and regenerative cytokines were increased with hMSC encapsulation, there were also a number of pro-inflammatory cytokines that showed increased expression. In considering these latter findings, it is important to consider that this hMSC paracrine response is an acute response and that the secretion of these pro-inflammatory cytokines may be critical in resolving the chronic OA inflammatory environment. Together, the data from the current study demonstrated that biomaterial encapsulation of hMSCs modulated the paracrine response to a simulated OA microenvironment and enhanced the *in vivo* therapeutic efficacy of the hMSCs in preventing further disease progression in treating established OA.

Acknowledgements

This work was supported in part by VA (SPiRE) Grant I21RX002372-01A1 from the United States (U.S.) Department of Veterans Affairs Rehabilitation Research and Development Service. The research was also supported in part by the DOD PRMRP Grant PR171379 and PHS Grant UL1TR000454 from the Clinical and Translational Science Award Program, National Institutes of Health, National Center for Advancing Translational Sciences. The authors would like to thank Mila Friedman for the histological analyses and Colleen Oliver for her support in the animal study.

Conflicts of interest

There are no conflicts to declare.

Disclaimer

The contents do not represent the views of the U.S. Department of Veterans Affairs or the United States Government.

References

1. M. G. Cisternas, L. Murphy, J. J. Sacks, D. H. Solomon, D. J. Pasta and C. G. Helmick, Arthritis Care Res., 2016, 68, 574–580.
2. J. Bertrand, C. Cromme, D. Umlauf, S. Frank and T. Pap, Int. J. Biochem. Cell Biol., 2010, 42, 1594–1601.

3. T. Vos, R. M. Barber, B. Bell, A. Bertozzi-Villa, S. Biryukov, I. Bolliger, F. Charlson, A. Davis, L. Degenhardt, D. Dicker, L. Duan, H. Erskine, V. L. Feigin, A. J. Ferrari, C. Fitzmaurice, T. Fleming, N. Graetz, C. Guinovart, J. Haagsma, G. M. Hansen, S. W. Hanson, K. R. Heuton, H. Higashi, N. Kassebaum, H. Kyu, E. Laurie, X. Liang, K. Lofgren, R. Lozano, M. F. MacIntyre, M. Moradi-Lakeh, M. Naghavi, G. Nguyen, S. Odell, K. Ortblad, D. A. Roberts, G. A. Roth, L. Sandar, P. T. Serina, J. D. Stanaway, C. Steiner, B. Thomas, S. E. Vollset, H. Whiteford, T. M. Wolock, P. Ye, M. Zhou, M. A. Ãvila, G. M. Aasvang, C. Abbafati, A. A. Ozgoren, F. Abd-Allah, M. I. A. Aziz, S. F. Abera, V. Aboyans, J. P. Abraham, B. Abraham, I. Abubakar, L. J. Abu-Raddad, N. M. E. Abu-Rmeileh, T. C. Aburto, T. Achoki, I. N. Ackerman, A. Adelekan, Z. Ademi, A. K. Adou, J. C. Adsuar, J. Arnlov, E. E. Agardh, M. J. Al Khabouri, S. S. Alam, D. Alasfoor, M. I. Albittar, M. A. Alegretti, A. V. Aleman, Z. A. Alemu, R. Alfonso-Cristancho, S. Alhabib, R. Ali, F. Alla, P. Allebeck, P. J. Allen, M. A. AlMazroa, U. Alsharif, E. Alvarez, N. Alvis-Guzman, O. Ameli, H. Amini, W. Ammar, B. O. Anderson, H. R. Anderson, C. A. T. Antonio, P. Anwari, H. Apfel, V. S. A. Arsenijevic, A. Artaman, R. J. Asghar, R. Assadi, L. S. Atkins, C. Atkinson, A. Badawi, M. C. Bahit, T. Bakfalouni, K. Balakrishnan, S. Balalla, A. Banerjee, S. L. Barker-Collo, S. Barquera, L. Barregard, L. H. Barrero, S. Basu, A. Basu, A. Baxter, J. Beardsley, N. Bedi, E. Beghi, T. Bekele, M. L. Bell, C. Benjet, D. A. Bennett, I. M. Bensenor, H. Benzian, E. Bernabe, T. J. Beyene, N. Bhala, A. Bhalla, Z. Bhutta, K. Bienhoff, B. Bikbov, A. Bin Abdulhak, J. D. Blore, F. M. Blyth, M. A. Bohensky, B. B. Basara, G. Borges, N. M. Bornstein, D. Bose, S. Boufous, R. R. Bourne, L. N. Boyers, M. Brainin, M. Brauer, C. E. G. Brayne, A. Brazinova, N. J. K. Breitborde, H. Brenner, A. D. M. Briggs, P. M. Brooks, J. Brown, T. S. Brugha, R. Buchbinder, G. C. Buckle, G. Bukhman, A. G. Bulloch, M. Burch, R. Burnett, R. Cardenas, N. L. Cabral, I. R. Campos-Nonato, J. C. Campuzano, J. R. Carapetis, D. O. Carpenter, V. Caso, C. A. Castaneda-Orjuela, F. Catala-Lopez, V. K. Chadha, J. C. Chang, H. Chen, W. Chen, P. P. Chiang, O. Chimed-Ochir, R. Chowdhury, H. Christensen, C. A. Christophi, S. S. Chugh, M. Cirillo, M. Coggeshall, A. Cohen, V. Colistro, S. M. Colquhoun, A. G. Contreras, L. T. Cooper, C. Cooper, K. Cooperrider, J. Coresh, M. Cortinovis, M. H. Criqui, J. A. Crump, L. Cuevas-Nasu, R. Dandona, L. Dandona, E. Dansereau, H. G. Dantes, P. I. Dargan, G. Davey, D. V. Davitoiu, A. Dayama, V. De La Cruz-Gongora, S. F. De La Vega, D. De Leo, B. Del Pozo-Cruz, R. P. Dellavalle, K. Deribe, S. Derrett, D. C. Des Jarlais, M. Dessalegn, G. A. DeVeber, S. D. Dharmaratne, C. Diaz-Torne, E. L. Ding, K. Dokova, E. R. Dorsey, T. R. Driscoll, H. Duber, A. M. Durrani, K. M. Edmond, R. G. Ellenbogen, M. Endres, S. P. Ermakov, B. Eshrati, A. Esteghamati, K. Estep, S. Fahimi, F. Farzadfar, D. F. J. Fay, D. T. Felson, S. M. Fereshtehnejad, J. G. Fernandes, C. P. Ferri, A. Flaxman, N. Foigt, K. J. Foreman, F. G. R. Fowkes, R. C. Franklin, T. Furst, N. D. Futran, B. J. Gabbe, F. G. Gankpe, F. A. Garcia-Guerra, J. M. Geleijnse, B. D. Gessner, K. B. Gibney, R. F. Gillum, I. A. Ginawi, M. Giroud, G. Giussani, S. Goenka, K. Goginashvili, P. Gona, T. G. De Cosio, R. A. Gosselin, C. C. Gotay, A. Goto, H. N. Gouda, R. L. Guerrant, H. C. Gugnani, D. Gunnell, R. Gupta, R. Gupta, R. A. Gutierrez, N. Hafezi-Nejad, H. Hagan, Y. Halasa, R. R. Hamadeh, H. Hamavid, M. Hammami, G. J. Hankey, Y. Hao, H. L. Harb, J. M. Haro, R. Havmoeller, R. J. Hay, S. Hay, M. T. Hedayati, I. B. H. Pi, P. Heydarpour, M. Hijar, H. W. Hoek, H. J. Hoffman, J. C. Hornberger, H. D. Hosgood, M. Hossain, P. J. Hotez, D. G. Hoy, M. Hsairi, H. Hu, G. Hu, J. J. Huang, C. Huang, L. Huiart, A. Husseini, M. Iannarone, K. M. Iburg, K. Innos, M. Inoue, K. H. Jacobsen, S. K. Jassal, P. Jeemon, P. N. Jensen, V. Jha, G. Jiang, Y. Jiang, J. B. Jonas, J. Joseph, K. Juel, H. Kan, A. Karch, C. Karimkhani, G. Karthikeyan, R. Katz, A. Kaul, N. Kawakami, D. S. Kazi, A. H. Kemp, A. P. Kengne, Y. S. Khader, S. E. A. H. Khalifa, E. A. Khan, G. Khan, Y. H. Khang, I. Khonelidze, C. Kieling, D. Kim, S. Kim, R. W. Kimokoti, Y. Kinfu, J. M. Kinge, B. M. Kissela, M. Kivipelto, L. Knibbs, A. K. Knudsen,

Y. Kokubo, S. Kosen, A. Kramer, M. Kravchenko, R. V. Krishnamurthi, S. Krishnaswami, B. K. Defo, B. K. Bicer, E. J. Kuipers, V. S. Kulkarni, K. Kumar, G. A. Kumar, G. F. Kwan, T. Lai, R. Lalloo, H. Lam, Q. Lan, V. C. Lansingh, H. Larson, A. Larsson, A. E. B. Lawrynowicz, J. L. Leasher, J. T. Lee, J. Leigh, R. Leung, M. Levi, B. Li, Y. Li, Y. Li, J. Liang, S. Lim, H. H. Lin, M. Lind, M. P. Lindsay, S. E. Lipshultz, S. Liu, B. K. Lloyd, S. L. Ohno, G. Logroscino, K. J. Looker, A. D. Lopez, N. Lopez-Olmedo, J. Lortet-Tieulent, P. A. Lotufo, N. Low, R. M. Lucas, R. Lunevicius, R. A. Lyons, J. Ma, S. Ma, M. T. MacKay, M. Majdan, R. Malekzadeh, C. C. Mapoma, W. Marcenes, L. M. March, C. Margono, G. B. Marks, M. B. Marzan, J. R. Masci, A. J. Mason-Jones, R. G. Matzopoulos, B. M. Mayosi, T. T. Mazorodze, N. W. McGill, J. J. McGrath, M. McKee, A. McLain, B. J. McMahon, P. A. Meaney, M. M. Mehndiratta, F. Mejia-Rodriguez, W. Mekonnen, Y. A. Melaku, M. Meltzer, Z. A. Memish, G. Mensah, A. Meretoja, F. A. Mhimbira, R. Micha, T. R. Miller, E. J. Mills, P. B. Mitchell, C. N. Mock, T. E. Moffitt, N. M. Ibrahim, K. A. Mohammad, A. H. Mokdad, G. L. Mola, L. Monasta, M. Montico, T. J. Montine, A. R. Moore, A. E. Moran, L. Morawska, R. Mori, J. Moschandreas, W. N. Moturi, M. Moyer, D. Mozaffarian, U. O. Mueller, M. Mukaigawara, M. E. Murdoch, J. Murray, K. S. Murthy, P. Naghavi, Z. Nahas, A. Naheed, K. S. Naidoo, L. Naldi, D. Nand, V. Nangia, K. M. V. Narayan, D. Nash, C. Nejjari, S. P. Neupane, L. M. Newman, C. R. Newton, M. Ng, F. N. Ngalesoni, N. T. Nhung, M. I. Nisar, S. Nolte, O. F. Norheim, R. E. Norman, B. Norrving, L. Nyakarahuka, I. H. Oh, T. Ohkubo, S. B. Omer, J. N. Opio, A. Ortiz, J. D. Pandian, C. I. A. Panelo, C. Papachristou, E. K. Park, C. D. Parry, A. J. P. Caicedo, S. B. Patten, V. K. Paul, B. I. Pavlin, N. Pearce, L. S. Pedraza, C. A. Pellegrini, D. M. Pereira, F. P. Perez-Ruiz, N. Perico, A. Pervaiz, K. Pesudovs, C. B. Peterson, M. Petzold, M. R. Phillips, D. Phillips, B. Phillips, F. B. Piel, D. Plass, D. Poenaru, G. V. Polanczyk, S. Polinder, C. A. Pope, S. Popova, R. G. Poulton, F. Pourmalek, D. Prabhakaran, N. M. Prasad, D. Qato, D. A. Quistberg, A. Rafay, K. Rahimi, V. Rahimi-Movaghar, S. U. Rahman, M. Raju, I. Rakovac, S. M. Rana, H. Razavi, A. Refaat, J. Rehm, G. Remuzzi, S. Resnikoff, A. L. Ribeiro, P. M. Riccio, L. Richardson, J. H. Richardus, A. M. Riederer, M. Robinson, A. Roca, A. Rodriguez, D. Rojas-Rueda, L. Ronfani, D. Rothenbacher, N. Roy, G. M. Ruhago, N. Sabin, R. L. Sacco, K. Ksoreide, S. Saha, R. Sahathevan, M. A. Sahraian, U. Sampson, J. R. Sanabria, L. Sanchez-Riera, I. S. Santos, M. Satpathy, J. E. Saunders, M. Sawhney, M. I. Saylan, P. Scarborough, B. Schoettker, I. J. C. Schneider, D. C. Schwebel, J. G. Scott, S. Seedat, S. G. Sepanlou, B. Serdar, E. E. Servan-Mori, K. Shackelford, A. Shaheen, S. Shahraz, T. S. Levy, S. Shangguan, J. She, S. Sheikhbahaei, D. S. Shepard, P. Shi, K. Shibuya, Y. Shinohara, R. Shiri, K. Shishani, I. Shiue, M. G. Shrime, I. D. Sigfusdottir, D. H. Silberberg, E. P. Simard, S. Sindi, J. A. Singh, L. Singh, V. Skirbekk, K. Sliwa, M. Soljak, S. Soneji, S. S. Soshnikov, P. Speyer, L. A. Sposato, C. T. Sreeramareddy, H. Stoeckl, V. K. Stathopoulou, N. Steckling, M. B. Stein, D. J. Stein, T. J. Steiner, A. Stewart, E. Stork, L. J. Stovner, K. Stroumpoulis, L. Sturua, B. F. Sunguya, M. Swaroop, B. L. Sykes, K. M. Tabb, K. Takahashi, F. Tan, N. Tandon, D. Tanne, M. Tanner, M. Tavakkoli, H. R. Taylor, B. J. Te Ao, A. M. Temesgen, M. Ten Have, E. Y. Tenkorang, A. S. Terkawi, A. M. Theadom, E. Thomas, A. L. Thorne-Lyman, A. G. Thrift, I. M. Tleyjeh, M. Tonelli, F. Topouzis, J. A. Towbin, H. Toyoshima, J. Traebert, B. X. Tran, L. Trasande, M. Trillini, T. Truelsen, U. Trujillo, M. Tsilimbaris, E. M. Tuzcu, K. N. Ukwaja, E. A. Undurraga, S. B. Uzun, W. H. Van Brakel, S. Van De Vijver, R. Van Dingenen, C. H. Van Gool, Y. Y. Varakin, T. J. Vasankari, M. S. Vavilala, L. J. Veerman, G. Velasquez-Melendez, N. Venketasubramanian, L. Vijayakumar, S. Villalpando, F. S. Violante, V. V. Vlassov, S. Waller, M. T. Wallin, X. Wan, L. Wang, J. Wang, Y. Wang, T. S. Warouw, S. Weichenthal, E. Weiderpass, R. G. Weintraub, A. Werdecker, K. R. Wessells, R. Westerman, J. D. Wilkinson, H. C. Williams, T. N. Williams, S. M. Woldeyohannes, C. D. A. Wolfe, J. Q. Wong, H. Wong, A. D. Woolf, J. L.

Wright, B. Wurtz, G. Xu, G. Yang, Y. Yano, M. A. Yenesew, G. K. Yentur, P. Yip, N. Yonemoto, S. J. Yoon, M. Younis, C. Yu, K. Y. Kim, M. E. S. Zaki, Y. Zhang, Z. Zhao, Y. Zhao, J. Zhu, D. Zonies, J. R. Zunt, J. A. Salomon and C. J. L. Murray, Lancet, 2015, 386, 743–800.
4. V. Kontis, J. E. Bennett, C. D. Mathers, G. Li, K. Foreman and M. Ezzati, Lancet, 2017, 389, 1323–1335.
5. J. Sokolove and C. M. Lepus, Ther. Adv. Musculoskelet. Dis., 2013, 5, 77–94.
6. M. B. Goldring and M. Otero, Curr. Opin. Rheumatol., 2011, 23, 471–478.
7. F. Berenbaum, Osteoarthr. Cartil., 2013, 21, 16–21.
8. K. B. Marcu, M. Otero, E. Olivotto, R. M. Borzi and M. B. Goldring, Curr. Drug Targets, 2010, 11, 599–613.
9. J. Shen, Y. Abu-Amer, R. J. O'Keefe and A. McAlinden, Connect. Tissue Res., 2017, 58, 49–63.
10. Y. Y. Chow and K. Y. Chin, Mediators Inflamm., 2020.
11. L. A. Yeh, A. J. Augustine, P. Lee, L. R. Riviere and A. Sheldon, J. Rheumatol., 1995, 22, 1740–1746.
12. D. M. Salter, S. J. Millward-Sadler, G. Nuki and M. O. Wright, in Biorheology, 2002, 39, 97–108.
13. P. Wojdasiewicz, Ł. A. Poniatowski and D. Szukiewicz, Mediators Inflamm., 2014.
14. H. De Jong, S. E. Berlo, P. Hombrink, H. G. Otten, W. Van Eden, F. P. Lafeber, A. H. M. Heurkens, J. W. J. Bijlsma, T. T. Glant and B. J. Prakken, Ann. Rheum. Dis., 2010, 69, 255–262.
15. M. Imamura, F. Ezquerro, F. Marcon Alfieri, L. Vilas Boas, T. R. Tozetto-Mendoza, J. Chen, L. Özçakar, L. Arendt-Nielsen and L. Rizzo Battistella, Int. J. Inflam., 2015.
16. N. Rajabzadeh, E. Fathi and R. Farahzadi, Stem Cell Investig., 2019.
17. M. Dominici, K. Le Blanc, I. Mueller, I. Slaper-Cortenbach, F. C. Marini, D. S. Krause, R. J. Deans, A. Keating, D. J. Prockop and E. M. Horwitz, Cytotherapy, 2006, 8, 315–317.
18. J. M. McKinney, T. N. Doan, L. Wang, J. Deppen, D. S. Reece, K. A. Pucha, S. Ginn, R. D. Levit and N. J. Willett, Eur. Cell. Mater., 2019, 37, 42–59.
19. P. Mancuso, S. Raman, A. Glynn, F. Barry and J. M. Murphy, Front. Bioeng. Biotechnol., 2019, 7.
20. M. Maumus, C. Jorgensen and D. Noël, Biochimie, 2013, 95, 2229–2234.
21. A. Colombini, C. Perucca Orfei, D. Kouroupis, E. Ragni, P. De Luca, M. ViganÒ, D. Correa and L. de Girolamo, Cytotherapy, 2019, 21, 1179–1197.
22. A. T. Wang, Y. Feng, H. H. Jia, M. Zhao and H. Yu, World J. Stem Cells, 2019, 11, 222–235.
23. Y. Shi, J. Su, A. I. Roberts, P. Shou, A. B. Rabson and G. Ren, Trends Immunol., 2012, 33, 136–143.
24. M. E. Bernardo and W. E. Fibbe, Cell Stem Cell, 2013, 13, 392–402.
25. N. Espagnolle, A. Balguerie, E. Arnaud, L. Sensebé and A. Varin, Stem Cell Reports, 2017, 8, 961–976.
26. Y. Chen, Z. Shu, K. Qian, J. Wang and H. Zhu, Tissue Eng. - Part B Rev., 2019, 25, 492–499.
27. J. K. Leach and J. Whitehead, ACS Biomater. Sci. Eng., 2018, 4, 1115–1127.
28. A. Papadimitropoulos, E. Piccinini, S. Brachat, A. Braccini, D. Wendt, A. Barbero, C. Jacobi and I. Martin, PLoS One, 2014, 9, e102359.
29. S. Duggal, K. B. Frønsdal, K. Szöke, A. Shahdadfar, J. E. Melvik and J. E. Brinchmann, Tissue Eng. - Part A, 2009, 15, 1763–1773.
30. M. W. Tibbitt and K. S. Anseth, Biotechnol. Bioeng., 2009, 103, 655–663.
31. E. C. Stucky, R. S. Schloss, M. L. Yarmush and D. I. Shreiber, Cytotherapy, 2015, 17, 1353–1364.

32. G. Choe, J. Park, H. Park and J. Y. Lee, Polymers (Basel)., 2018, 10.
33. J. Barminko, J. H. Kim, S. Otsuka, A. Gray, R. Schloss, M. Grumet and M. L. Yarmush, Biotechnol. Bioeng., 2011, 108, 2747–2758.
34. L. M. Li, M. Han, X. C. Jiang, X. Z. Yin, F. Chen, T. Y. Zhang, H. Ren, J. W. Zhang, T. J. Hou, Z. Chen, H. W. Ou-Yang, Y. Tabata, Y. Q. Shen and J. Q. Gao, ACS Appl. Mater. Interfaces, 2017, 9, 3330–3342.
35. B. Follin, M. Juhl, S. Cohen, A. E. Pedersen, M. Gad, J. Kastrup and A. Ekblond, Cytotherapy, 2015, 17, 1104–1118.
36. J. Sun and H. Tan, Materials (Basel)., 2013, 6, 1285–1309.
37. N. Landázuri, R. D. Levit, G. Joseph, J. M. Ortega-Legaspi, C. A. Flores, D. Weiss, A. Sambanis, C. J. Weber, S. A. Safley and W. R. Taylor, J. Tissue Eng. Regen. Med., 2016, 10, 222–232.
38. R. D. Levit, N. Landázuri, E. A. Phelps, M. E. Brown, A. J. García, M. E. Davis, G. Joseph, R. Long, S. A. Safley, J. D. Suever, A. N. Lyle, C. J. Weber and W. R. Taylor, J. Am. Heart Assoc., 2013, 2, e000367–e000367.
39. O. Levy, R. Kuai, E. M. J. Siren, D. Bhere, Y. Milton, N. Nissar, M. De Biasio, M. Heinelt, B. Reeve, R. Abdi, M. Alturki, M. Fallatah, A. Almalik, A. H. Alhasan, K. Shah and J. M. Karp, Sci. Adv., 2020, 6, eaba6884.
40. A. M. Bendele, Animal models of osteoarthritis, 2001, 1.
41. M. J. Janusz, A. M. Bendele, K. K. Brown, Y. O. Taiwo, L. Hsieh and S. A. Heitmeyer, Osteoarthr. Cartil., 2002, 10, 785–791.
42. A. W. Palmer, R. E. Guldberg and M. E. Levenston, Proc. Natl. Acad. Sci. U. S. A., 2006, 103, 19255–19260.
43. N. J. Willett, T. Thote, M. Hart, S. Moran, R. E. Guldberg and R. V. Kamath, Osteoarthr. Cartil., 2016, 24, 1604–1612.
44. T. Thote, A. S. P. Lin, Y. Raji, S. Moran, H. Y. Stevens, M. Hart, R. V. Kamath, R. E. Guldberg and N. J. Willett, Osteoarthr. Cartil., 2013, 21, 1132–1141.
45. D. S. Reece, T. Thote, A. S. P. Lin, N. J. Willett and R. E. Guldberg, Osteoarthr. Cartil., 2018, 26, 118–127.
46. Y. Wang and S. Lou, Chin. Med. J. (Engl)., 2001, 114, 723–725.
47. R. Vézina Audette, A. Lavoie-Lamoureux, J. P. Lavoie and S. Laverty, Osteoarthr. Cartil., 2013, 21, 1116–1124.
48. L. Eriksson, T. Byrne, E. Johansson, J. Trygg and C. and Vikström, Multi- and Megavariate Data Analysis Basic Principles and Applications Volume 1 (3rd ed.), 2013.
49. L. D. Weinstock, A. M. Furness, S. S. Herron, S. S. Smith, S. B. Sankar, S. G. Derosa, D. Gao, M. E. Mepyans, A. Scotto Rosato, D. L. Medina, A. Vardi, N. S. Ferreira, S. M. Cho, A. H. Futerman, S. A. Slaugenhaupt, L. B. Wood and Y. Grishchuk, Hum. Mol. Genet., 2018, 27, 2725–2738.
50. I. Barroeta-Espar, L. D. Weinstock, B. G. Perez-Nievas, A. C. Meltzer, M. Siao Tick Chong, A. C. Amaral, M. E. Murray, K. L. Moulder, J. C. Morris, N. J. Cairns, J. E. Parisi, V. J. Lowe, R. C. Petersen, J. Kofler, M. D. Ikonomovic, O. López, W. E. Klunk, R. P. Mayeux, M. P. Frosch, L. B. Wood and T. Gomez-Isla, Neurobiol. Dis., 2019, 121, 327–337.
51. L. Kong, L. Z. Zheng, L. Qin and K. K. W. Ho, J. Orthop. Transl., 2017, 9, 89–103.
52. J. H. Kellgren and J. S. Lawrence, Ann. Rheum. Dis., 1957, 16, 494–502.
53. R. D. Altman and G. E. Gold, Osteoarthr. Cartil., 2007, 15, 1–56.
54. J. A. Buckwalter, H. J. Mankin and A. J. Grodzinsky, Instr. Course Lect., 2005, 54, 465–480.
55. N. J. Willett, T. Thote, A. S. P. Lin, S. Moran, Y. Raji, S. Sridaran, H. Y. Stevens and R. E. Guldberg, Arthritis Res. Ther., 2014, 16, R47.

56. R. F. Loeser, S. R. Goldring, C. R. Scanzello and M. B. Goldring, Arthritis Rheum., 2012, 64, 1697–1707.
57. T. Boegard, O. Rudling, I. F. Petersson and K. Jonsson, Ann. Rheum. Dis., 1998, 57, 401–407.
58. K. D. Brandt, R. S. Fife, E. M. Braunstein and B. Katz, Arthritis Rheum., 1991, 34, 1381–1386.
59. K. A. Pucha, J. M. McKinney, J. M. Fuller and N. J. Willett, Osteoarthr. Cartil. Open, 2020, 100066.
60. P. M. van der Kraan and W. B. van den Berg, Osteoarthr. Cartil., 2007, 15, 237–244.
61. S. Bloom, D. Lebel, E. Cohen, D. Atar and E. Rath, Harefuah, 2008, 147, 330–333.
62. A. J. Barr, T. M. Campbell, D. Hopkinson, S. R. Kingsbury, M. A. Bowes and P. G. Conaghan, Arthritis Res. Ther., 2015, 17, 228.
63. M. Al-Rawahi, J. Luo, P. Pollintine, P. Dolan and M. A. Adams, Spine (Phila. Pa. 1976)., 2011, 36, 770–777.
64. S. Khatab, M. J. Leijs, G. van Buul, J. Haeck, N. Kops, M. Nieboer, P. K. Bos, J. A. N. Verhaar, M. Bernsen and G. J. V. M. van Osch, Cell Biol. Toxicol., 2020.
65. J. Sellam and F. Berenbaum, Nat. Rev. Rheumatol., 2010, 6, 625–635.
66. A. C. Bakker, F. A. J. van de Loo, H. M. van Beuningen, P. Sime, P. L. E. M. van Lent, P. M. van der Kraan, C. D. Richards and W. B. van den Berg, Osteoarthr. Cartil., 2001, 9, 128–136.
67. S. Zoricic, I. Maric, D. Bobinac and S. Vukicevic, J. Anat., 2003, 202, 269–277.
68. A. Scharstuhl, E. L. Vitters, P. M. Van Der Kraan and W. B. Van Den Berg, Arthritis Rheum., 2003, 48, 3442–3451.
69. E. Redondo-Castro, C. Cunningham, J. Miller, L. Martuscelli, S. Aoulad-Ali, N. J. Rothwell, C. M. Kielty, S. M. Allan and E. Pinteaux, Stem Cell Res. Ther., 2017.
70. J. O. Voss, C. Loebel, J. J. Bara, M. A. Fussinger, F. Duttenhoefer, M. Alini and M. J. Stoddart, Biomed Res. Int., 2015.
71. M. Kapoor, J. Martel-Pelletier, D. Lajeunesse, J. P. Pelletier and H. Fahmi, Nat. Rev. Rheumatol., 2011, 7, 33–42.
72. D. Long, S. Blake, X. Y. Song, M. Lark and R. F. Loeser, Arthritis Res. Ther., 2008.
73. P. R. Elford and P. H. Cooper, Arthritis Rheum., 1991, 34, 325–332.
74. L. D. Weinstock, J. E. Forsmo, A. Wilkinson, J. Ueda and L. B. Wood, Front. Bioeng. Biotechnol., 2020, 8, 666.
75. T. Velnar, T. Bailey and V. Smrkolj, The wound healing process: An overview of the cellular and molecular mechanisms, 2009, 37.
76. S. Werner and R. Grose, Physiol. Rev., 2003, 83, 835–870.
77. M. Kucharzewski, E. Rojczyk, K. Wilemska-Kucharzewska, R. Wilk, J. Hudecki and M. J. Los, Eur. J. Pharmacol., 2019, 843, 307–315.
78. Z.-Q. Lin, T. Kondo, Y. Ishida, T. Takayasu and N. Mukaida, J. Leukoc. Biol., 2003, 73, 713–721.
79. A. Bartlett, A. J. Sanders, F. Ruge, K. G. Harding and W. G. Jiang, Exp. Ther. Med., 2016, 12, 33–40.
80. J. M. David, C. Dominguez, D. H. Hamilton and C. Palena, Vaccines, 2016, 4.
81. K. A. Elsaid, L. Zhang, Z. Shaman, C. Patel, T. A. Schmidt and G. D. Jay, Osteoarthr. Cartil., 2015, 23, 114–121.
82. J. P. Caron, J. C. Fernandes, J. Martel-Pelletier, G. Tardif, F. Mineau, C. Geng and J. P. Pelletier, Arthritis Rheum., 1996, 39, 1535–1544.
83. P. B. Bolno, D. Morgan, A. Wechsler and J. Y. Kresh, J. Am. Coll. Surg., 2004, 199, 33.
84. T. Sasaki, R. Akagi, Y. Akatsu, T. Fukawa, H. Hoshi, Y. Yamamoto, T. Enomoto, Y. Sato, R. Nakagawa, K. Takahashi, S. Yamaguchi and T. Sasho, Bone Jt. Res., 2017, 6, 123–131.

85. H. A. Flytlie, M. Hvid, E. Lindgreen, E. Kofod-Olsen, E. L. Petersen, A. Jørgensen, M. Deleuran, C. Vestergaard and B. Deleuran, *Cytokine*, 2010, **49**, 24–29.
86. C. Manferdini, E. Gabusi, D. Trucco, Y. Saleh and G. Lisignoli, *Osteoarthr. Cartil.*, 2020, **28**, S507–S508.
87. I. Shachar and N. Karin, *J. Leukoc. Biol.*, 2013, **93**, 51–61.
88. R. Rabani, M. Chan, A. Gómez-Aristizábal and S. Viswanathan, *Cytotherapy*, 2019, **21**, S15–S16.
89. R. A. Gadient and U. H. Otten, *Prog. Neurobiol.*, 1997, **52**, 379–390.
90. T. H. Qazi, D. J. Mooney, G. N. Duda and S. Geissler, *Biomaterials*, 2017, **140**, 103–114.
91. T. H. Qazi, D. J. Mooney, G. N. Duda and S. Geissler, *Biomaterials*, 2020, **230**, 119639.
92. M. E. Klontzas, S. Reakasame, R. Silva, J. C. F. Morais, S. Vernardis, R. J. MacFarlane, M. Heliotis, E. Tsiridis, N. Panoskaltsis, A. R. Boccaccini and A. Mantalaris, *Acta Biomater.*, 2019, **88**, 224–240.

Fig. 1. (a) Principle component analysis (PCA) identifies axes of maximum variation among samples in the data when measurement variables (**X1** and **X2**) are plotted against one another. Through incorporation of a response variable **Y**, partial least squares regression (PLSR), enables identification of maximum co-variation between the **X** variables and different **Y** responses. PLSR outputs new linear combinations of **X** variables, referred to as latent variables (LVs). (b) Each latent variable is comprised of weights, which ranks the importance of each input variable X_i, in determining the final composite values for each sample data point. (c) To obtain the PLSR scores plot, the raw data is multiplied by the calculated weights for each latent variable (**LV1** and **LV2**). The new axes defined by these latent variables (**LV1** and **LV2**) better separates the data with respect to the identity of the **Y** response variables.

Fig. 2. (a-j) Serial hematoxylin and eosin (H&E; a-e) and safranin-O and fast green (Saf-O; f-j) coronal sections of rat medial tibial plateaus at six weeks after Sham or MMT operation of rat hindlimbs. For MMT-induced OA there is presence of increased articular cartilage degeneration [increased proteoglycan loss (loss of red coloration in Saf-O images), loss of articular chondrocytes (lack of hematoxylin stain), surface fibrillations, formation of erosions and lesions] and the presence of osteophyte formations on the marginal edges for all MMT conditions (b-e&g-j). Sham operated hindlimbs (a&f) did not show any damage to articular cartilage or the presence of osteophyte formations. The MMT/Encap hMSC group (e&j) showed less overall cartilage damage (smoother cartilage surface with less erosion and lesion formation) with respect to all other MMT conditions. (k-o) MATLAB generated representative topographic maps of the articular cartilage surfaces depict the deviation of a sample's cartilage surface from a 3D polynomial fitted surface. Representative surface renderings were matched with representative histology and microCT. These surface renderings demonstrate elevations (red) and depressions (blue) in articular cartilage surfaces of MMT groups which were not found in the Sham. All images are oriented with the medial aspect of the tibia on the left. Scale bar (bottom right corner) is universal for all histology representative images. Scale bar for the topographic surface renderings (bottom center) is also included.

Fig. 3. (a) Total articular cartilage volume for all MMT groups are significantly greater than Sham animals; total articular cartilage volume for MMT/Encap hMSC group is significantly lower than MMT/Saline and MMT/Empty Cap groups. (b) Medial 1/3 articular cartilage volumes for MMT/Saline, MMT/Empty Caps and MMT/hMSC groups were significantly greater than Sham; hMSC/Encap hMSC group was not significantly different from Sham. (c&d) Total and medial 1/3 articular cartilage thickness values for MMT/Saline, MMT/Empty Caps and MMT/hMSC groups were significantly greater than Sham; no differences were found for either parameter between MMT/Encap hMSC and Sham; medial 1/3 articular cartilage thickness for MMT/Encap hMSC

group was significantly lower than MMT/Saline and MMT/Empty Caps groups. (e) Total articular cartilage attenuation for the MMT/hMSC group was significantly greater than the Sham group. (f) Medial 1/3 cartilage attenuation values for all MMT groups were significantly greater than the Sham group and no differences were found among MMT conditions. (g) Total cartilage surface roughness showed significantly higher values for all MMT groups relative to Sham; the MMT/Encap hMSC group did show significantly less surface roughness than all other MMT conditions. (h) Medial 1/3 analysis of surface roughness yielded identical findings to total analysis except no difference was found between Sham and MMT/Encap hMSC groups. (i&j) A difference in total exposed bone was found only for the MMT/hMSC group compared to all other groups; for medial 1/3 analysis of exposed bone, MMT/Saline and MMT/hMSC groups were significantly increased from Sham group. (k) PLSDA assessment of the overall effect of the therapeutics applied on articular cartilage damage showed distinct separation with Sham and MMT Encap hMSC separating to the left and all other MMT conditions separating to the right along LV1. (l) Quantification of the scores obtained from PLSDA analysis demonstrated that all MMT conditions had significantly more cartilage damage than Sham; in addition, MMT/Encap hMSC had significantly less damage than all other MMT conditions. Data presented as mean +/- SD. *n* = 6 for Sham, *n* = 7 for MMT/Saline, *n* = 7 for MMT/Empty Caps, *n* = 8 for MMT/hMSC and *n* = 7 for MMT/Encap hMSC. * represents significant differences ($p < 0.05$) between individual MMT conditions and Sham. Horizontal black bars indicate significance ($p < 0.05$) between individual MMT groups.

Fig. 4. (a&b) Total and medial 1/3 subchondral bone volumes for all MMT groups, except MMT/Encap hMSC, were significantly greater than the Sham group. (c&d) Total and medial 1/3 subchondral bone thickness analysis yielded significant increases in all MMT groups relative to Sham. (e) MMT/Empty Caps and MMT/Saline total subchondral bone attenuation was significantly greater than the Sham while showing no differences with MMT/hMSC and MMT/Encap hMSC groups. (f) In the medial 1/3 region, all MMT groups had significantly greater attenuation values compared to Shams; the only difference found between MMT conditions was between MMT/Empty Caps and MMT/Encap hMSC. (g) PLSDA analysis of total and medial 1/3 subchondral bone parameters depicted significant separation between Sham, to the left, from all MMT conditions, to the right, along LV1 based on the level of subchondral bone remodeling. (h) Statistical analysis of these scores demonstrated a significant difference between the Sham group and all the MMT groups, with no differences between the respective MMT groups. Data presented as mean +/- SD. *n* = 6 for Sham, *n* = 7 for MMT/Saline, *n* = 7 for MMT/Empty Caps, *n* = 8 for MMT/hMSC and *n* = 7 for MMT/Encap hMSC. * represents significant differences ($p < 0.05$) between individual MMT conditions and Sham. Horizontal black bars indicate significance ($p < 0.05$) between individual MMT groups.

Fig. 5. (a) Mineralized osteophyte volumes for all MMT groups were significantly greater than the Sham group; MMT/Encap hMSC and MMT/hMSC groups yielded significant increases in mineralized osteophyte volume compared to MMT/Saline and MMT/Empty Caps groups. (b) Cartilaginous osteophyte volumes for all MMT groups were significantly greater than the Sham group; MMT/Encap hMSC demonstrated significant increases in cartilaginous volume relative to MMT/hMSC and MMT/Empty Caps. (c) Total osteophyte volumes (Mineralized volume + Cartilaginous volume) for all MMT groups were again significantly greater than the Sham group; MMT/Encap hMSC yielded significantly greater total osteophyte volumes than all MMT conditions. (d) PLSDA analysis of overall osteophyte volumes depicted distinct separation of all groups based on osteophyte size, with Sham to the left and MMT/Encap hMSC to the right along LV1. (e) Statistical analysis of LV1 scores demonstrated significantly higher values for all MMT conditions, compared to Sham, with MMT/Encap hMSC showing increased volumes relative to all MMT conditions. Data presented as mean +/- SD. *n* = 6 for Sham, *n* = 7 for

MMT/Saline, *n* = 7 for MMT/Empty Caps, *n* = 8 for MMT/hMSC and *n* = 7 for MMT/Encap hMSC. * represents significant differences ($p < 0.05$) between individual MMT conditions and Sham. Horizontal black bars indicate significance ($p < 0.05$) between individual MMT groups.

Fig. 6. (a) Luminex analysis of 41 cytokines (columns; z-scored) secreted from hMSCs with (Encap hMSC) and without encapsulation (hMSC) in non-stimulated (+CTRL) and stimulated environments (+IL-1β; each row represents a single sample). (b) PLSDA analysis identified two profiles of cytokines, LV1 and LV2, that identified a distinct separation between treatment groups for both encapsulated and non-encapsulated hMSCs. (c&d) Independent analysis of scores on each of the respective latent variables demonstrated significant differences between non-stimulated (+CTRL) and stimulated environments (+IL-1β) for both encapsulated and non-encapsulated hMSCs. Data presented as mean +/- SD. *n* = 6 for all groups. Horizontal black bars indicate significant differences between non-stimulated (+CTRL) and stimulated (+IL-1β) groups.

Fig. 7. (a) PLSDA analysis of encapsulated hMSCs identified a single latent variable, LV1, that distinguished between Encap hMSC + CTRL on the left and Encap hMSC + IL-1β to the right. (b) The weighted profiles of cytokines showed relative expression of cytokines in CTRL conditions (blue) and IL-1β conditions (red). Error bars on each cytokine were computed by PLSDA model regeneration using iterative (1000 iterations) leave one out cross validation (LOOCV). (c-j) All measured cytokines that showed significant increased expression with IL-1β stimulation were assessed independently, using t-test with Bonferroni correction, for significance between CTRL and IL-1β conditions, with all significant findings presented. Encap hMSCs + IL-1β yielded increased expression in pro-inflammatory (IL-1β, IL-6, IL-7, IL-8), anti-inflammatory (IL-1RA), and chemotactic (G-CSF, MDC, IP10) cytokines. Data presented as mean +/- SD. *n* = 6 for all groups. Horizontal black bars indicate significant differences between non-stimulated (+CTRL) and stimulated (+IL-1β) groups.

Figure 1

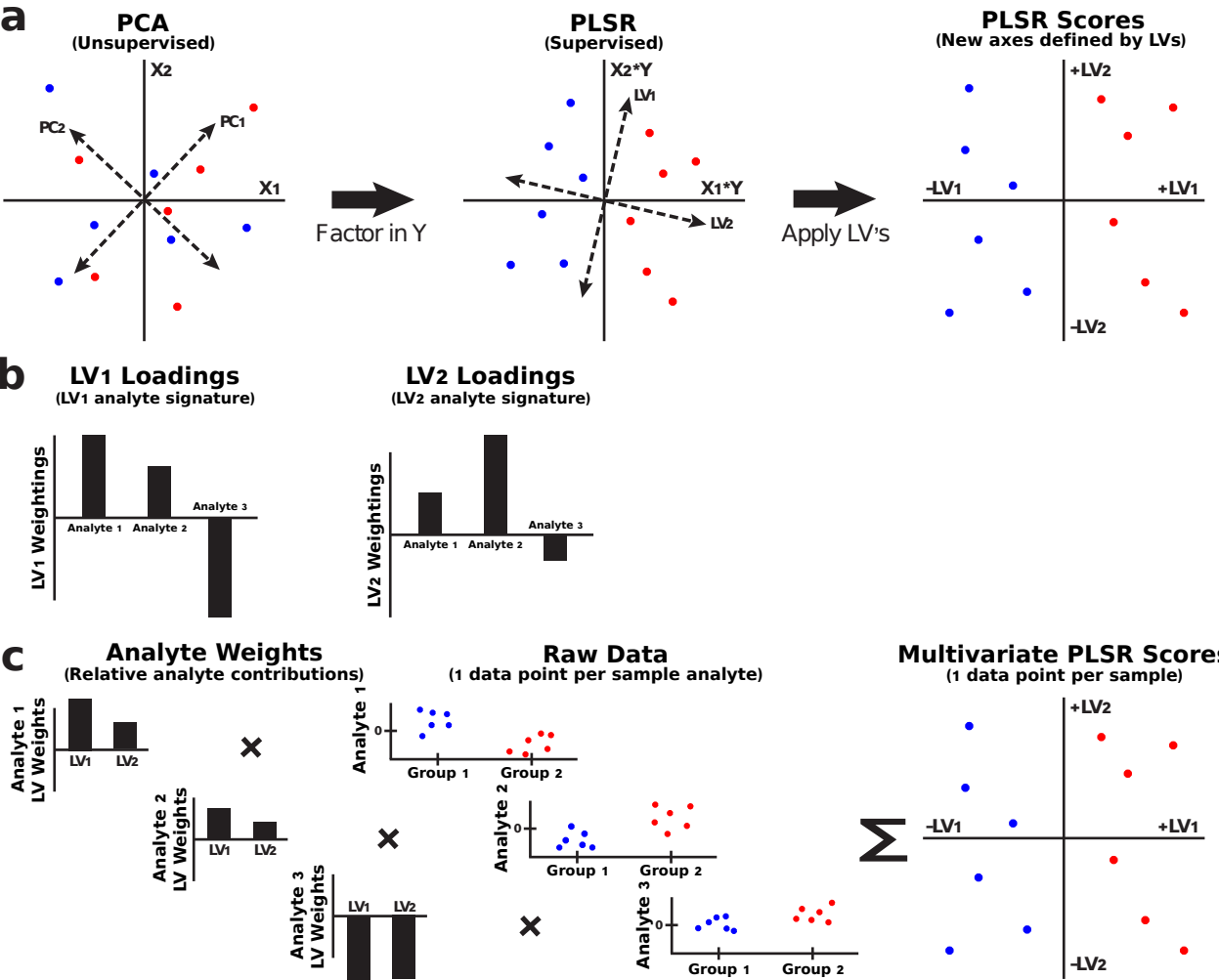
a
PCA
(Unsupervised)
X2
PC2
PC1
X1
Factor in Y
PLSR
(Supervised)
X2*Y
LV1
X1*Y
LV2
Apply LV's
PLSR Scores
(New axes defined by LVs)
+LV2
-LV1
+LV1
-LV2
b
LV1 Loadings
(LV1 analyte signature)
LV1 Weightings
Analyte 1
Analyte 2
Analyte 3
LV2 Loadings
(LV2 analyte signature)
LV2 Weightings
Analyte 1
Analyte 2
Analyte 3
c
Analyte Weights
(Relative analyte contributions)
Analyte 1 LV Weights
LV1
LV2
Analyte 2 LV Weights
LV1
LV2
Analyte 3 LV Weights
LV1
LV2
Raw Data
(1 data point per sample analyte)
Analyte 1
0
Group 1
Group 2
Analyte 2
0
Group 1
Group 2
Analyte 3
0
Group 1
Group 2
Multivariate PLSR Scores
(1 data point per sample)
+LV2
-LV1
+LV1
-LV2

Figure 2

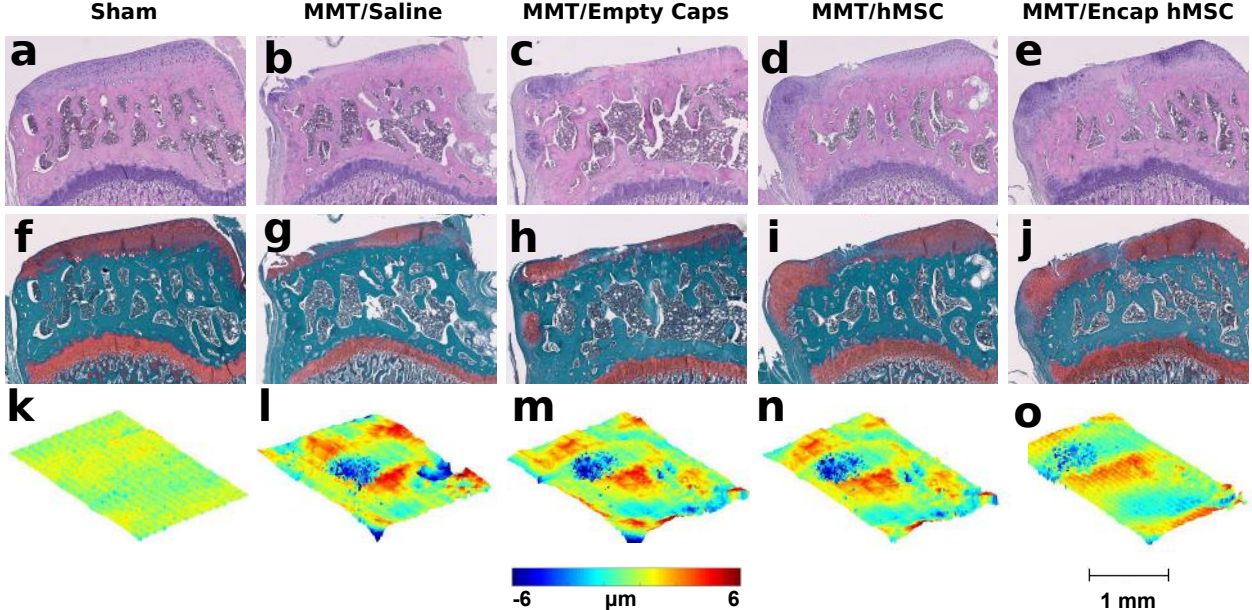
Sham
MMT/Saline
MMT/Empty Caps
MMT/hMSC
MMT/Encap hMSC
H&E
Saf-O
Diff. Surf.
a
b
c
d
e
f
g
h
i
j
k
l
m
n
o
-6
µm
6
1 mm

Figure 3

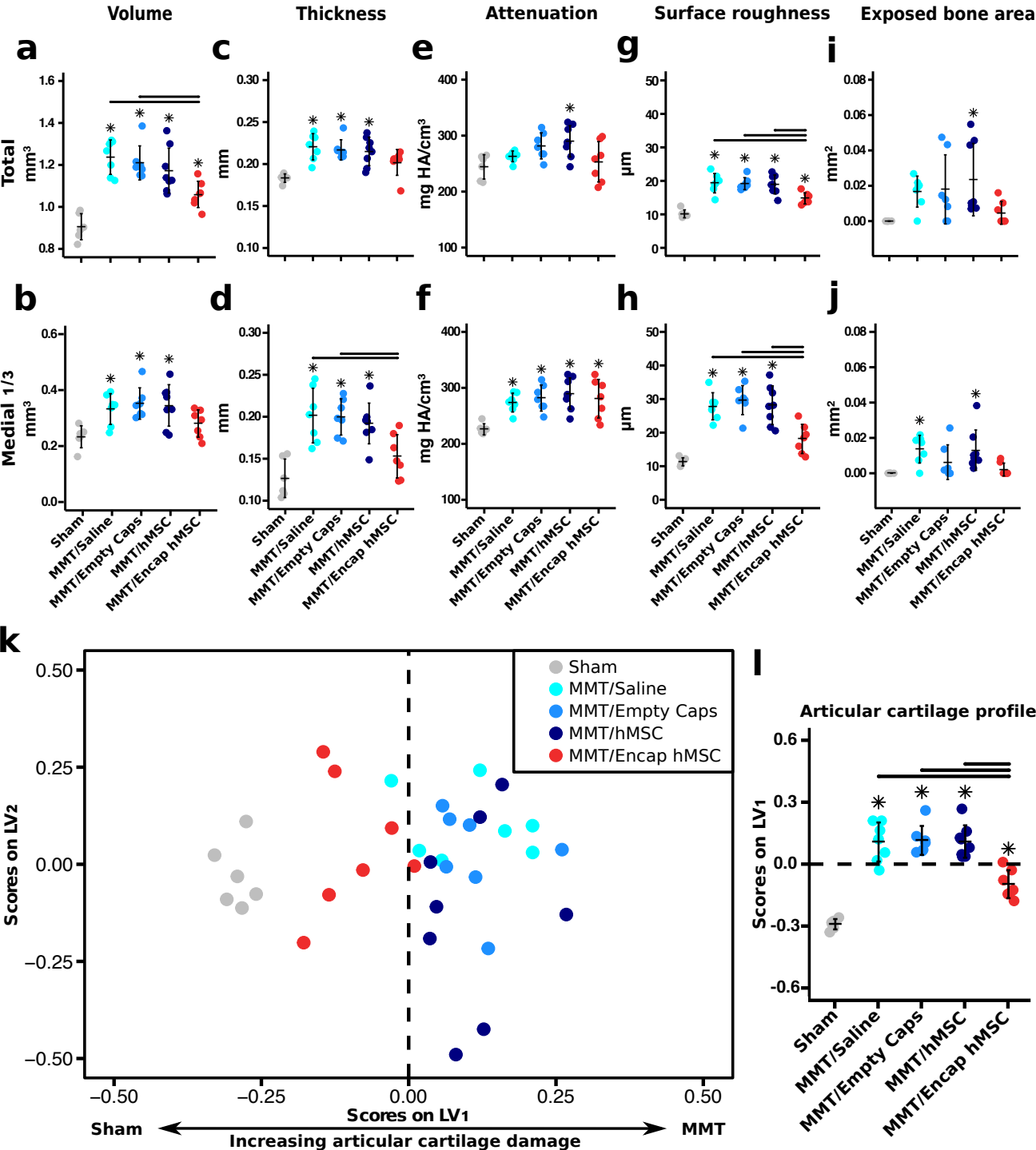
Volume
Thickness
Attenuation
Surface roughness
Exposed bone area
a
c
e
g
i
b
d
f
h
j
Total mm³
Medial 1/3 mm³
mm
mg HA/cm³
µm
mm²
Sham
MMT/Saline
MMT/Empty Caps
MMT/hMSC
MMT/Encap hMSC
k
l
Sham
MMT/Saline
MMT/Empty Caps
MMT/hMSC
MMT/Encap hMSC
Scores on LV2
Scores on LV1
Articular cartilage profile
Sham
MMT
Increasing articular cartilage damage

Figure 4

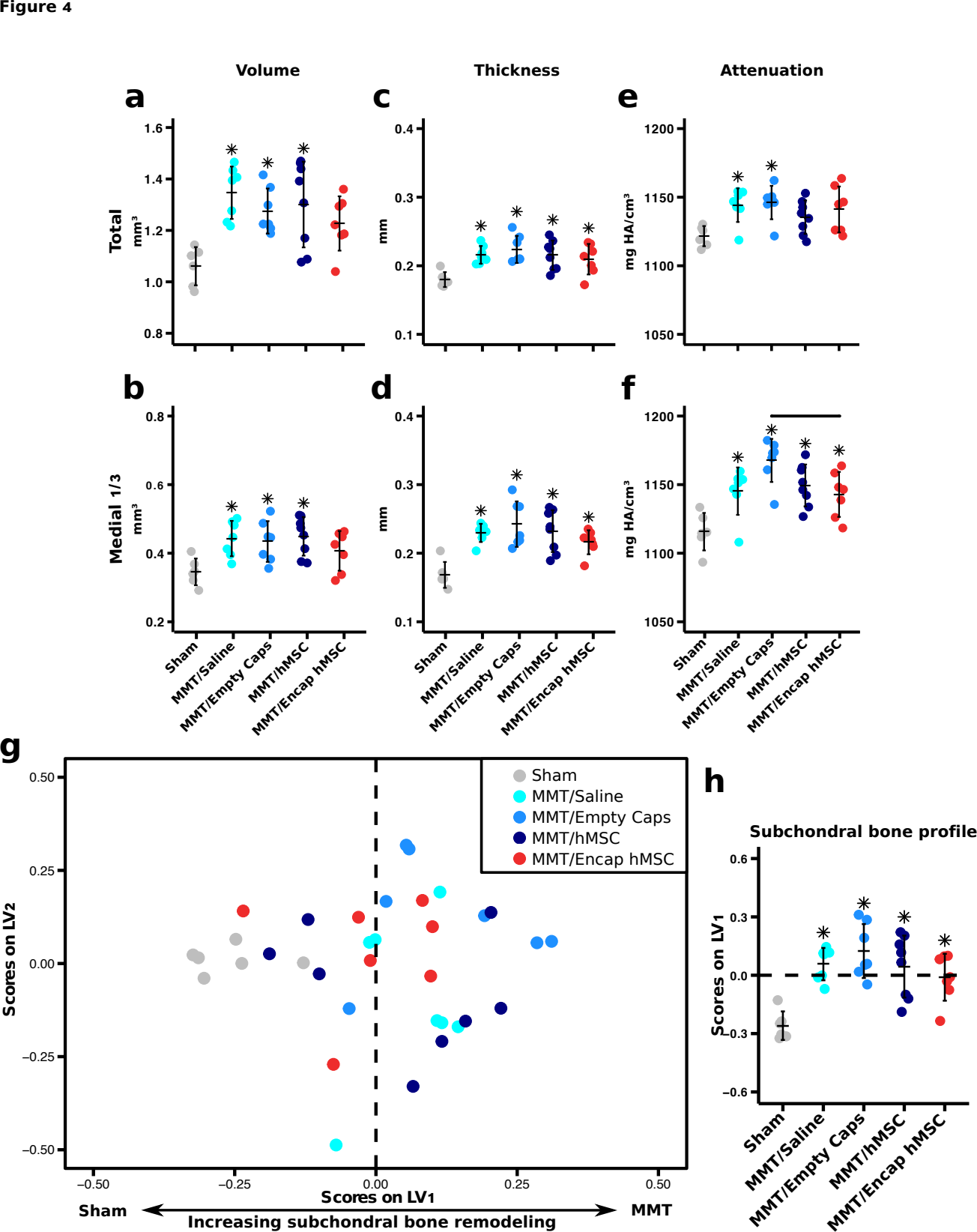
Volume
Thickness
Attenuation
a
c
e
b
d
f
Total mm³
mm
mg HA/cm³
Medial 1/3 mm³
Sham
MMT/Saline
MMT/Empty Caps
MMT/hMSC
MMT/Encap hMSC
g
h
Scores on LV2
Scores on LV1
Sham
MMT
Increasing subchondral bone remodeling
Subchondral bone profile

Figure 5

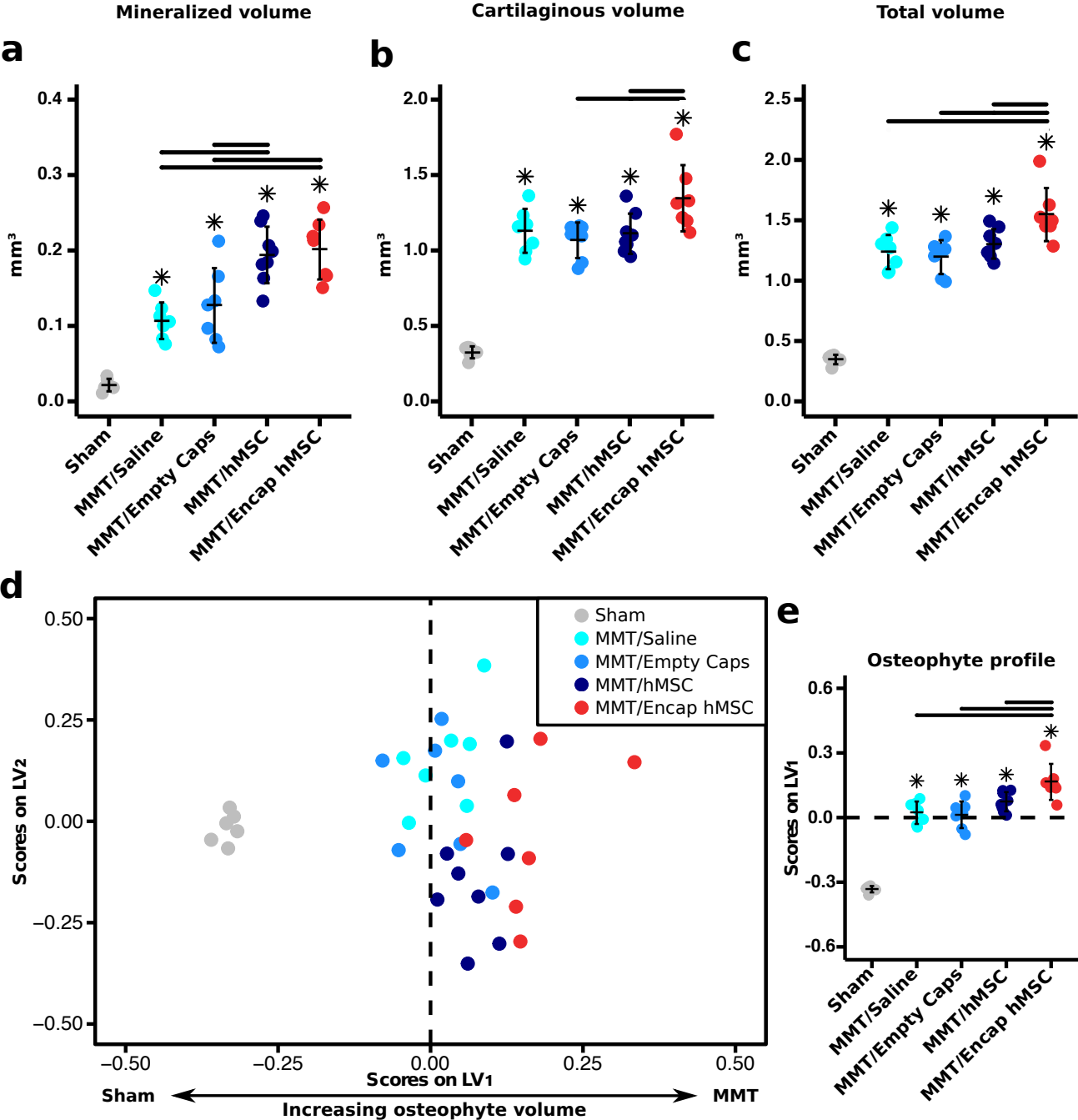
Mineralized volume
Cartilaginous volume
Total volume
a
b
c
mm³
Sham
MMT/Saline
MMT/Empty Caps
MMT/hMSC
MMT/Encap hMSC
d
e
Sham
MMT/Saline
MMT/Empty Caps
MMT/hMSC
MMT/Encap hMSC
Scores on LV2
Scores on LV1
Osteophyte profile
Scores on LV1
Sham
MMT
Increasing osteophyte volume

Figure 6

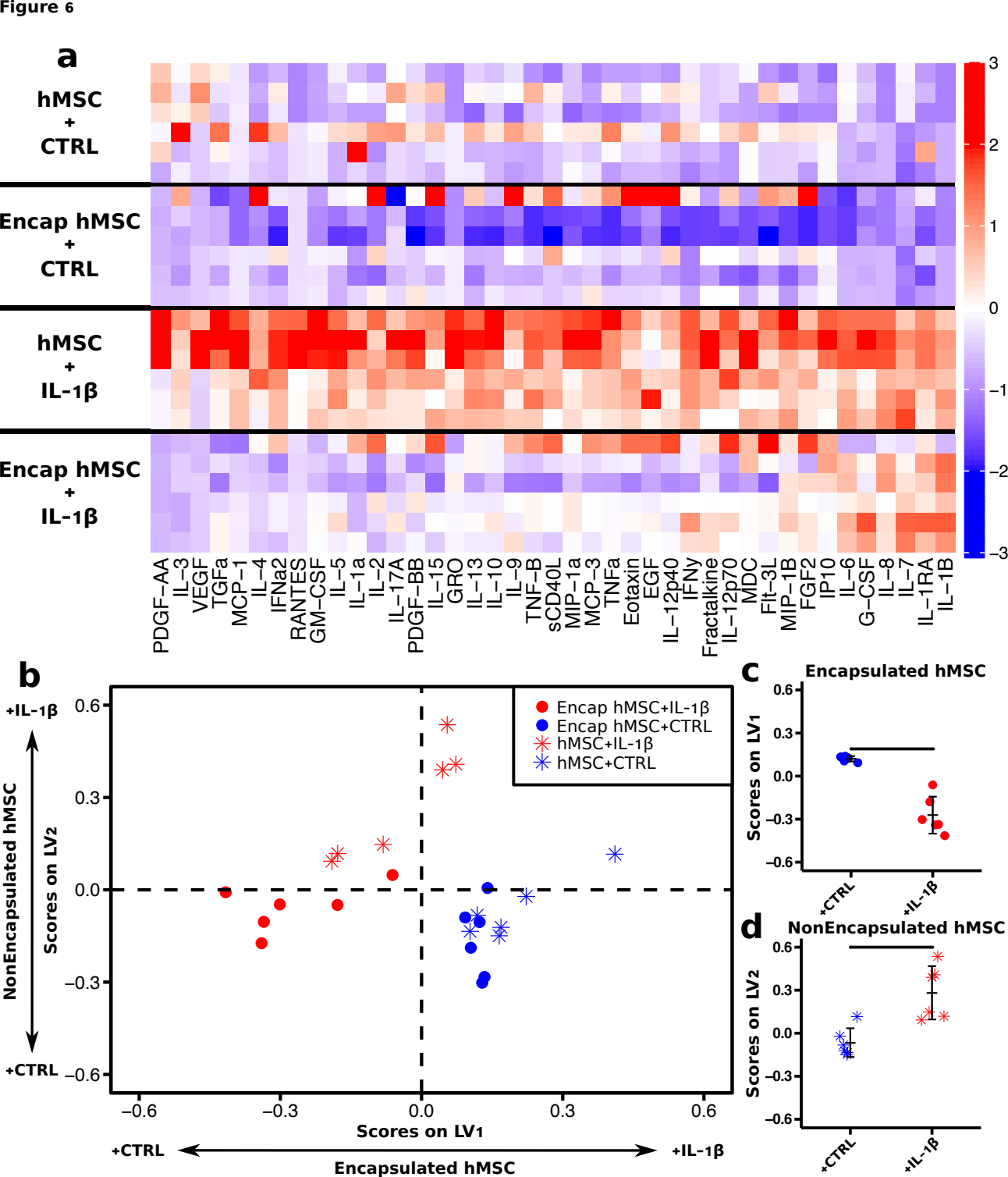
a
hMSC + CTRL
Encap hMSC + CTRL
hMSC + IL-1β
Encap hMSC + IL-1β
3
2
1
0
−1
−2
−3
PDGF−AA
IL−3
VEGF
TGFa
MCP−1
IL−4
IFNa2
RANTES
GM−CSF
IL−5
IL−1a
IL−2
IL−17A
PDGF−BB
IL−15
GRO
IL−13
IL−10
IL−9
TNF−B
sCD40L
MIP−1a
MCP−3
TNFa
Eotaxin
EGF
IL−12p40
IFNγ
Fractalkine
IL−12p70
MDC
Flt−3L
MIP−1B
FGF2
IP10
IL−6
G−CSF
IL−8
IL−7
IL−1RA
IL−1B
b
+IL-1β
+CTRL
NonEncapsulated hMSC
Scores on LV2
Encap hMSC+IL-1β
Encap hMSC+CTRL
hMSC+IL-1β
hMSC+CTRL
0.6
0.3
0.0
−0.3
−0.6
Scores on LV1
+CTRL
+IL-1β
Encapsulated hMSC
c
Encapsulated hMSC
Scores on LV1
+CTRL
+IL-1β
d
NonEncapsulated hMSC
Scores on LV2
+CTRL
+IL-1β

Figure 7

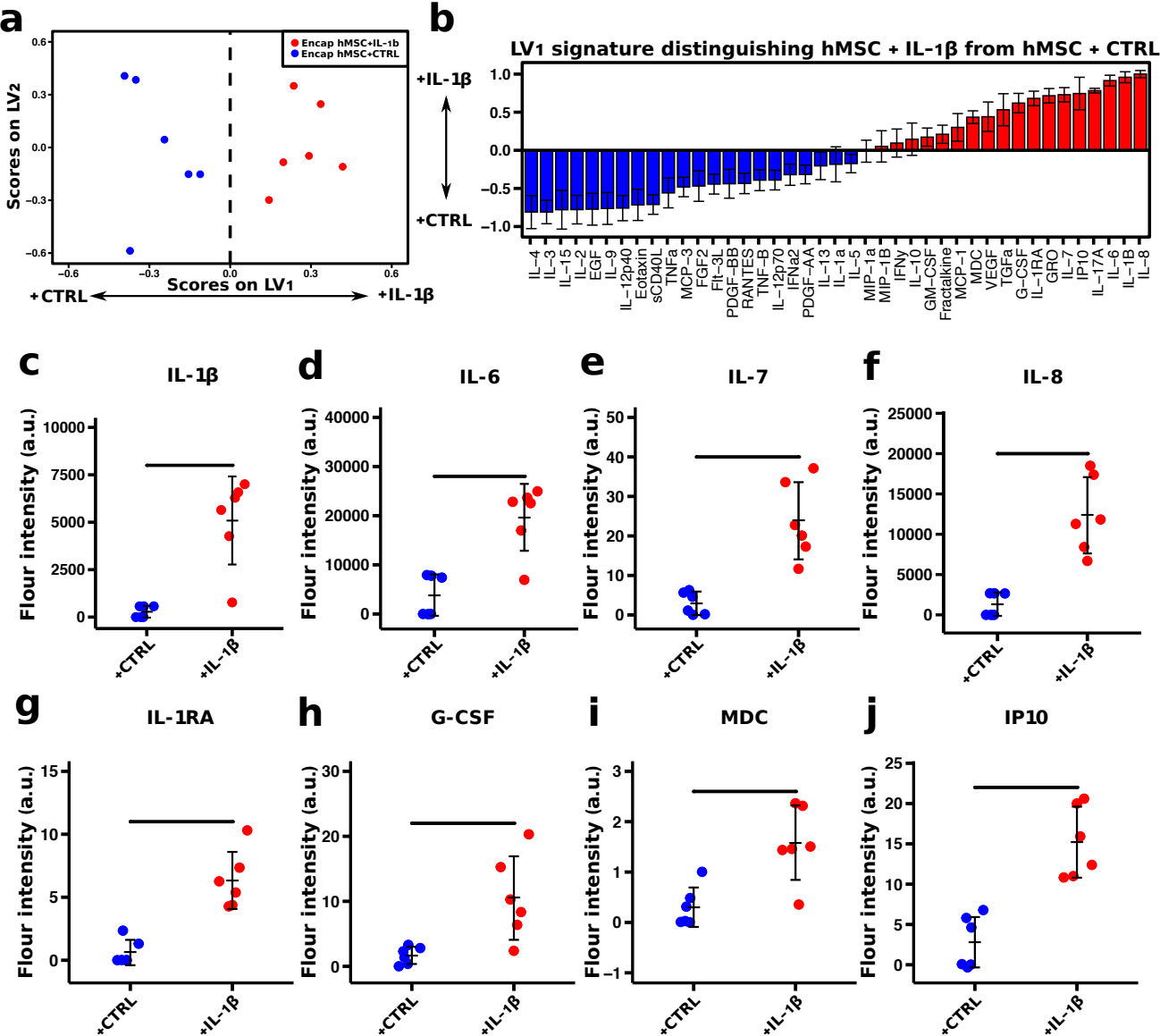
a
Encap hMSC+IL-1b
Encap hMSC+CTRL
Scores on LV2
Scores on LV1
+CTRL
+IL-1β
b
LV1 signature distinguishing hMSC + IL-1β from hMSC + CTRL
+IL-1β
+CTRL
IL−4
IL−3
IL−15
IL−2
EGF
IL−9
IL−12p40
Eotaxin
sCD40L
TNFa
MCP−3
FGF2
Flt−3L
PDGF−BB
RANTES
TNF−B
IL−12p70
IFNa2
PDGF−AA
IL−13
IL−1a
IL−5
MIP−1a
MIP−1B
IFNγ
IL−10
GM−CSF
Fractalkine
MCP−1
MDC
VEGF
TGFa
G−CSF
IL−1RA
GRO
IL−7
IP10
IL−17A
IL−6
IL−1B
IL−8
c
IL-1β
d
IL-6
e
IL-7
f
IL-8
Flour intensity (a.u.)
+CTRL
+IL-1β
g
IL-1RA
h
G-CSF
i
MDC
j
IP10

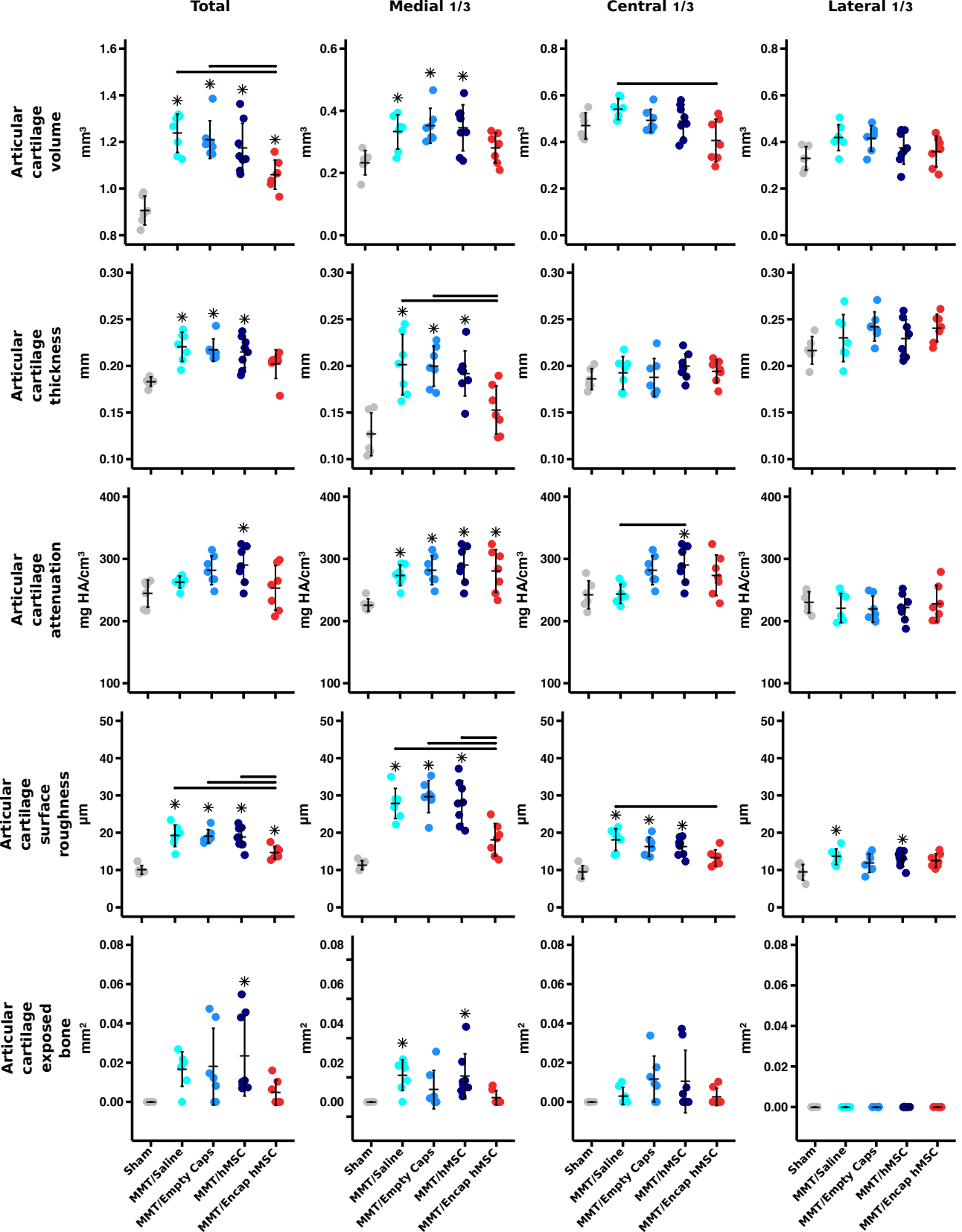
Total
Medial 1/3
Central 1/3
Lateral 1/3
Articular cartilage volume
mm³
Articular cartilage thickness
mm
Articular cartilage attenuation
mg HA/cm³
Articular cartilage surface roughness
µm
Articular cartilage exposed bone
mm²
Sham
MMT/Saline
MMT/Empty Caps
MMT/hMSC
MMT/Encap hMSC

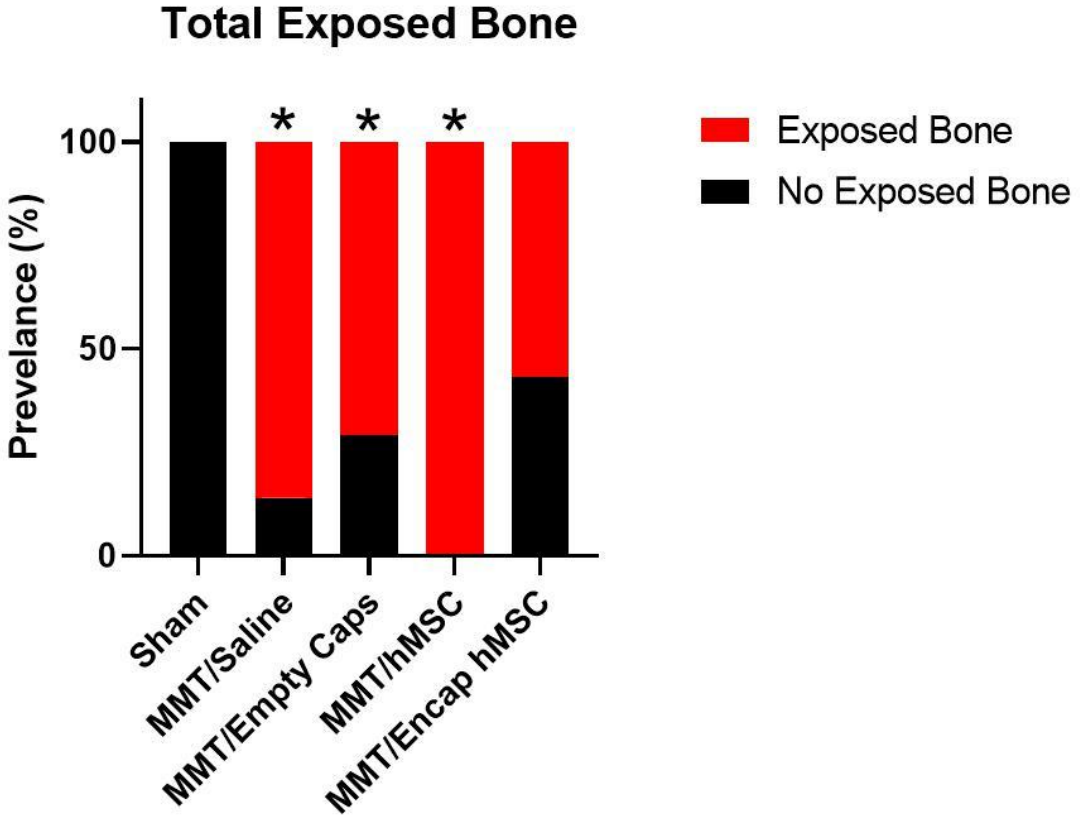
Total Exposed Bone
Prevelance (%)
100
50
0
*
*
*
Exposed Bone
No Exposed Bone
Sham
MMT/Saline
MMT/Empty Caps
MMT/hMSC
MMT/Encap hMSC

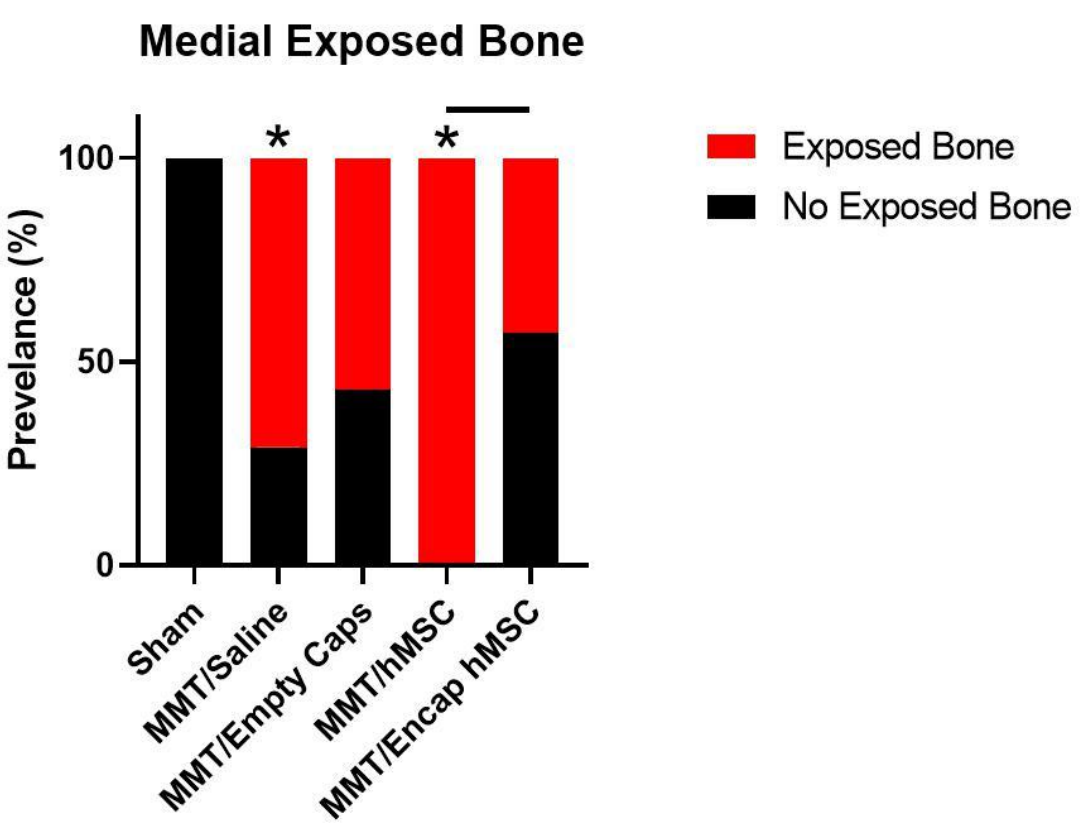
Medial Exposed Bone
Prevelance (%)
100
50
0
*
*
Exposed Bone
No Exposed Bone
Sham
MMT/Saline
MMT/Empty Caps
MMT/hMSC
MMT/Encap hMSC

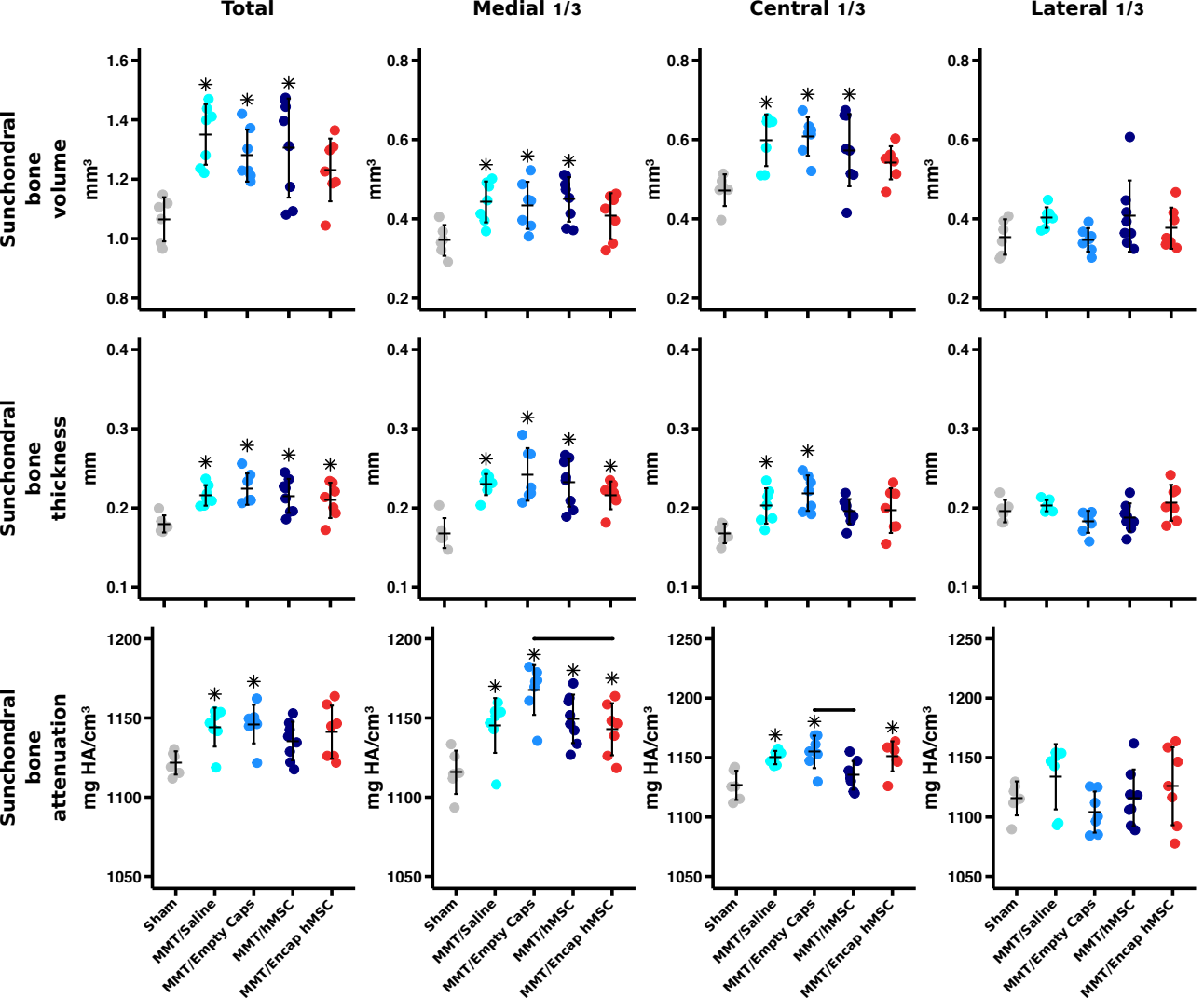
Total
Medial 1/3
Central 1/3
Lateral 1/3
Sunchondral bone volume
Sunchondral bone thickness
Sunchondral bone attenuation
mm³
mm
mg HA/cm³
Sham
MMT/Saline
MMT/Empty Caps
MMT/hMSC
MMT/Encap hMSC